Density Model for Short-Beaked Common Dolphin (*Delphinus delphis*) for the U.S. East Coast: Supplementary Report

Model Version 5.1

Duke University Marine Geospatial Ecology Laboratory*

2023-05-27

Citation

When citing our methodology or results generally, please cite Roberts et al. (2016, 2023). The complete references appear at the end of this document. We are preparing a new article for a peer-reviewed journal that will eventually replace those. Until that is published, those are the best general citations.

When citing this model specifically, please use this reference:

Roberts JJ, Yack TM, Cañadas A, Fujioka E, Halpin PN, Barco SG, Boisseau O, Chavez-Rosales S, Cole TVN, Cotter MP, Cummings EW, Davis GE, DiGiovanni Jr. RA, Garrison LP, Gowan TA, Jackson KA, Kenney RD, Khan CB, Lockhart GG, Lomac-MacNair KS, McAlarney RJ, McLellan WA, Mullin KD, Nowacek DP, O'Brien O, Pabst DA, Palka DL, Quintana-Rizzo E, Redfern JV, Rickard ME, White M, Whitt AD, Zoidis AM (2022) Density Model for Short-Beaked Common Dolphin (*Delphinus delphis*) for the U.S. East Coast, Version 5.1, 2023-05-27, and Supplementary Report. Marine Geospatial Ecology Laboratory, Duke University, Durham, North Carolina.

Copyright and License

Model Version History

Version	Date	Description
1	2014-11-17	Initial version.
2	2014-12-04	Fixed bug that applied the wrong detection function to segments NE_narwss_1999_widgeon_hapo dataset. Refitted model. Updated documentation.
2.1	2015-03-06	Updated the documentation. No changes to the model.
2.2	2015-05-14	Updated calculation of CVs. Switched density rasters to logarithmic breaks. No changes to the model.
3	2015-10-06	Switched our selection of the "best model" to the contemporaneous model, from the climatological model fitted to all segments (see Discussion). Updated the documentation.
3.1	2016-04-21	Switched calculation of monthly 5% and 95% confidence interval rasters to the method used to produce the year-round rasters. (We intended this to happen in version 2.2 but I did not implement it properly.) No changes to the other rasters or the model itself. Model files released as supplementary information to Roberts et al. (2016).

*For questions or to offer feedback please contact Jason Roberts (jason.roberts@duke.edu) and Tina Yack (tina.yack@duke.edu)

(continued)

Version	Date	Description
4	2018-04-14	Began update to Roberts et al. (2015) model. Introduced new surveys from AMAPPS, NARWSS, UNCW, VAMSC, and the SEUS NARW teams. Updated modeling methodology. Refitted detection functions and spatial models from scratch using new and reprocessed covariates. Model released as part of a scheduled update to the U.S. Navy Marine Species Density Database (NMSDD).
5	2022-06-20	This model is a major update over the prior version, with substantial additional data, improved statistical methods, and an increased spatial resolution. It was released as part of the final delivery of the U.S. Navy Marine Species Density Database (NMSDD) for the Atlantic Fleet Testing and Training (AFTT) Phase IV Environmental Impact Statement. Several new collaborators joined and contributed survey data: New York State Department of Environmental Conservation, TetraTech, HDR, and Marine Conservation Research. We incorporated additional surveys from all continuing and new collaborators through the end of 2020. (Because some environmental covariates were only available through 2019, certain models only extend through 2019.) We increased the spatial resolution to 5 km and, at NOAA's request, we extended the model further inshore from New York through Maine. We reformulated and refitted all detection functions and spatial models. We updated all enviromental covariates to newer products, when available, and added several covariates to the set of candidates. For models that incorporated dynamic covariates, we estimated model uncertainty using a new method that accounts for both model parameter error and temporal variability.
5.1	2023-05-27	Completed the supplementary report documenting the details of this model. The model itself was not changed.

1 Survey Data

We built this model from data collected between 1998-2019 (Table 1, Figure 1). We excluded surveys that did not target small cetaceans or were otherwise problematic for modeling them. In keeping with our primary strategy for the 2022 modeling cycle, we excluded data prior to 1998 in order to utilize biological covariates derived from satellite ocean color observations, which were only available for a few months before 1998. We excluded data after 2019 in order to utilize zooplankton and micronekton biomass estimates from SEAPODYM (Lehodey et al. 2008), which preliminary modeling indicated were were effective spatial covariates but were only available through 2019. We restricted the model to aerial survey transects with sea states of Beaufort 4 or less (for a few surveys we used Beaufort 3 or less) and shipboard transects with Beaufort 5 or less (for a few we used Beaufort 4 or less). We also excluded transects with poor weather or visibility for surveys that reported those conditions.

Table 1: Survey effort and observations considered for this model. Effort is tallied as the cumulative length of on-effort transects. Observations are the number of groups and individuals encountered while on effort. Off effort observations and those lacking an estimate of group size or distance to the group were excluded.

			Effort	Observations		
Institution	Program	Period	1000s km	Groups	Individuals	Mean Group Size
Aerial Surveys						
HDR	Navy Norfolk Canyon	2018-2019	10	47	8,736	185.9
NEFSC	AMAPPS	2010-2019	83	817	12,948	15.8
NEFSC	NARWSS	2003-2016	380	607	16,412	27.0
NEFSC	Pre-AMAPPS	1999-2008	45	237	5,985	25.3
SEFSC	AMAPPS	2010-2019	110	177	8,576	48.5
SEFSC	MATS	2002-2005	27	2	3,000	1,500.0
UNCW	MidA Bottlenose	2002-2002	15	5	64	12.8
UNCW	Navy Cape Hatteras	2011-2017	34	27	7,614	282.0
UNCW	Navy Jacksonville	2009-2017	92	0	0	
UNCW	Navy Norfolk Canyon	2015-2017	14	49	5,785	118.1
UNCW	Navy Onslow Bay	2007-2011	49	1	20	20.0
UNCW	SEUS NARW EWS	2005-2008	106	26	496	19.1
VAMSC	MD DNR WEA	2013-2015	15	22	169	7.7
VAMSC	Navy VACAPES	2016-2017	18	8	303	37.9
VAMSC	VA CZM WEA	2012-2015	19	22	333	15.1
		Total	**1,017**	**2,047**	**70,441**	**34.4**
Shipboard Surveys						
MCR	SOTW Visual	2012-2019	9	60	583	9.7
NEFSC	AMAPPS	2011-2016	15	334	14,096	42.2
NEFSC	Pre-AMAPPS	1998-2007	13	136	5,441	40.0
NJDEP	NJEBS	2008-2009	14	19	241	12.7
SEFSC	AMAPPS	2011-2016	16	2	63	31.5
SEFSC	Pre-AMAPPS	1998-2006	30	40	5,064	126.6
		Total	**96**	**591**	**25,488**	**43.1**
		Grand Total	**1,113**	**2,638**	**95,929**	**36.4**

Table 2: Institutions that contributed surveys used in this model.

Institution	Full Name
HDR	HDR, Inc.
MCR	Marine Conservation Research
NEFSC	NOAA Northeast Fisheries Science Center
NJDEP	New Jersey Department of Environmental Protection
SEFSC	NOAA Southeast Fisheries Science Center
UNCW	University of North Carolina Wilmington
VAMSC	Virginia Aquarium & Marine Science Center

Table 3: Descriptions and references for survey programs used in this model.

Program	Description	References
AMAPPS	Atlantic Marine Assessment Program for Protected Species	Palka et al. (2017), Palka et al. (2021)
MATS	Mid-Atlantic Tursiops Surveys	
MD DNR WEA	Aerial Surveys of the Maryland Wind Energy Area	Barco et al. (2015)
MidA Bottlenose	Mid-Atlantic Onshore/Offshore Bottlenose Dolphin Surveys	Torres et al. (2005)
NARWSS	North Atlantic Right Whale Sighting Surveys	Cole et al. (2007)
Navy Cape Hatteras	Aerial Surveys of the Navy's Cape Hatteras Study Area	McLellan et al. (2018)
Navy Jacksonville	Aerial Surveys of the Navy's Jacksonville Study Area	Foley et al. (2019)
Navy Norfolk Canyon	Aerial Surveys of the Navy's Norfolk Canyon Study Area	Cotter (2019), McAlarney et al. (2018)
Navy Onslow Bay	Aerial Surveys of the Navy's Onslow Bay Study Area	Read et al. (2014)
Navy VACAPES	Aerial Survey Baseline Monitoring in the Continental Shelf Region of the VACAPES OPAREA	Mallette et al. (2017)
NJEBS	New Jersey Ecological Baseline Study	Geo-Marine, Inc. (2010), Whitt et al. (2015)
Pre-AMAPPS	Pre-AMAPPS Marine Mammal Abundance Surveys	Mullin and Fulling (2003), Garrison et al. (2010), Palka (2006)
SEUS NARW EWS	Southeast U.S. Right Whale Early Warning System Surveys	
SOTW Visual	R/V Song of the Whale Visual Surveys	Ryan et al. (2013)
VA CZM WEA	Virginia CZM Wind Energy Area Surveys	Mallette et al. (2014), Mallette et al. (2015)

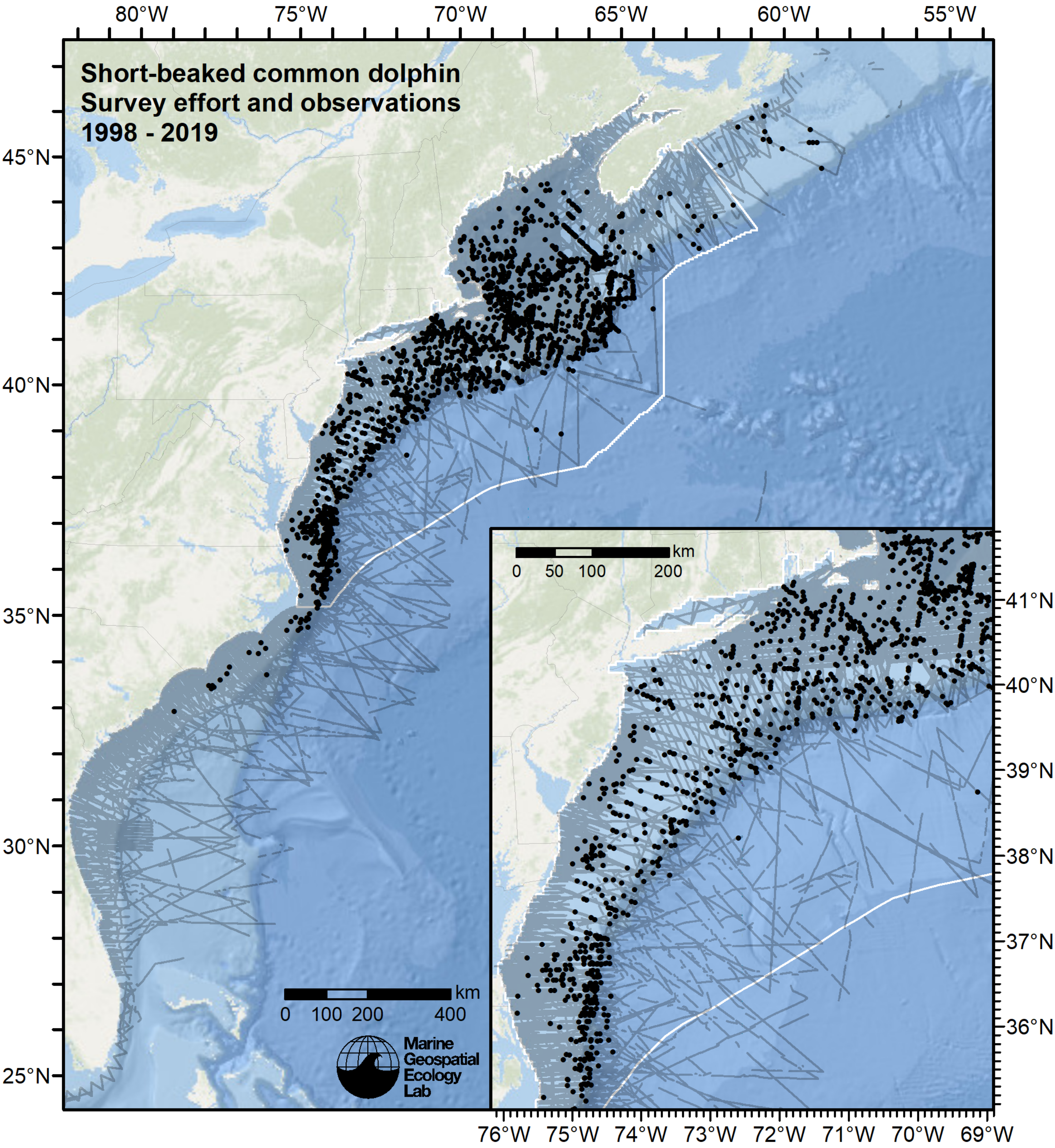

Figure 1: Survey effort and short-beaked common dolphin observations available for density modeling, after detection functions were applied, and excluded segments and truncated observations were removed.

2 Classification of Ambiguous Sightings

Observers occasionally experience difficulty identifying species, due to poor sighting conditions or phenotypic similarities between the possible choices. For example, observers may not always be able to distinguish fin whales from sei whales due their similiar size and shape. When this happens, observers will report an ambiguous identification, such as "fin or sei whale". In our density models, we handled ambiguous identifications in three ways:

1. For sightings with very generic identifications such as "large whale", we discarded the sightings. These sightings represented a clear minority when compared to those with definitive species identifications, but they are uncounted animals and our density models may therefore underestimate density to some degree.

2. For sightings of certain taxa in which a large majority of identifications were ambiguous (e.g. "unidentified pilot whale") rather than specific (e.g. "short-finned pilot whale" or "long-finned pilot whale"), it was not tractable to model the individual species so we modeled the generic taxon instead.

3. For sightings that reported an ambiguous identification of two species (e.g. "fin or sei whale") that are known to exhibit different habitat preferences or typically occur in different group sizes, and for which we had sufficient number of definitive sightings of both species, we first fitted a predictive model that classified the ambiguous sightings into one species or the other and then included the resulting classified sightings in the density models for each of the two species.

This section describes how we classified the third category of ambiguous sightings reported as "common or white-sided dolphin" into one species or the other.

For the predictive model, we used the cforest classifier (Hothorn et al. 2006), an elaboration of the classic random forest classifier (Breiman 2001). First, we trained a binary classifier using the sightings that reported definitive species identifications ("short-beaked common dolphin" and "Atlantic white-sided dolphin"). To increase the range of sampling of the classification model's covariates, the training data may have included additional surveys not considered for the density model, as well as transects from outside the spatial and temporal extents of the density model. Only on-effort sightings were used. We used the species ID as the response variable and environmental variables as covariates.

We used receiver operating characteristic (ROC) curve analysis to select a threshold for classifying the probabilistic predictions of species identifications made by the model into a binary result of one species or another. For the classification threshold, we selected the value that maximized the Youden index (Perkins and Schisterman 2006). Then, for all sightings reporting the ambiguous identification, we classified each as either one species or the other by processing the covariate values observed for it through the fitted model. We then included the classified sightings in the detection functions and density models. The sightings reported elsewhere in this document incorporate both the definitive sightings and the classified sightings, unless otherwise noted.

2.1 Classification Model

```
MODEL SUMMARY:
==============

Random Forest using Conditional Inference Trees

Number of trees: 750

Response: factor(OriginalScientificName)
Inputs: ClimChl, ClimDistToFront207, ClimMnkEpi, ClimPP_CAFE, ClimSST_CMC, ClimWindSpeed,
ClimZoo_SEAPODYM, Depth, DistTo125m, DistTo300m, Slope
Number of observations: 4877

Number of variables tried at each split: 5

Estimated predictor variable importance (conditional = FALSE):

Importance
DistTo300m 0.0818
ClimZoo_SEAPODYM 0.0688
ClimMnkEpi 0.0659
```

```
ClimWindSpeed 0.0343
ClimSST_CMC 0.0266
ClimPP_CAFE 0.0250
ClimDistToFront207 0.0244
DistTo125m 0.0204
ClimChl 0.0180
Depth 0.0111
Slope 0.0063

MODEL PERFORMANCE SUMMARY:
=========================

Statistics calculated from the training data.

Area under the ROC curve (auc)           = 0.981
Mean cross-entropy (mxe)                 = 0.210
Precision-recall break-even point (prbe) = 0.907
Root-mean square error (rmse)            = 0.244

User-specified cutoff = 0.524

Confusion matrix for that cutoff:

                                 Actual Lagenorhynchus acutus  Actual Delphinus delphis  Total
Predicted Lagenorhynchus acutus                          1880                       193   2073
Predicted Delphinus delphis                               192                      2612   2804
Total                                                    2072                      2805   4877

Model performance statistics for that cutoff:

Accuracy (acc)                                = 0.921
Error rate (err)                              = 0.079
Rate of positive predictions (rpp)            = 0.425
Rate of negative predictions (rnp)            = 0.575

True positive rate (tpr, or sensitivity)      = 0.907
False positive rate (fpr, or fallout)         = 0.069
True negative rate (tnr, or specificity)      = 0.931
False negative rate (fnr, or miss)            = 0.093

Positive prediction value (ppv, or precision) = 0.907
Negative prediction value (npv)               = 0.932
Prediction-conditioned fallout (pcfall)       = 0.093
Prediction-conditioned miss (pcmiss)          = 0.068

Matthews correlation coefficient (mcc)        = 0.838
Odds ratio (odds)                             = 132.517
SAR                                           = 0.715

Cohen's kappa (K)                             = 0.838
```

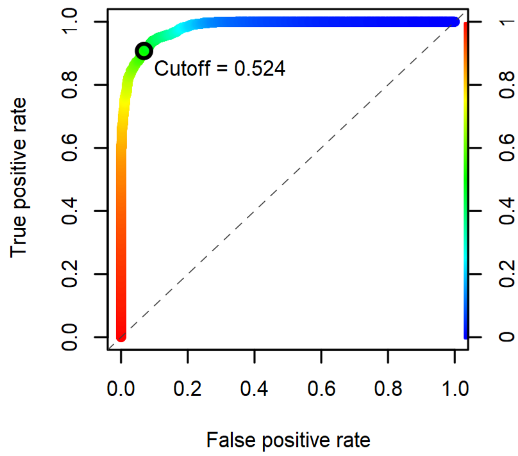

Figure 2: Receiver operating characteristic (ROC) curve summarizing the predictive performance of the ambiguous sighting classification model.

Table 4: Covariates used in the ambiguous sighting classification model.

Covariate	Description
ClimChl	Climatological monthly mean chlorophyll a concentration (mg m^{-3}) from Copernicus GlobColour (Garnesson et al. (2019)), provided by E.U. Copernicus Marine Service (product OCEANCOLOUR_GLO_CHL_L4_REP_OBSERVATIONS_009_082)
ClimDistToFront207	Climatological monthly mean distance (km) to the closest sea surface temperature front detected in daily GHRSST Level 4 CMC0.2deg and CMC0.1deg images (Brasnett (2008); Canada Meteorological Center (2012); Meissner et al. (2016); Canada Meteorological Center (2016)) with MGET's implementation of the Canny edge detector (Roberts et al. (2010); Canny (1986))
ClimMnkEpi	Climatological monthly mean micronekton biomass available in the epipelagic zone, expressed as wet weight (g m^{-2}), from SEAPODYM (Lehodey et al. (2008); Lehodey et al. (2015)), provided by E.U. Copernicus Marine Service. doi: 10.48670/moi-00020. Computed as the sum of the SEAPODYM mnkc_epi, mnkc_mumeso, and mnkc_hmlmeso variables.
ClimPP_CAFE	Climatological monthly mean net primary productivity (mg C m^{-2} day^{-1}) from the Carbon, Absorption, and Fluorescence Euphotic-resolving (CAFE) model (Silsbe et al. (2016))
ClimSST_CMC	Climatological monthly mean sea surface temperature (°C) from GHRSST Level 4 CMC0.2deg and CMC0.1deg (Brasnett (2008); Canada Meteorological Center (2012); Meissner et al. (2016); Canada Meteorological Center (2016))
ClimWindSpeed	Climatological monthly mean wind speed (m s^{-1}) 10 m above sea level from CCMP V2 Level 3 surface wind vectors (Atlas et al. (2011); Wentz et al. (2015))
ClimZoo_SEAPODYM	Climatological monthly mean zooplankton biomass expressed in carbon (g C m^{-2}) from SEAPODYM (Lehodey et al. (2008); Lehodey et al. (2015)), provided by E.U. Copernicus Marine Service. doi: 10.48670/moi-00020
Depth	Depth (m) of the seafloor, from SRTM30_PLUS (Becker et al. (2009))
DistTo125m	Distance (km) to the 125m isobath, derived from SRTM30_PLUS (Becker et al. (2009))
DistTo300m	Distance (km) to the 300m isobath, derived from SRTM30_PLUS (Becker et al. (2009))
Slope	Slope (percent rise) of the seafloor, derived from SRTM30_PLUS (Becker et al. (2009))

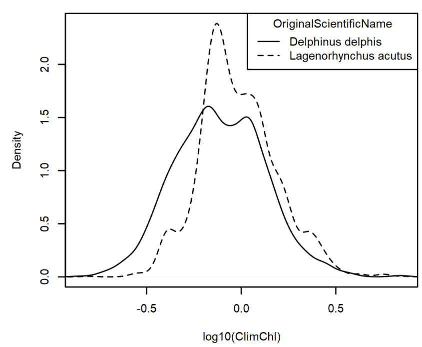

(a) Chlorophyll a concentration (mg m^{-3})

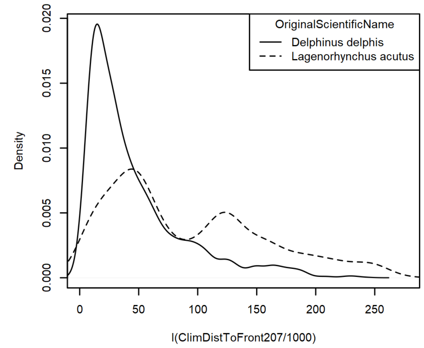

(b) Climatological distance to SST front (km)

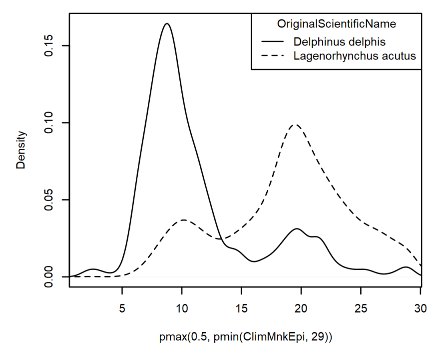

(c) Climatological epipelagic micronekton biomass (g m^{-2})

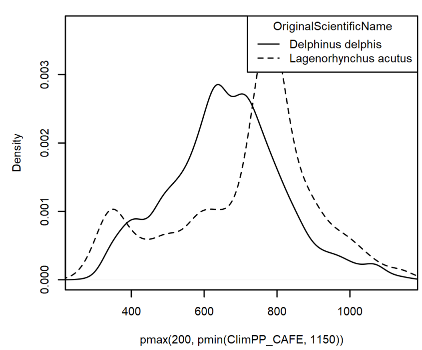

(d) Climatological net primary productivity (mg C m^{-2} day^{-1}) (CAFE model)

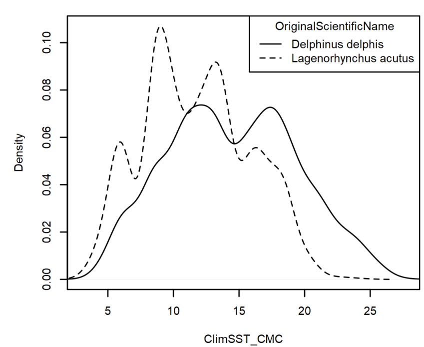

(e) Climatological sea surface temperature (°C)

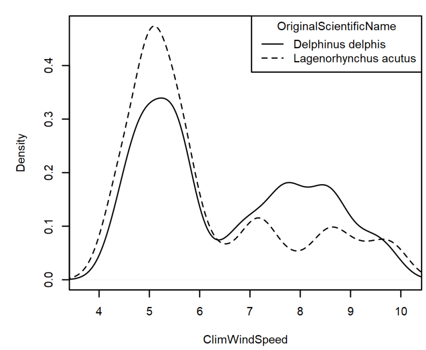

(f) Climatological wind speed (m s^{-1})

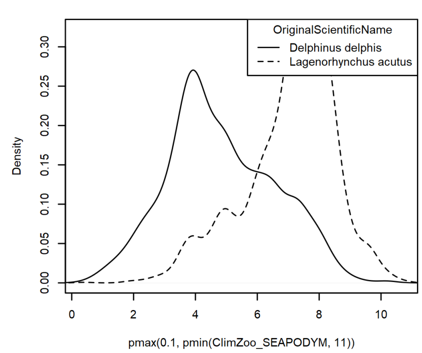

(g) Climatological zooplankton biomass (g C m^{-2})

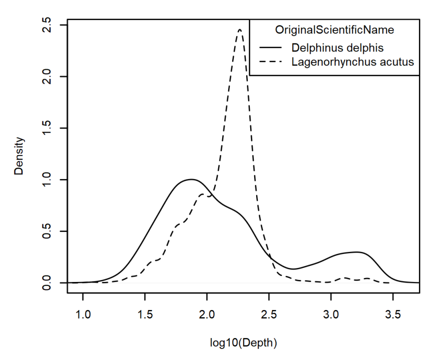

(h) Seafloor depth (m)

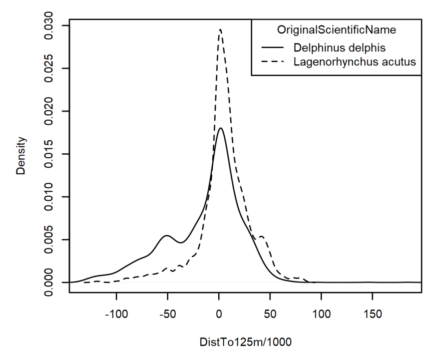

(i) Distance to 125m isobath (km)

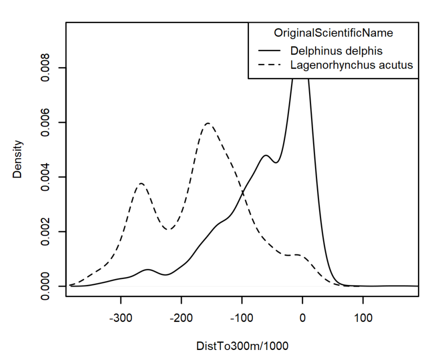

(j) Distance to 300m isobath (km)

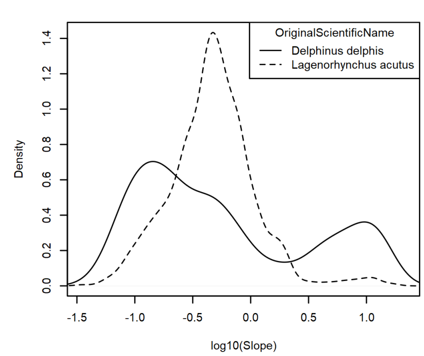

(k) Seafloor slope (percent rise)

Figure 3: Density histograms showing the per-species distribution of each covariate in the ambiguous sighting classification model. When a covariate exhibits a substantially different distribution for each species, it is a good candidate for differentiating the species. Transforms and other treatments are indicated in axis labels. *log10* indicates the covariate was $\log_{10}$ transformed. *pmax* and *pmin* indicate the covariate's minimum and maximum values, respectively, were Winsorized to the values shown. */1000* indicates meters were transformed to kilometers for interpretation convenience.

2.2 Classifications Performed

Table 5: Summary of the definitive sightings used to train the classification model, the ambiguous sightings to which the model was applied, and their resulting classifications. To increase the range of sampling of the classification model's covariates, the training data may have included additional surveys not considered for the density model, as well as transects from outside the spatial and temporal extents of the density model. Only on-effort sightings were used.

		Definitive			Classified	
Institution	Program	D. delphis	L. acutus	Ambiguous	D. delphis	L. acutus
Aerial Surveys						
HDR	Navy Norfolk Canyon	84	0	0	0	0
NEAq	CNM	21	0	0	0	0
NEAq	MMS-WEA	61	8	3	3	0
NEAq	NLPSC	44	6	5	4	1
NEFSC	AMAPPS	742	225	165	103	62
NEFSC	NARWSS	372	1,536	1,472	325	1,147
NEFSC	Pre-AMAPPS	302	207	9	7	2
NJDEP	NJEBS	5	0	0	0	0
NYS-DEC/TT	NYBWM	67	0	0	0	0
SEFSC	AMAPPS	300	0	0	0	0
SEFSC	MATS	3	0	0	0	0
UNCW	MidA Bottlenose	5	0	0	0	0
UNCW	Navy Cape Hatteras	30	0	0	0	0
UNCW	Navy Norfolk Canyon	51	0	0	0	0
UNCW	Navy Onslow Bay	1	0	0	0	0
UNCW	SEUS NARW EWS	26	0	0	0	0
VAMSC	MD DNR WEA	44	0	0	0	0
VAMSC	Navy VACAPES	9	0	0	0	0
VAMSC	VA CZM WEA	25	0	0	0	0
	Total	**2,192**	**1,982**	**1,654**	**442**	**1,212**
Shipboard Surveys						
MCR	SOTW Visual	9	1	0	0	0
NEFSC	AMAPPS	368	24	2	2	0
NEFSC	Pre-AMAPPS	173	65	0	0	0
NJDEP	NJEBS	19	0	0	0	0
SEFSC	AMAPPS	2	0	0	0	0
SEFSC	Pre-AMAPPS	42	0	0	0	0
	Total	**613**	**90**	**2**	**2**	**0**
	Grand Total	**2,805**	**2,072**	**1,656**	**444**	**1,212**

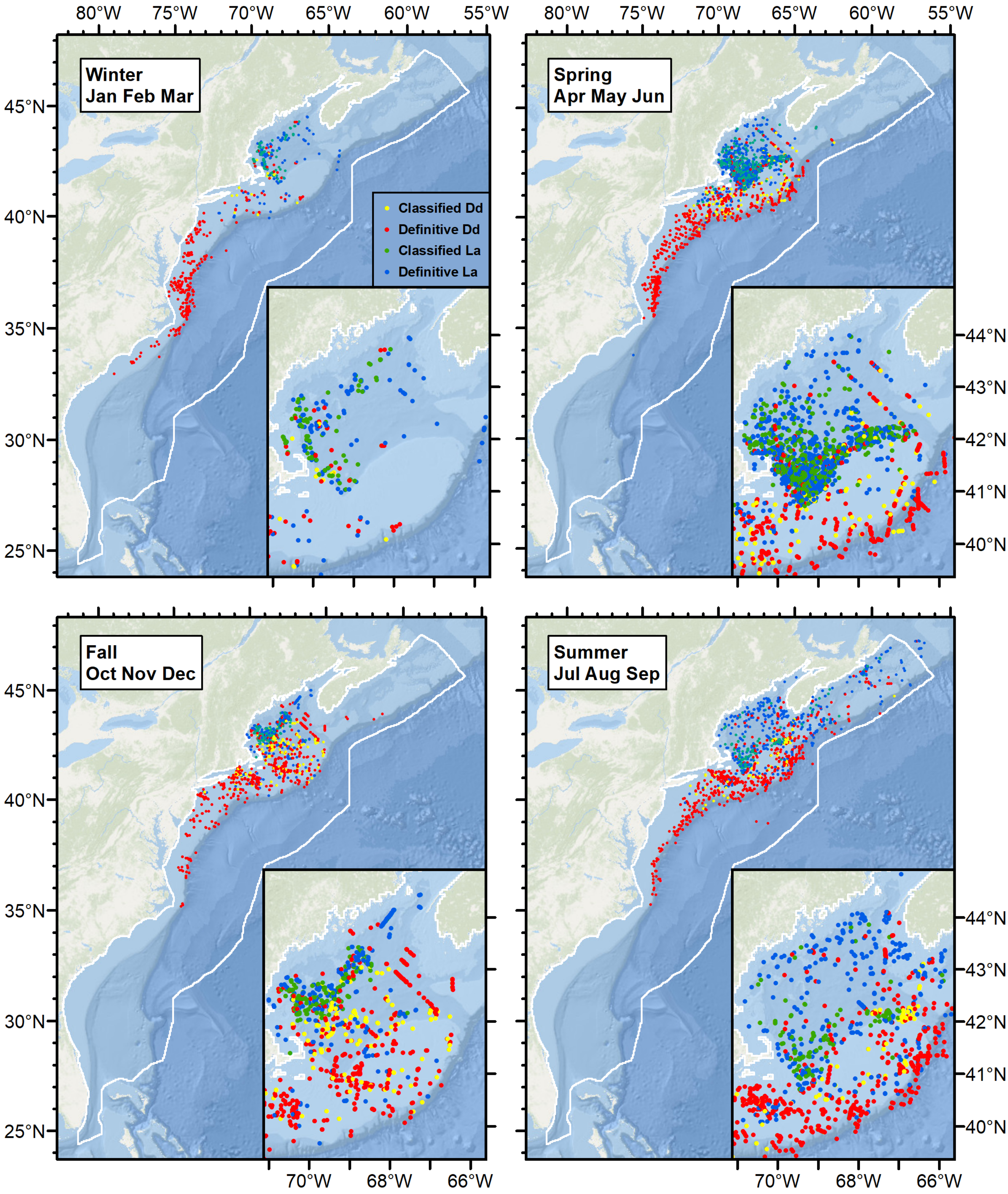

Figure 4: Definitive sightings used to train the model and ambiguous sightings classified by the model.

3 Detection Functions

3.1 With a Taxonomic Covariate

We fitted the detection functions in this section to pools of species with similar detectability characteristics and used the taxonomic identification as a covariate (ScientificName) to account for differences between them. We consulted the literature and observer teams to determine appropriate poolings. We usually employed this approach to boost the counts of observations in the detection functions, which increased the chance that other covariates such as Beaufort sea state could be used to account for differences in observing conditions. When defining the taxonomic covariate, we sometimes had too few observations of species to allocate each of them their own level of the covariate and had to group them together, again consulting the literature and observers for advice on species similarity. Also, when species were observed frequently enough to be allocated their own levels but statistical tests indicated no significant difference between the levels, we usually grouped them together into a single level.

3.1.1 Aerial Surveys

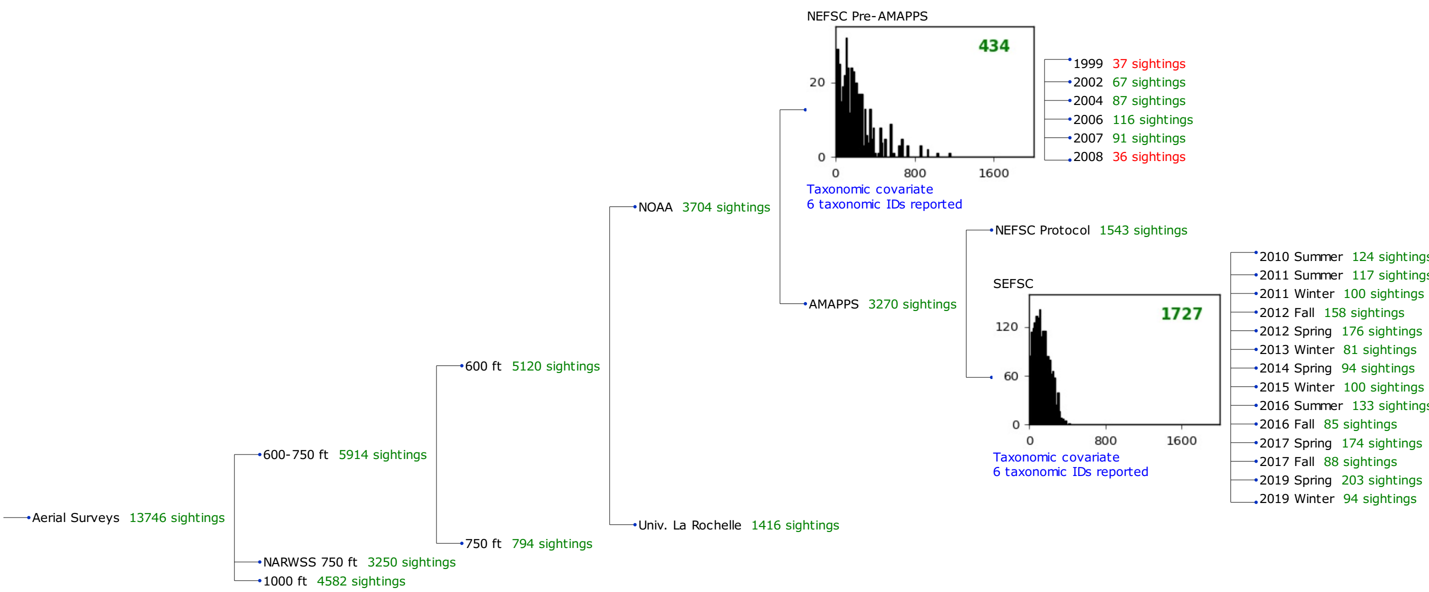

Figure 5: Detection hierarchy for aerial surveys, showing how they were pooled during detectability modeling, for detection functions that pooled multiple taxa and used used a taxonomic covariate to account for differences between them. Each histogram represents a detection function and summarizes the perpendicular distances of observations that were pooled to fit it, prior to truncation. Observation counts, also prior to truncation, are shown in green when they met the recommendation of Buckland et al. (2001) that detection functions utilize at least 60 sightings, and red otherwise. For rare taxa, it was not always possible to meet this recommendation, yielding higher statistical uncertainty. During the spatial modeling stage of the analysis, effective strip widths were computed for each survey using the closest detection function above it in the hierarchy (i.e. moving from right to left in the figure). Surveys that do not have a detection function above them in this figure were either addressed by a detection function presented in a different section of this report, or were omitted from the analysis.

3.1.1.1 NEFSC Pre-AMAPPS

After right-truncating observations greater than 600 m, we fitted the detection function to the 413 observations that remained (Table 6). The selected detection function (Figure 6) used a hazard rate key function with Beaufort (Figure 7) and ScientificName (Figure 8) as covariates.

Table 6: Observations used to fit the NEFSC Pre-AMAPPS detection function.

ScientificName	n
Delphinus, Lagenodelphis, Stenella	239
Lagenorhynchus	128
Tursiops, Steno	46
Total	**413**

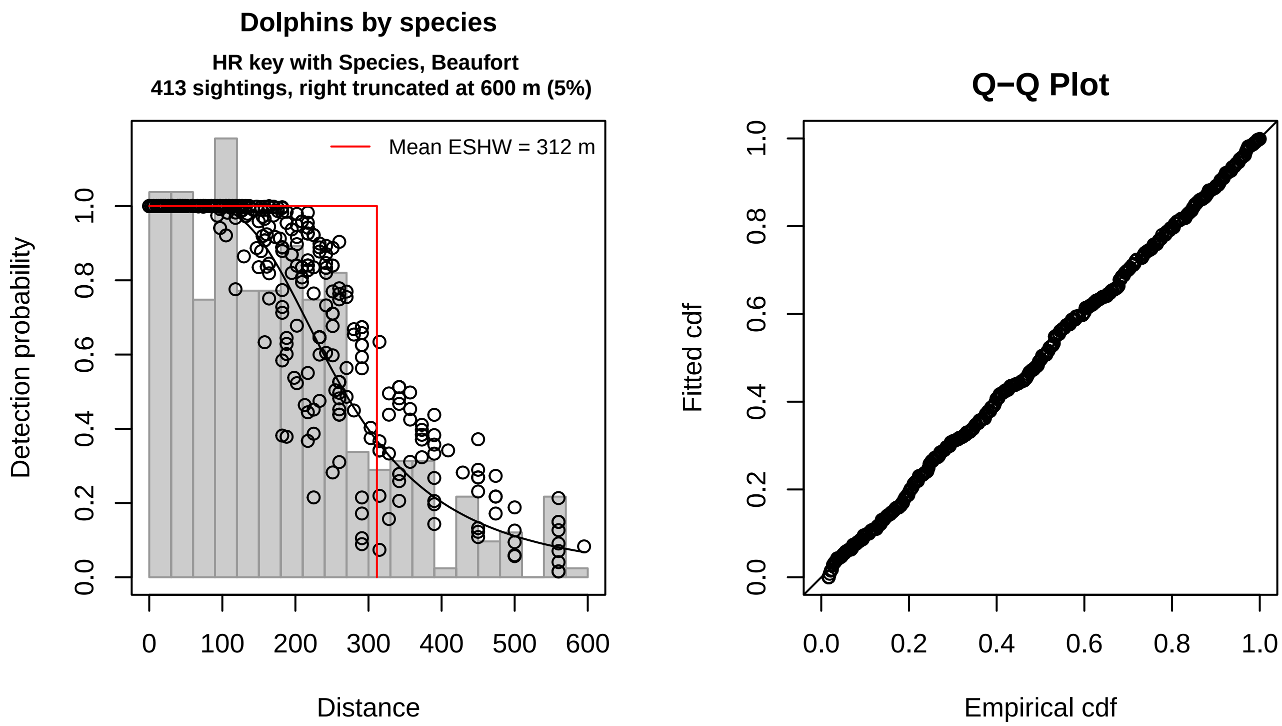

Figure 6: NEFSC Pre-AMAPPS detection function and Q-Q plot showing its goodness of fit.

Statistical output for this detection function:

```
Summary for ds object
Number of observations :  413
Distance range         :  0  -  600
AIC                    :  5043.994

Detection function:
 Hazard-rate key function

Detection function parameters
Scale coefficient(s):
                                 estimate         se
(Intercept)                     5.3188665 0.15126469
ScientificNameLagenorhynchus   -0.1872175 0.11165678
ScientificNameTursiops, Steno -0.5457529 0.14785313
Beaufort                        0.1451869 0.05844944

Shape coefficient(s):
            estimate        se
(Intercept) 1.107015 0.1176733

                       Estimate          SE          CV
```

```
Average p              0.4982478  0.02373666 0.04764026
N in covered region 828.9047438 49.28440455 0.05945726

Distance sampling Cramer-von Mises test (unweighted)
Test statistic = 0.023324  p = 0.992716
```

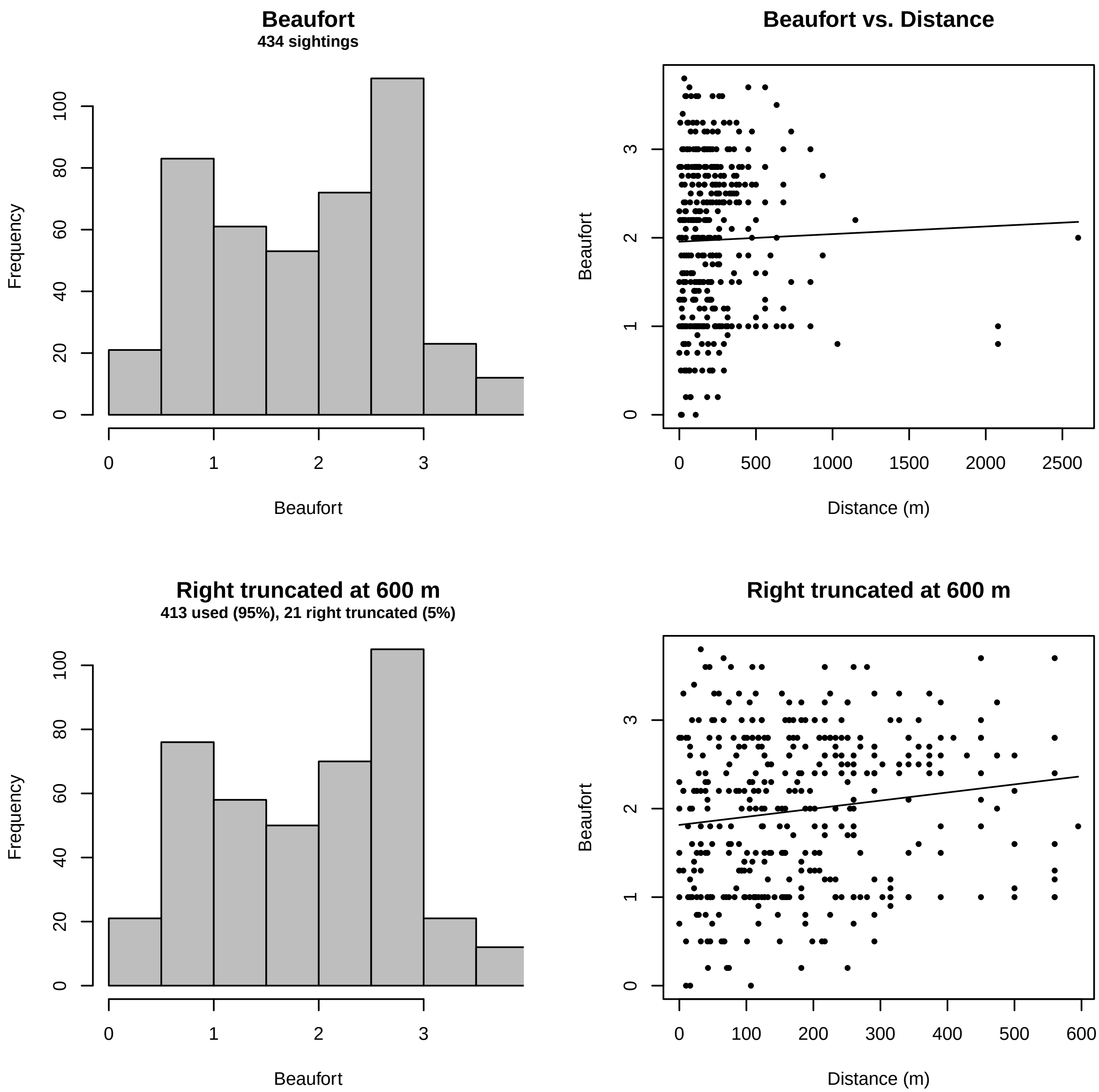

Figure 7: Distribution of the Beaufort covariate before (top row) and after (bottom row) observations were truncated to fit the NEFSC Pre-AMAPPS detection function.

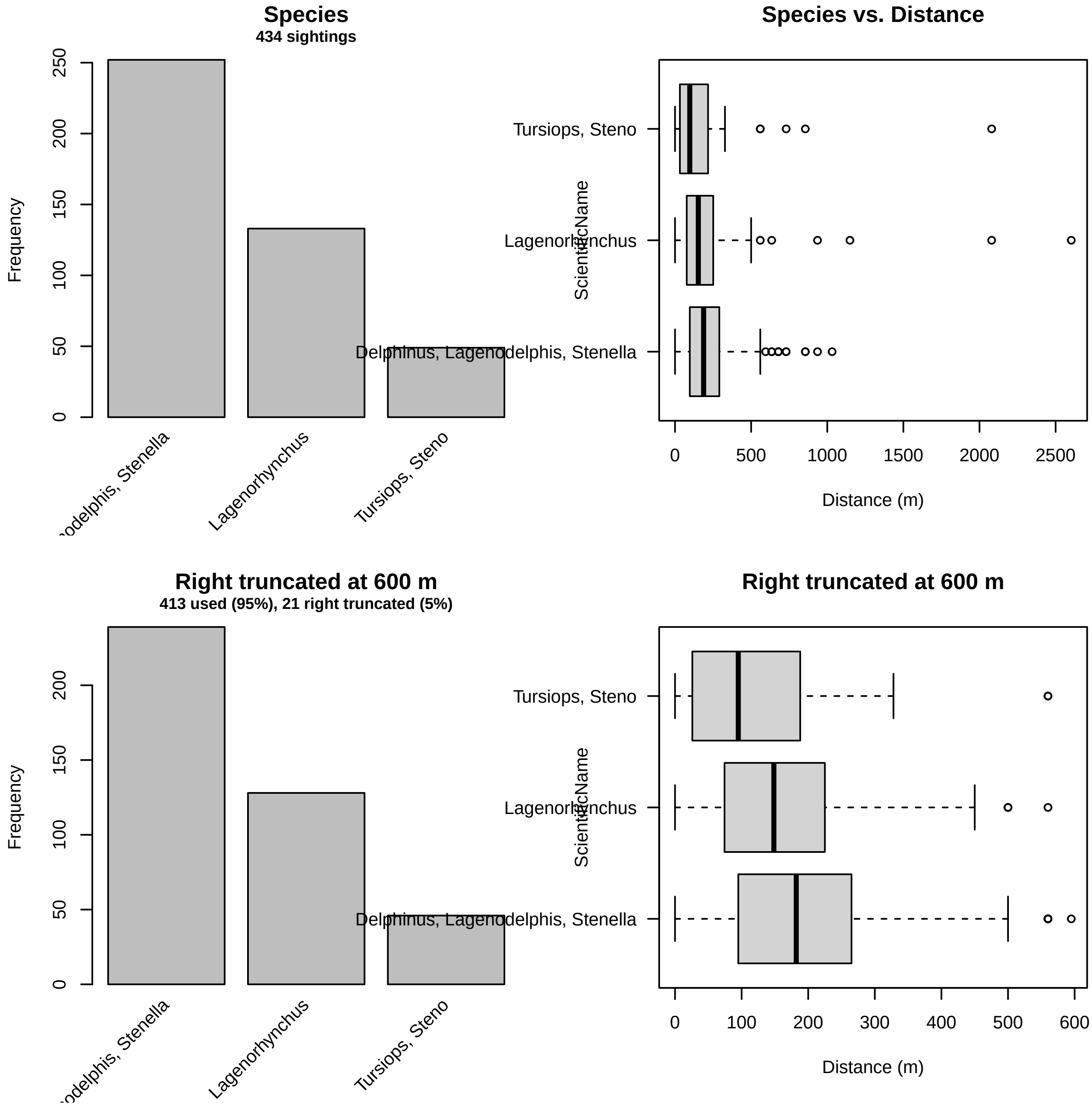

Figure 8: Distribution of the ScientificName covariate before (top row) and after (bottom row) observations were truncated to fit the NEFSC Pre-AMAPPS detection function.

3.1.1.2 SEFSC AMAPPS

After right-truncating observations greater than 325 m and left-truncating observations less than 15 m (Figure 10), we fitted the detection function to the 1628 observations that remained (Table 7). The selected detection function (Figure 9) used a hazard rate key function with Beaufort (Figure 11), ScientificName (Figure 12) and Season (Figure 13) as covariates.

Table 7: Observations used to fit the SEFSC AMAPPS detection function.

ScientificName	n
Delphinus, Tursiops, Lagenorhynchus, Steno	1422
Stenella, Lagenodelphis	206
Total	**1628**

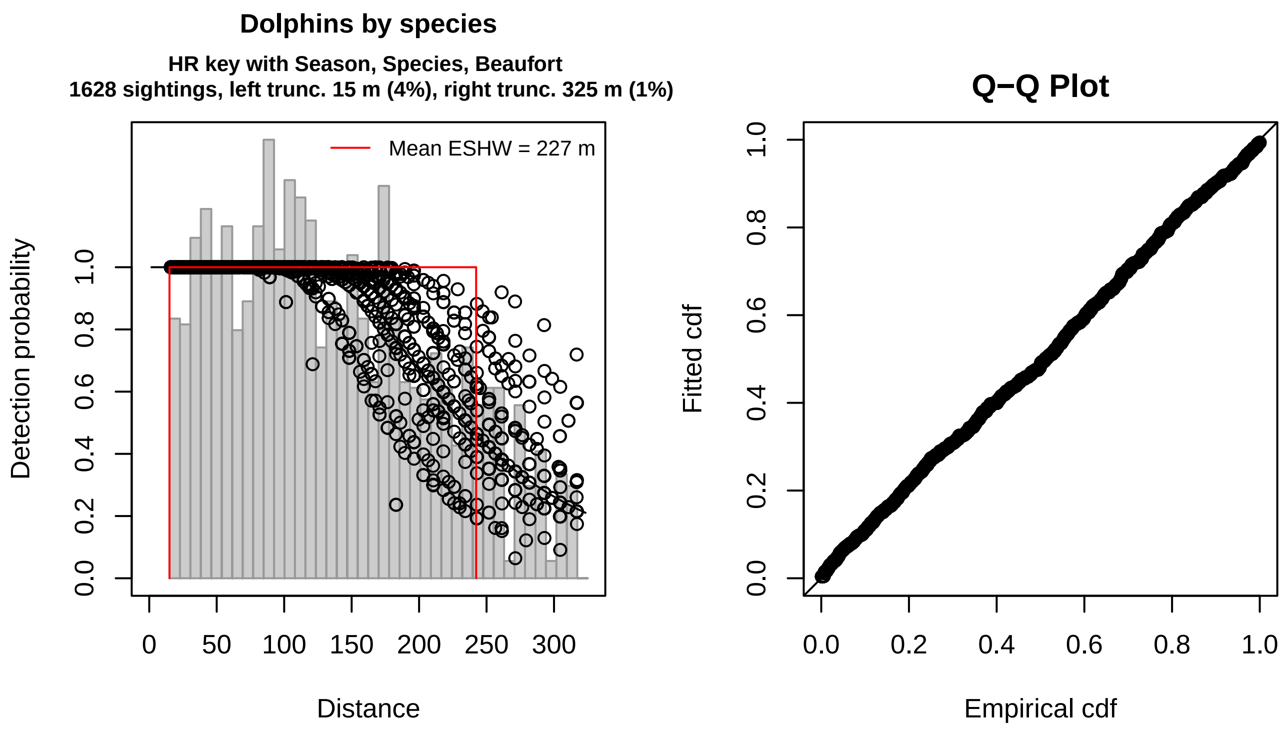

Figure 9: SEFSC AMAPPS detection function and Q-Q plot showing its goodness of fit.

Statistical output for this detection function:

```
Summary for ds object
Number of observations :  1628
Distance range         :  15  -  325
AIC                    :  18351.39

Detection function:
 Hazard-rate key function

Detection function parameters
Scale coefficient(s):
                                      estimate         se
(Intercept)                          5.4780735 0.08251975
SeasonSummer                         0.1269645 0.06172358
SeasonWinter                        -0.2356803 0.06102237
ScientificNameStenella, Lagenodelphis  0.2204074 0.08699872
Beaufort2                           -0.1192230 0.08713320
Beaufort3                           -0.1846083 0.08971655
Beaufort4                           -0.4027356 0.12330363

Shape coefficient(s):
            estimate        se
(Intercept) 1.266688 0.1150367

                       Estimate          SE         CV
Average p              0.720161  0.01522909 0.02114679
N in covered region 2260.605761 56.60731047 0.02504077

Distance sampling Cramer-von Mises test (unweighted)
Test statistic = 0.138923  p = 0.425167
```

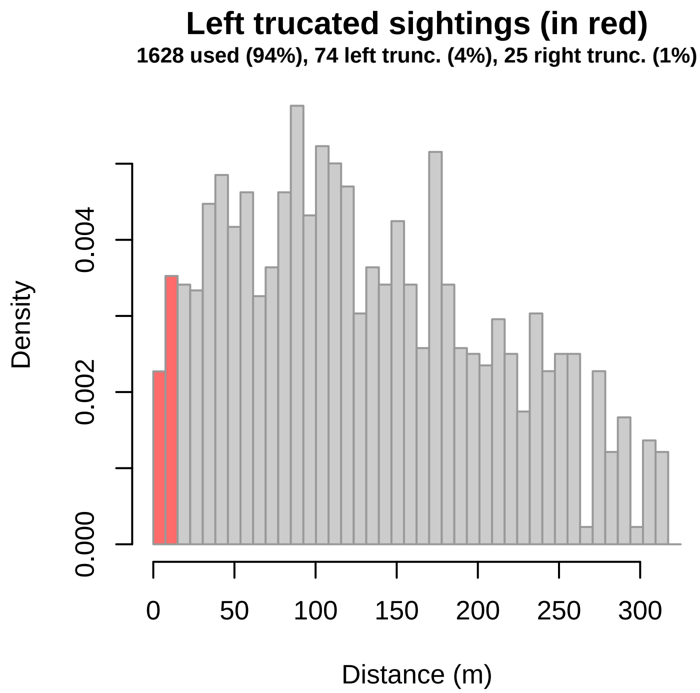

Figure 10: Density histogram of observations used to fit the SEFSC AMAPPS detection function, with the left-most bar showing observations at distances less than 15 m, which were left-truncated and excluded from the analysis [Buckland et al. (2001)]. (This bar may be very short if there were very few left-truncated sightings, or very narrow if the left truncation distance was very small; in either case it may not appear red.)

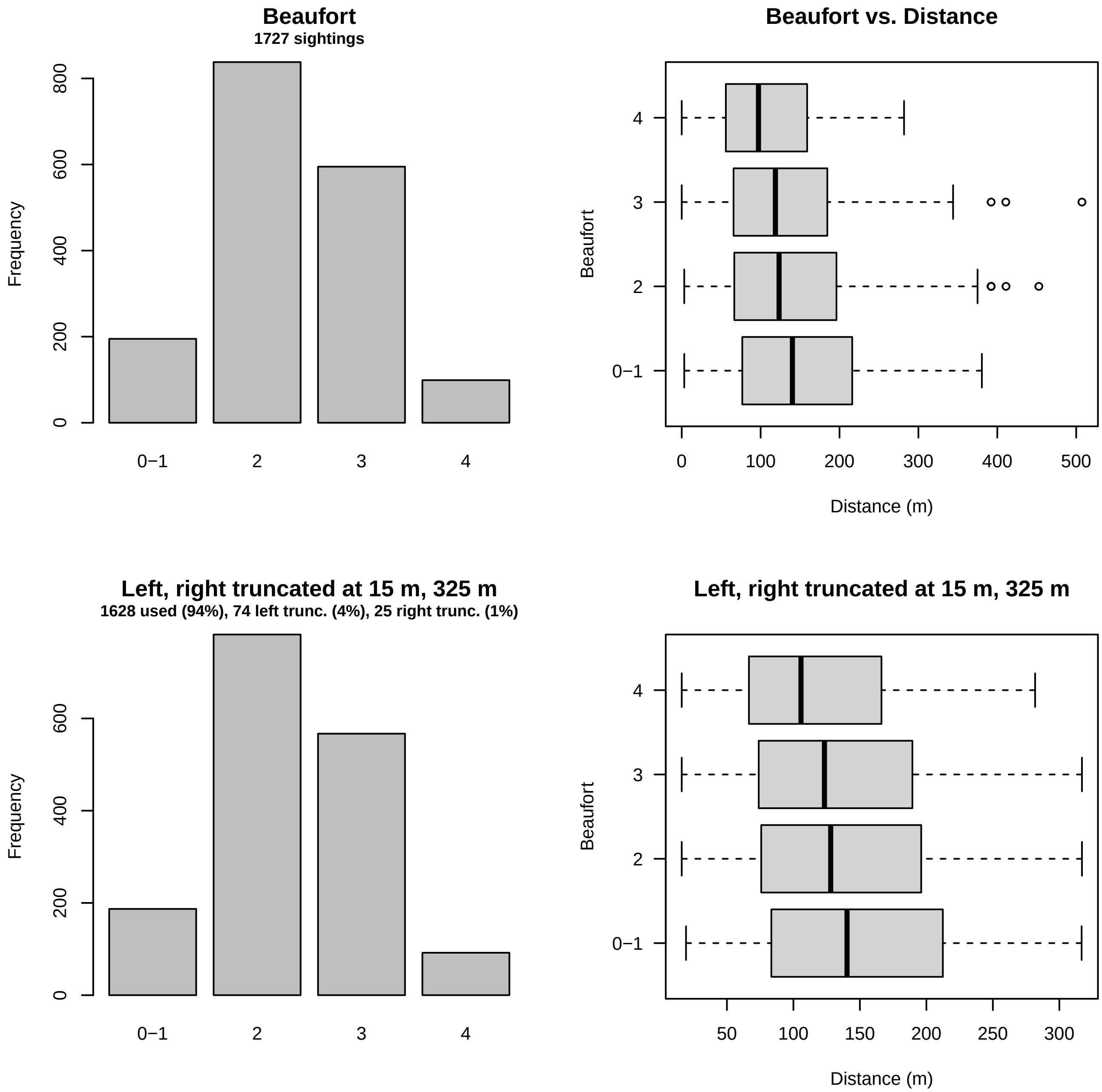

Figure 11: Distribution of the Beaufort covariate before (top row) and after (bottom row) observations were truncated to fit the SEFSC AMAPPS detection function.

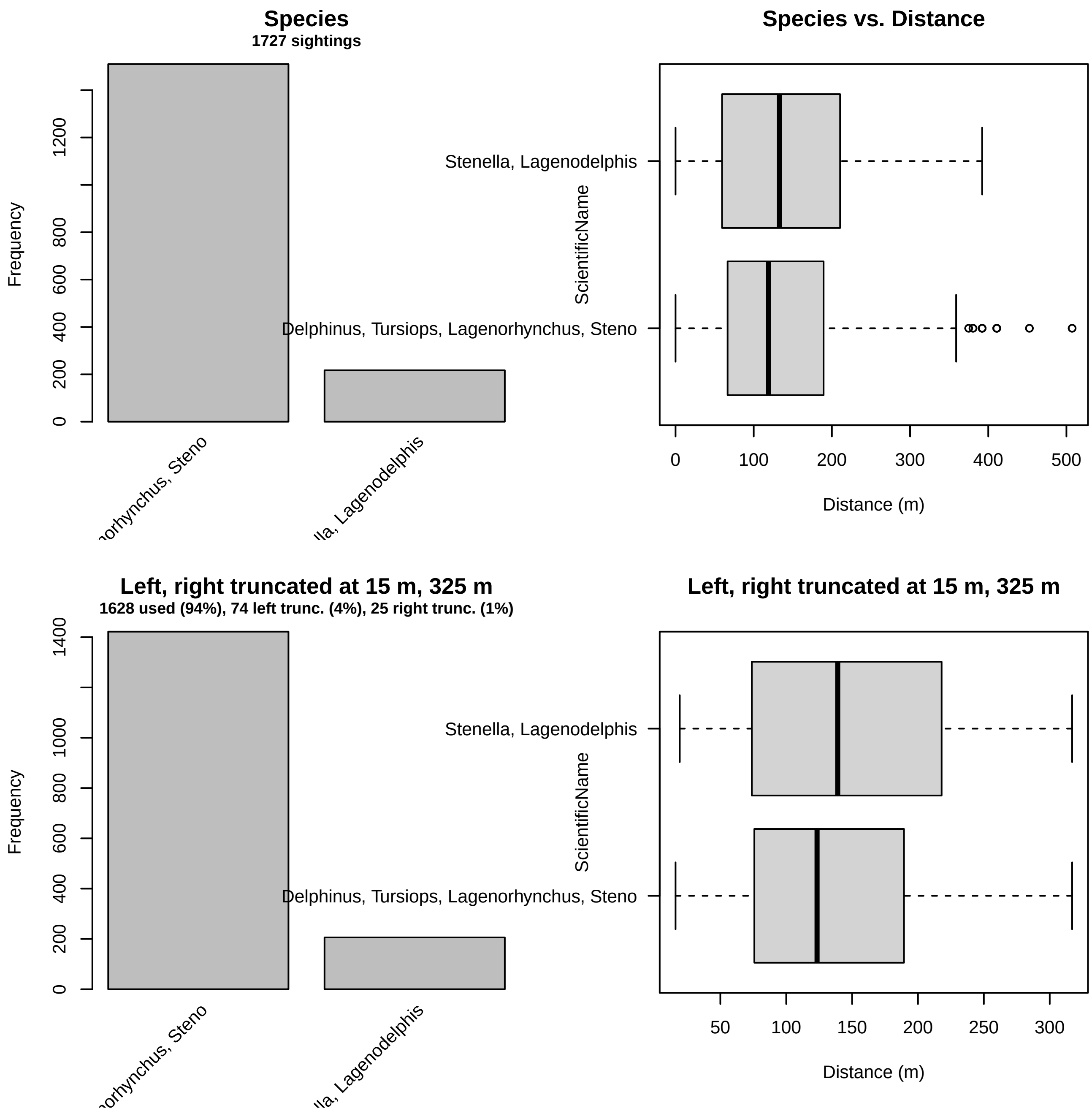

Figure 12: Distribution of the ScientificName covariate before (top row) and after (bottom row) observations were truncated to fit the SEFSC AMAPPS detection function.

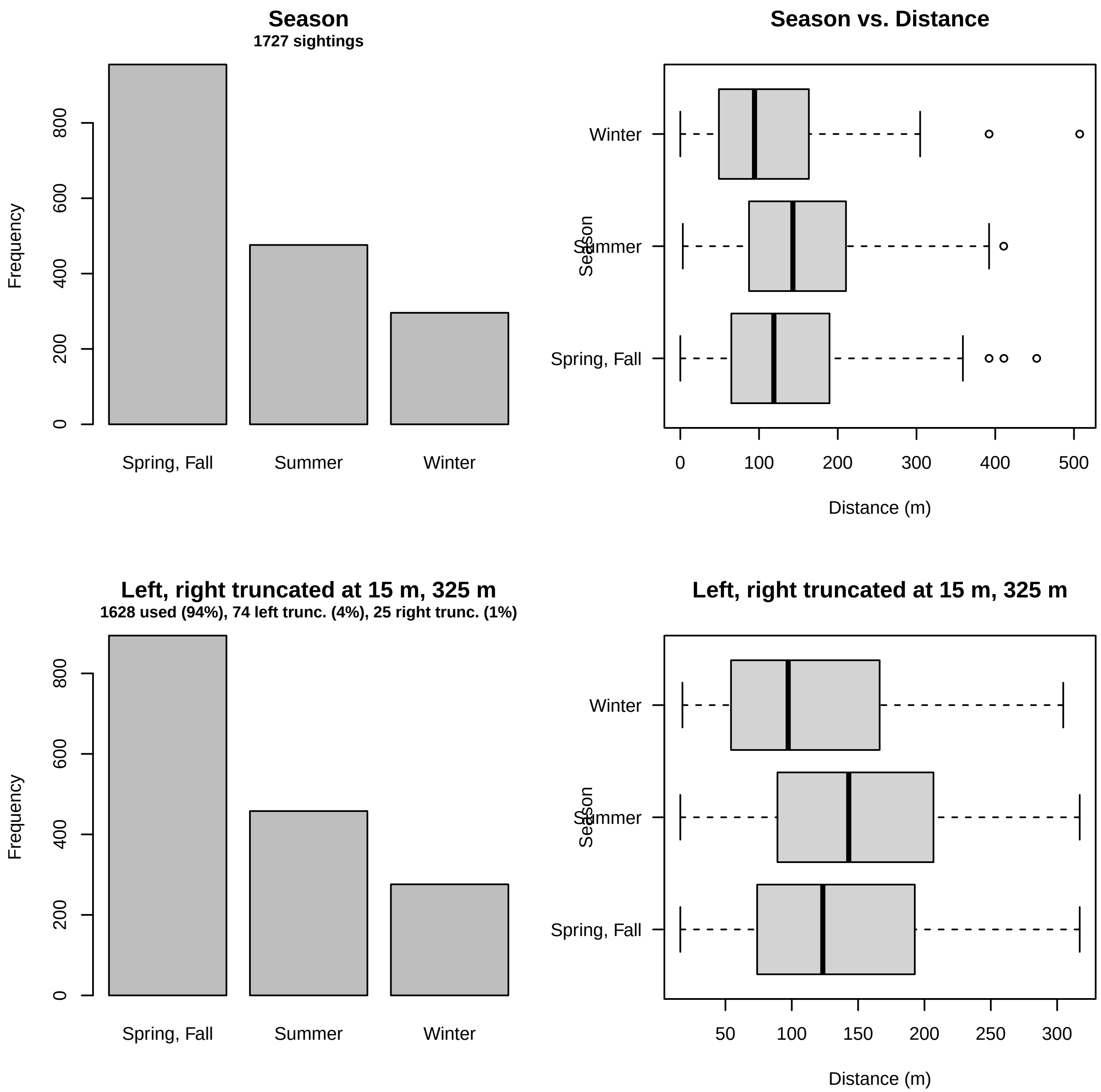

Figure 13: Distribution of the Season covariate before (top row) and after (bottom row) observations were truncated to fit the SEFSC AMAPPS detection function.

3.1.2 Shipboard Surveys

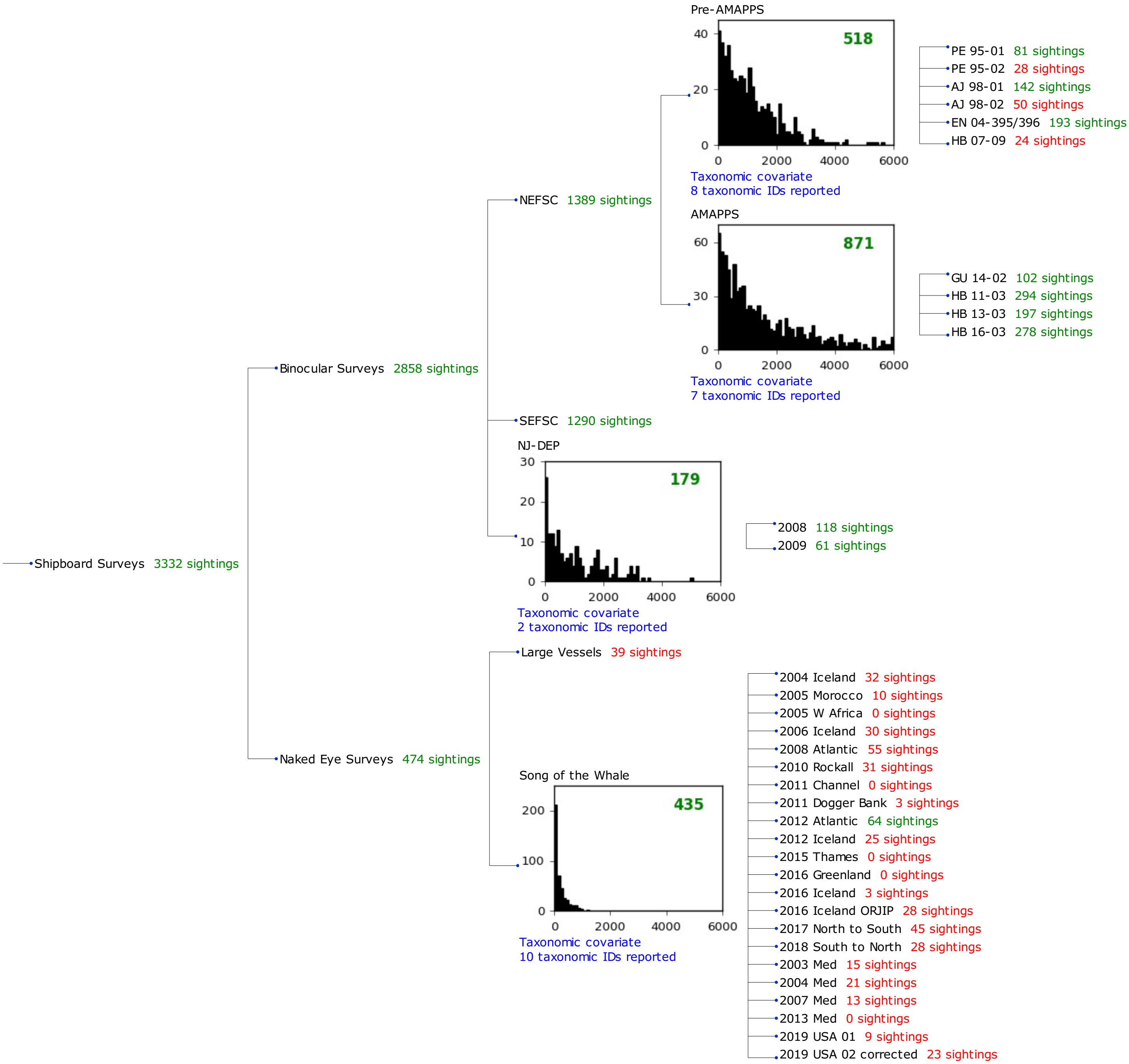

Figure 14: Detection hierarchy for shipboard surveys, showing how they were pooled during detectability modeling, for detection functions that pooled multiple taxa and used used a taxonomic covariate to account for differences between them. Each histogram represents a detection function and summarizes the perpendicular distances of observations that were pooled to fit it, prior to truncation. Observation counts, also prior to truncation, are shown in green when they met the recommendation of Buckland et al. (2001) that detection functions utilize at least 60 sightings, and red otherwise. For rare taxa, it was not always possible to meet this recommendation, yielding higher statistical uncertainty. During the spatial modeling stage of the analysis, effective strip widths were computed for each survey using the closest detection function above it in the hierarchy (i.e. moving from right to left in the figure). Surveys that do not have a detection function above them in this figure were either addressed by a detection function presented in a different section of this report, or were omitted from the analysis.

3.1.2.1 NEFSC Pre-AMAPPS

After right-truncating observations greater than 4000 m, we fitted the detection function to the 508 observations that remained (Table 8). The selected detection function (Figure 15) used a hazard rate key function with Beaufort (Figure 16), ScientificName (Figure 17) and VesselName (Figure 18) as covariates.

Table 8: Observations used to fit the NEFSC Pre-AMAPPS detection function.

ScientificName	n
Delphinus, Lagenorhynchus, Tursiops, Steno	365
Other Stenella, Lagenodelphis	130
Stenella frontalis	13
Total	**508**

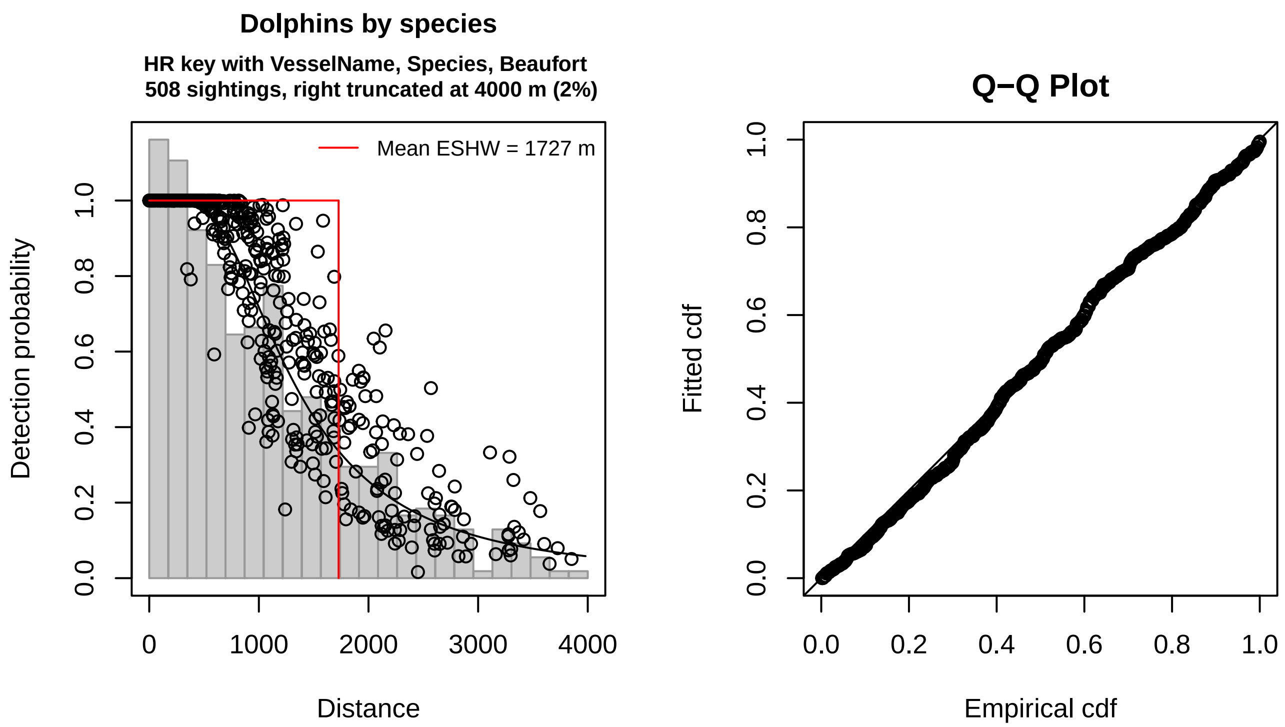

Figure 15: NEFSC Pre-AMAPPS detection function and Q-Q plot showing its goodness of fit.

Statistical output for this detection function:

```
Summary for ds object
Number of observations :  508
Distance range         :  0  -  4000
AIC                    :  8058.614

Detection function:
 Hazard-rate key function

Detection function parameters
Scale coefficient(s):
                                              estimate        se
(Intercept)                                  7.3979634 0.1986065
VesselNameEndeavor, Bigelow                  0.2529041 0.1095209
ScientificNameOther Stenella, Lagenodelphis  0.3555978 0.1258179
ScientificNameStenella frontalis            -0.8556981 0.3078540
```

```
Beaufort                                          -0.1897812 0.0694737

Shape coefficient(s):
             estimate        se
(Intercept) 0.8752144 0.1006522

                         Estimate          SE         CV
Average p               0.4071518  0.02118698 0.05203705
N in covered region 1247.6919609 78.15195776 0.06263722

Distance sampling Cramer-von Mises test (unweighted)
Test statistic = 0.120847  p = 0.492001
```

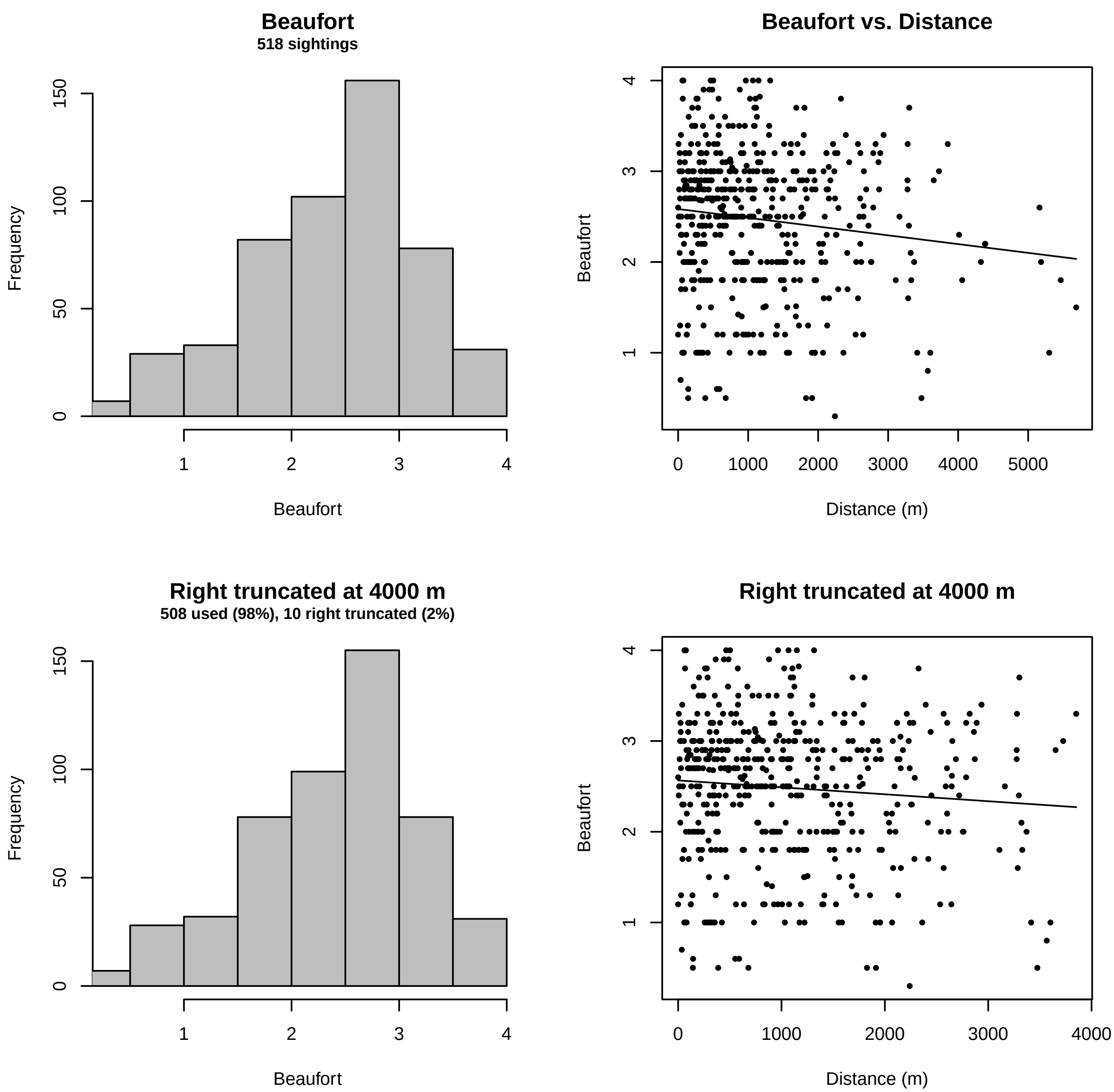

Figure 16: Distribution of the Beaufort covariate before (top row) and after (bottom row) observations were truncated to fit the NEFSC Pre-AMAPPS detection function.

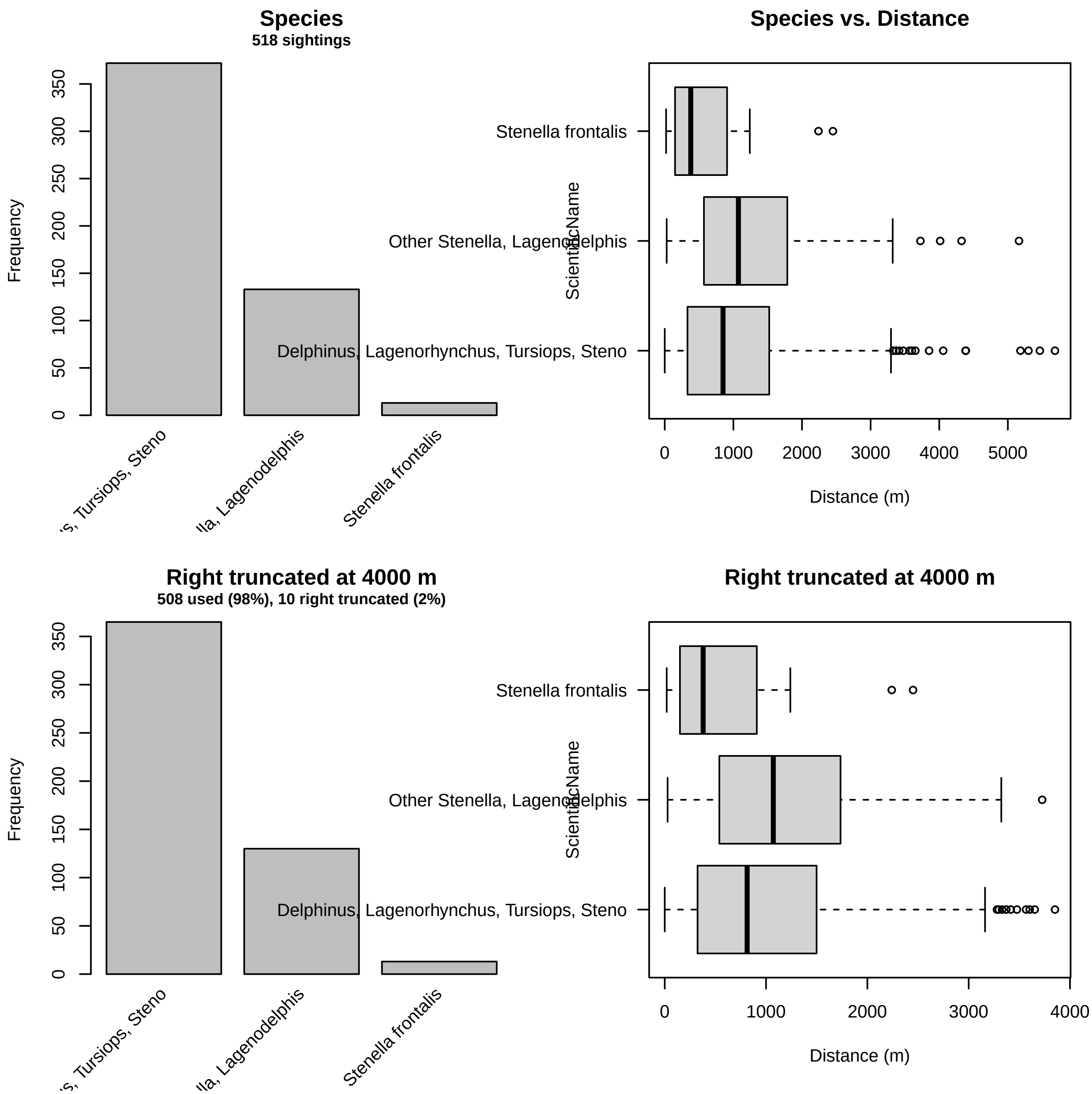

Figure 17: Distribution of the ScientificName covariate before (top row) and after (bottom row) observations were truncated to fit the NEFSC Pre-AMAPPS detection function.

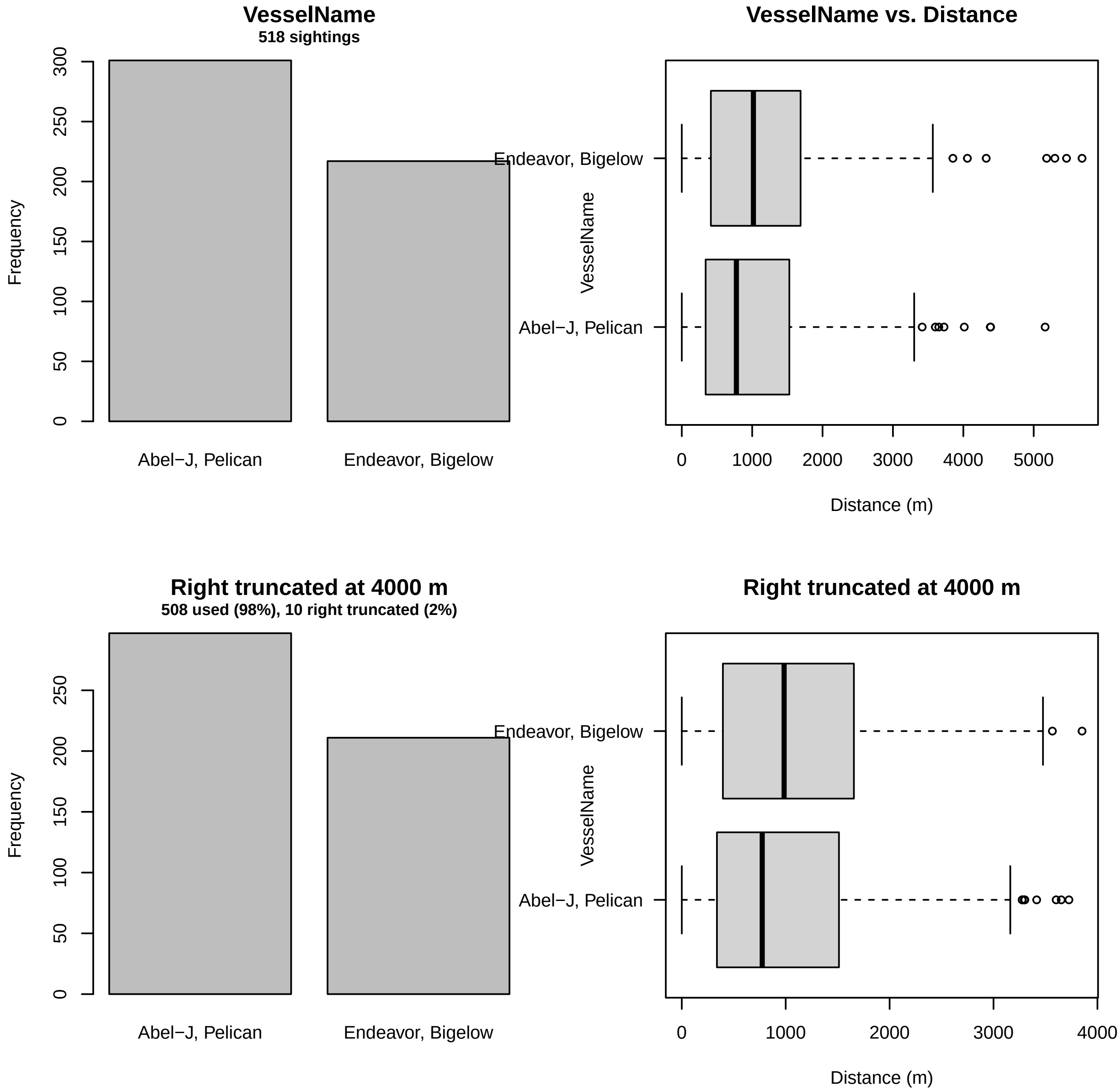

Figure 18: Distribution of the VesselName covariate before (top row) and after (bottom row) observations were truncated to fit the NEFSC Pre-AMAPPS detection function.

3.1.2.2 NEFSC AMAPPS

After right-truncating observations greater than 6000 m, we fitted the detection function to the 857 observations that remained (Table 9). The selected detection function (Figure 19) used a hazard rate key function with Beaufort (Figure 20) and ScientificName (Figure 21) as covariates.

Table 9: Observations used to fit the NEFSC AMAPPS detection function.

ScientificName	n
Delphinus, Lagenorhynchus	358
Other Stenella, Lagenodelphis	175
Stenella frontalis	53
Tursiops, Steno	271
Total	**857**

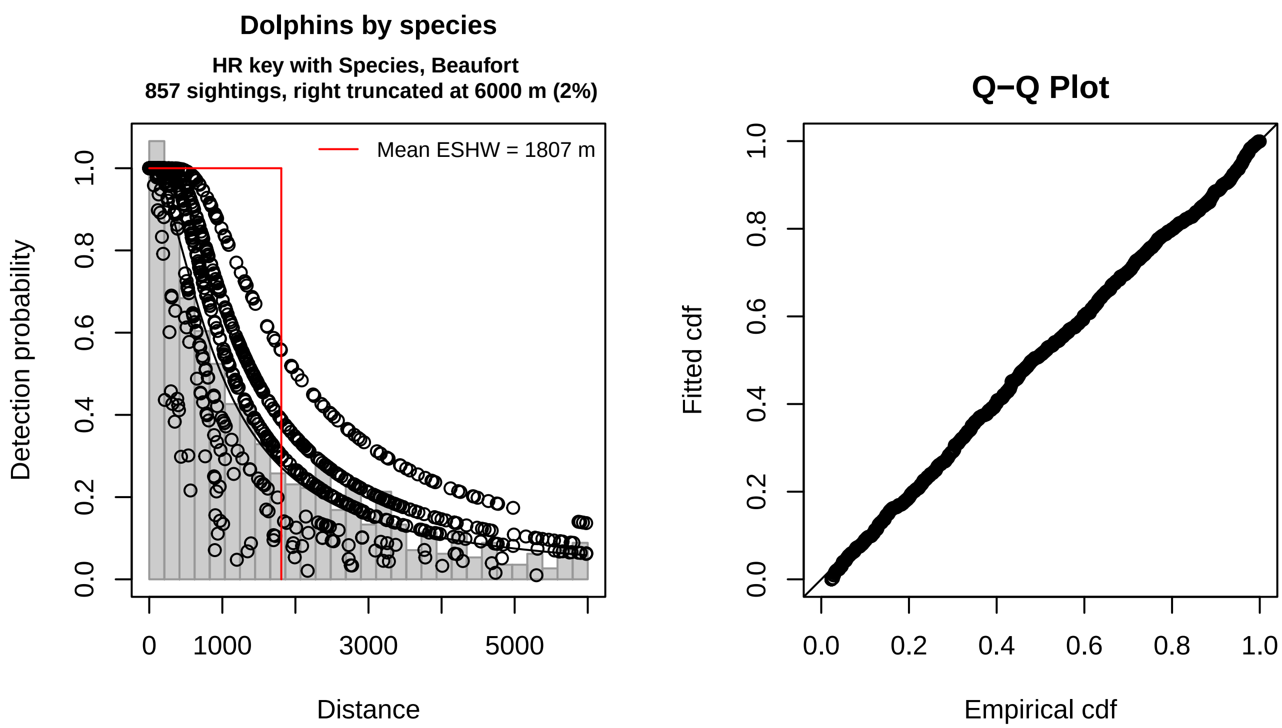

Figure 19: NEFSC AMAPPS detection function and Q-Q plot showing its goodness of fit.

Statistical output for this detection function:

```
Summary for ds object
Number of observations :  857
Distance range         :  0  -  6000
AIC                    :  14222.66

Detection function:
 Hazard-rate key function

Detection function parameters
Scale coefficient(s):
                                                estimate        se
(Intercept)                                    7.0022801 0.1342692
ScientificNameOther Stenella, Lagenodelphis    0.3515378 0.1854896
ScientificNameStenella frontalis              -0.5910499 0.3033455
ScientificNameTursiops, Steno                 -0.2176361 0.1602756
Beaufort3-4                                   -0.5842019 0.1839783
Beaufort4-5                                   -1.4374209 0.2667762

Shape coefficient(s):
            estimate        se
```

```
(Intercept) 0.356339 0.0663051

                        Estimate          SE         CV
Average p              0.2624967  0.01868208 0.07117073
N in covered region 3264.8026106 252.27662296 0.07727163

Distance sampling Cramer-von Mises test (unweighted)
Test statistic = 0.089267  p = 0.640081
```

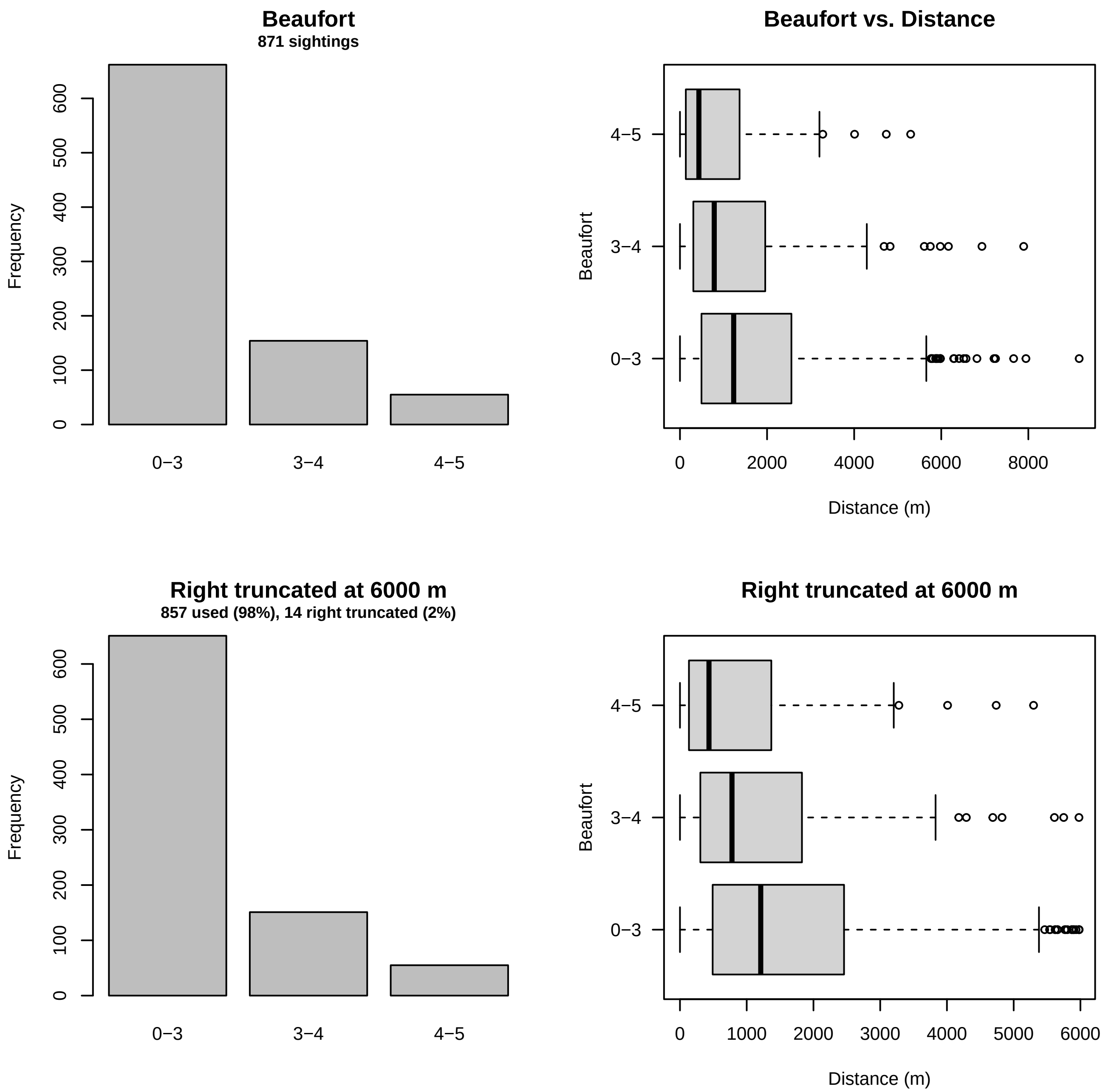

Figure 20: Distribution of the Beaufort covariate before (top row) and after (bottom row) observations were truncated to fit the NEFSC AMAPPS detection function.

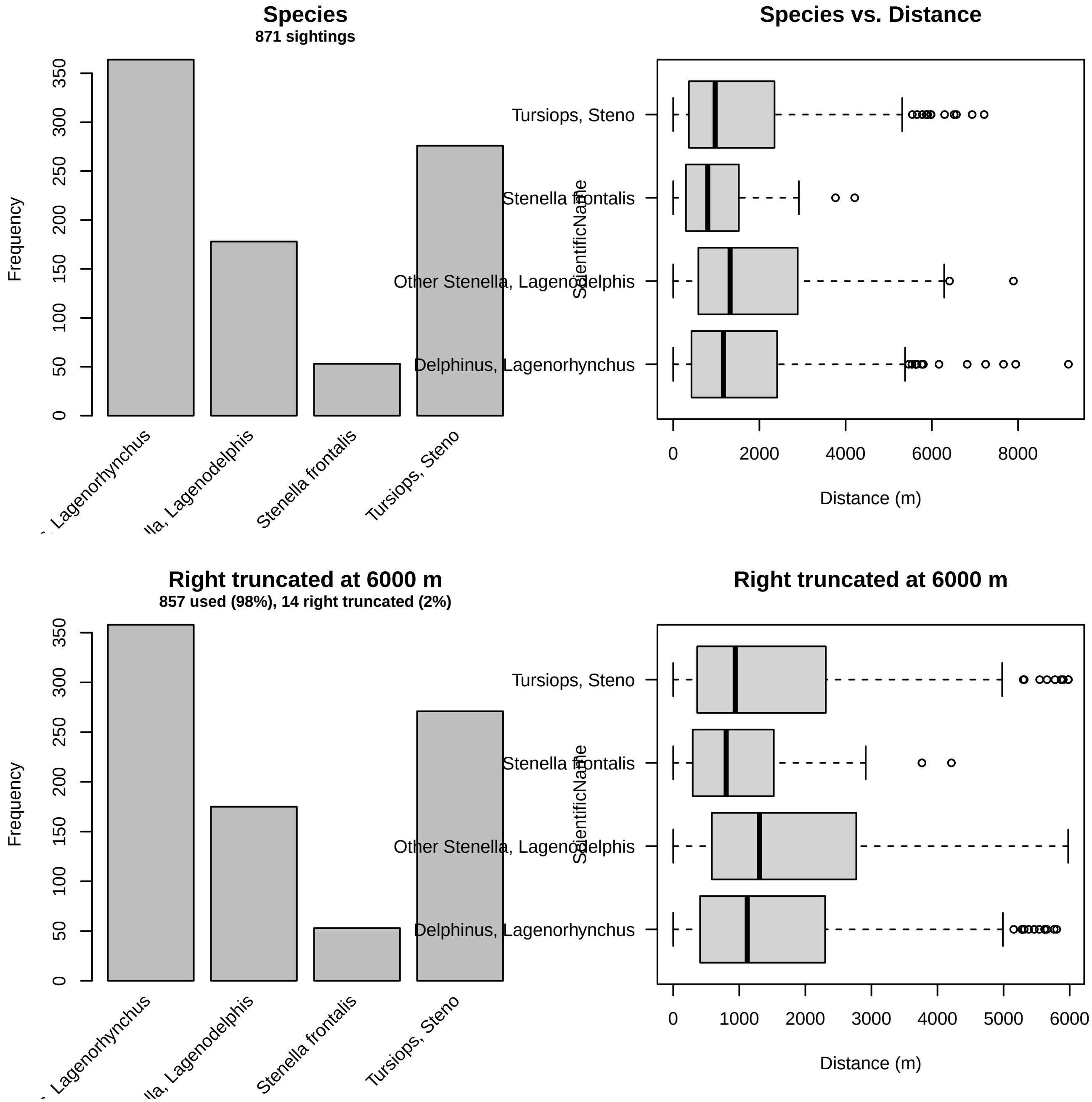

Figure 21: Distribution of the ScientificName covariate before (top row) and after (bottom row) observations were truncated to fit the NEFSC AMAPPS detection function.

3.1.2.3 NJ-DEP

After right-truncating observations greater than 3200 m, we fitted the detection function to the 175 observations that remained (Table 10). The selected detection function (Figure 22) used a hazard rate key function with ScientificName (Figure 23) as a covariate.

Table 10: Observations used to fit the NJ-DEP detection function.

ScientificName	n
Delphinus delphis	19
Tursiops truncatus	156
Total	**175**

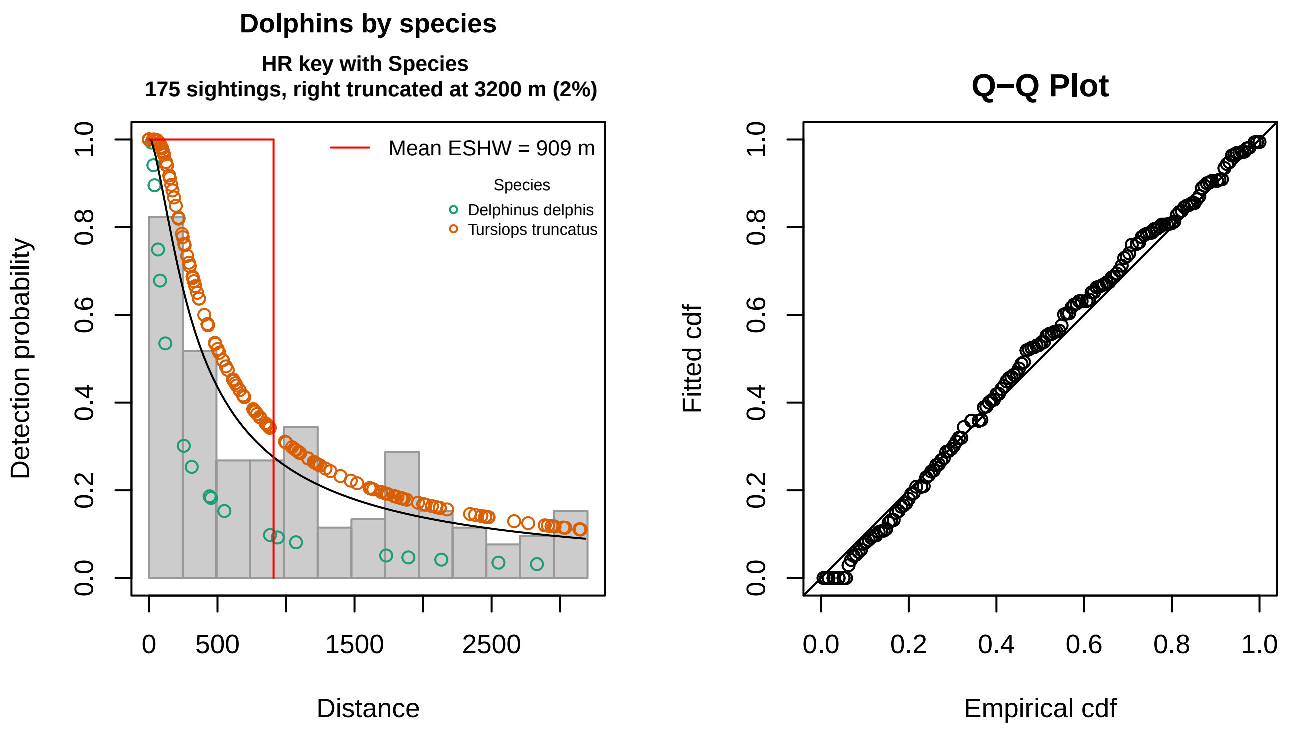

Figure 22: NJ-DEP detection function and Q-Q plot showing its goodness of fit.

Statistical output for this detection function:

```
Summary for ds object
Number of observations :  175
Distance range         :  0  -  3200
AIC                    :  2750.465

Detection function:
 Hazard-rate key function

Detection function parameters
Scale coefficient(s):
                                 estimate        se
(Intercept)                      4.512698 0.9620506
ScientificNameTursiops truncatus 1.400338 0.8543953

Shape coefficient(s):
            estimate        se
(Intercept)        0 0.1617129

                       Estimate           SE        CV
Average p             0.2578318   0.05821781 0.2257976
N in covered region 678.7370004 159.72027878 0.2353198

Distance sampling Cramer-von Mises test (unweighted)
Test statistic = 0.132198  p = 0.448683
```

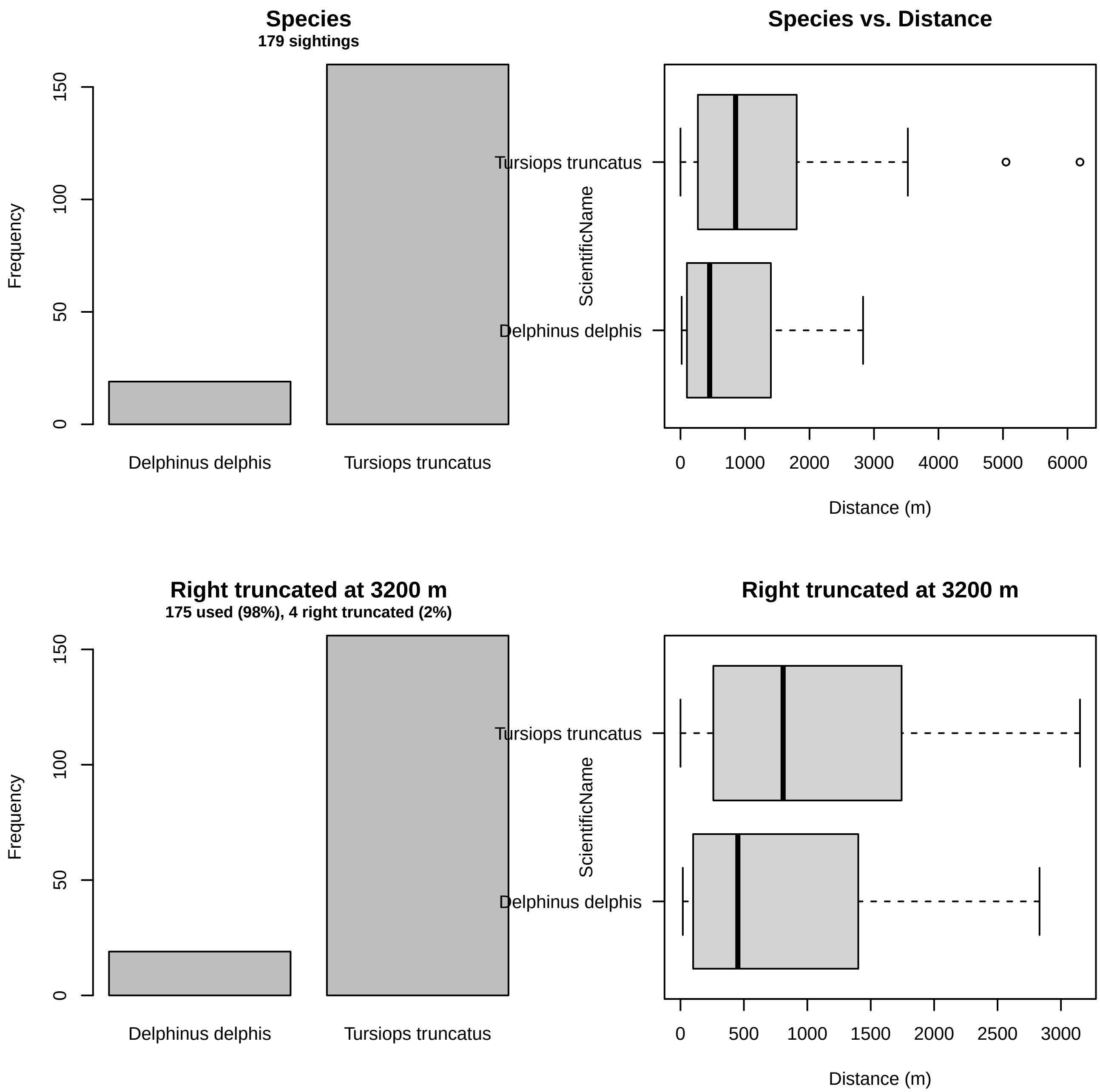

Figure 23: Distribution of the ScientificName covariate before (top row) and after (bottom row) observations were truncated to fit the NJ-DEP detection function.

3.1.2.4 Song of the Whale

After right-truncating observations greater than 700 m and left-truncating observations less than 1 m (Figure 25), we fitted the detection function to the 360 observations that remained (Table 11). The selected detection function (Figure 24) used a hazard rate key function with Beaufort (Figure 26), ScientificName (Figure 27) and Visibility (Figure 28) as covariates.

Table 11: Observations used to fit the Song of the Whale detection function.

ScientificName	n
All others	211
Delphinus	149
Total	**360**

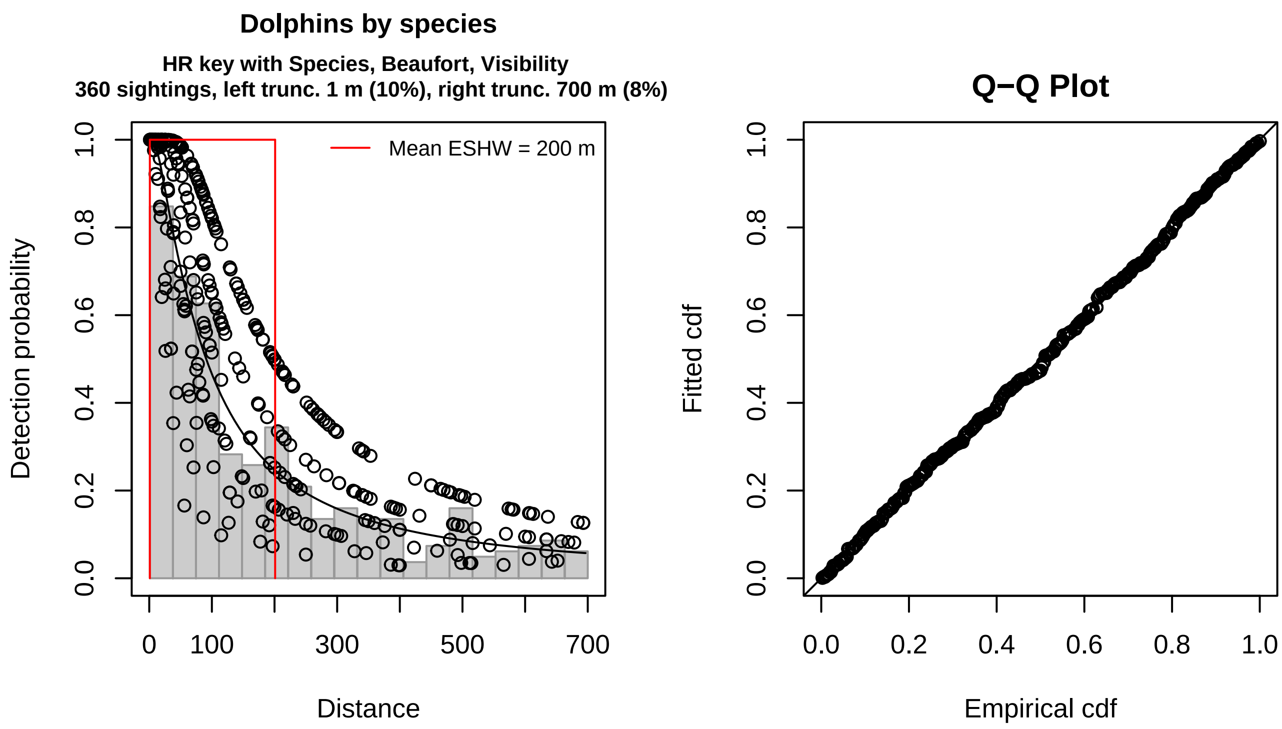

Figure 24: Song of the Whale detection function and Q-Q plot showing its goodness of fit.

Statistical output for this detection function:

```
Summary for ds object
Number of observations :  360
Distance range         :  1  -  700
AIC                    :  4434.06

Detection function:
 Hazard-rate key function

Detection function parameters
Scale coefficient(s):
                              estimate        se
(Intercept)                  5.0168382 0.2118228
ScientificNameDelphinus     -0.3746003 0.2526245
Beaufort3                   -0.6586604 0.2922112
Beaufort3.5-4               -1.3223280 0.3841776
VisibilityModerate (2-5nmi) -0.9687696 0.4363084

Shape coefficient(s):
             estimate         se
(Intercept) 0.2728327 0.09542948

                       Estimate           SE        CV
Average p              0.232512   0.02944422 0.1266352
N in covered region 1548.306965 209.54903632 0.1353408

Distance sampling Cramer-von Mises test (unweighted)
Test statistic = 0.019198  p = 0.997687
```

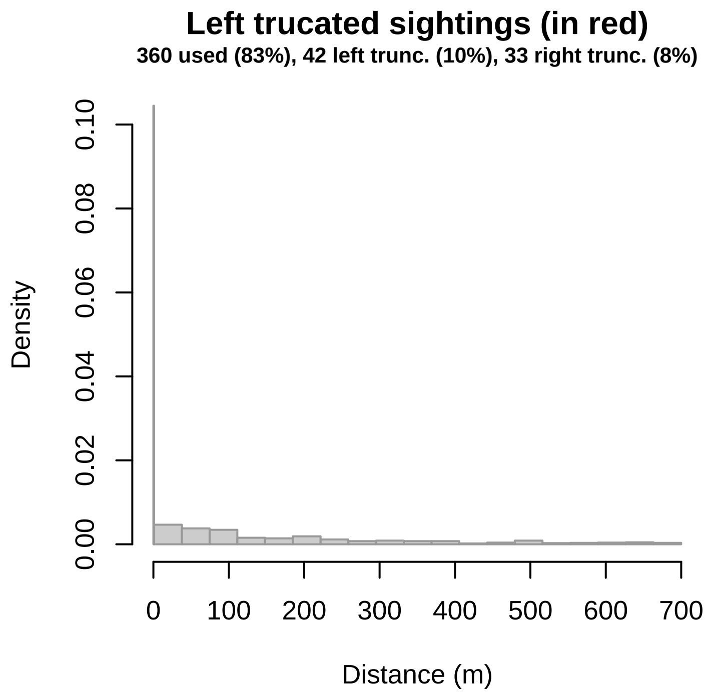

Figure 25: Density histogram of observations used to fit the Song of the Whale detection function, with the left-most bar showing observations at distances less than 1 m, which were left-truncated and not used to fit the detection function. (This bar may be very short if there were very few left-truncated sightings, or very narrow if the left truncation distance was very small; in either case it may not appear red.) These were excluded because they formed a problematic "spike" in detections close to the trackline, suggesting that animals approached the vessel (e.g. to bow-ride) prior to being detected. To address this, we fitted the detection function to the observations beyond the spike and assumed that within it, detection probability was 1, effectively treating it like a strip transect. We then added the left-truncated observations back into the analysis as if they occurred in this strip. This treatment may have resulted in an underestimation of detection probability.

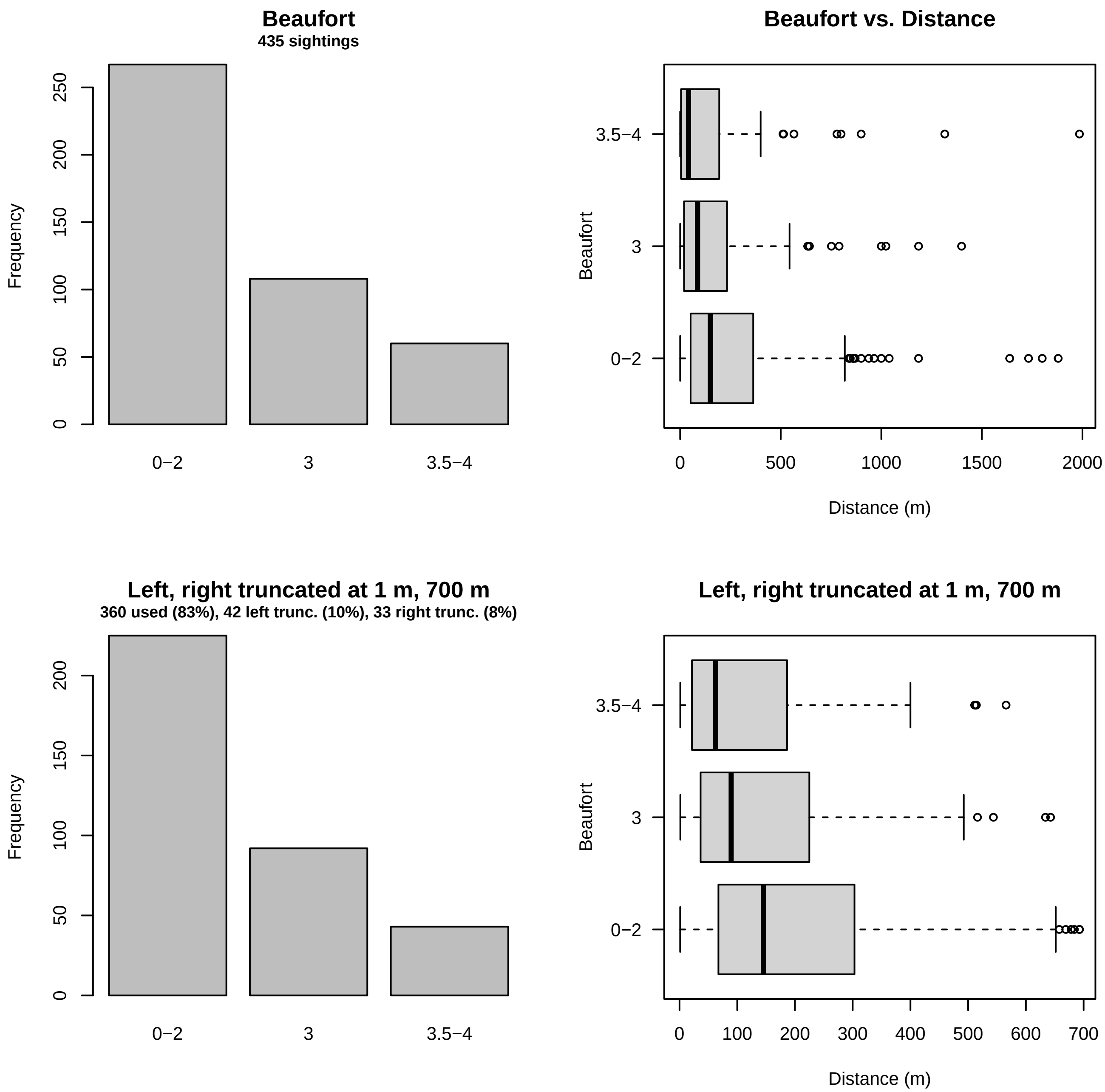

Figure 26: Distribution of the Beaufort covariate before (top row) and after (bottom row) observations were truncated to fit the Song of the Whale detection function.

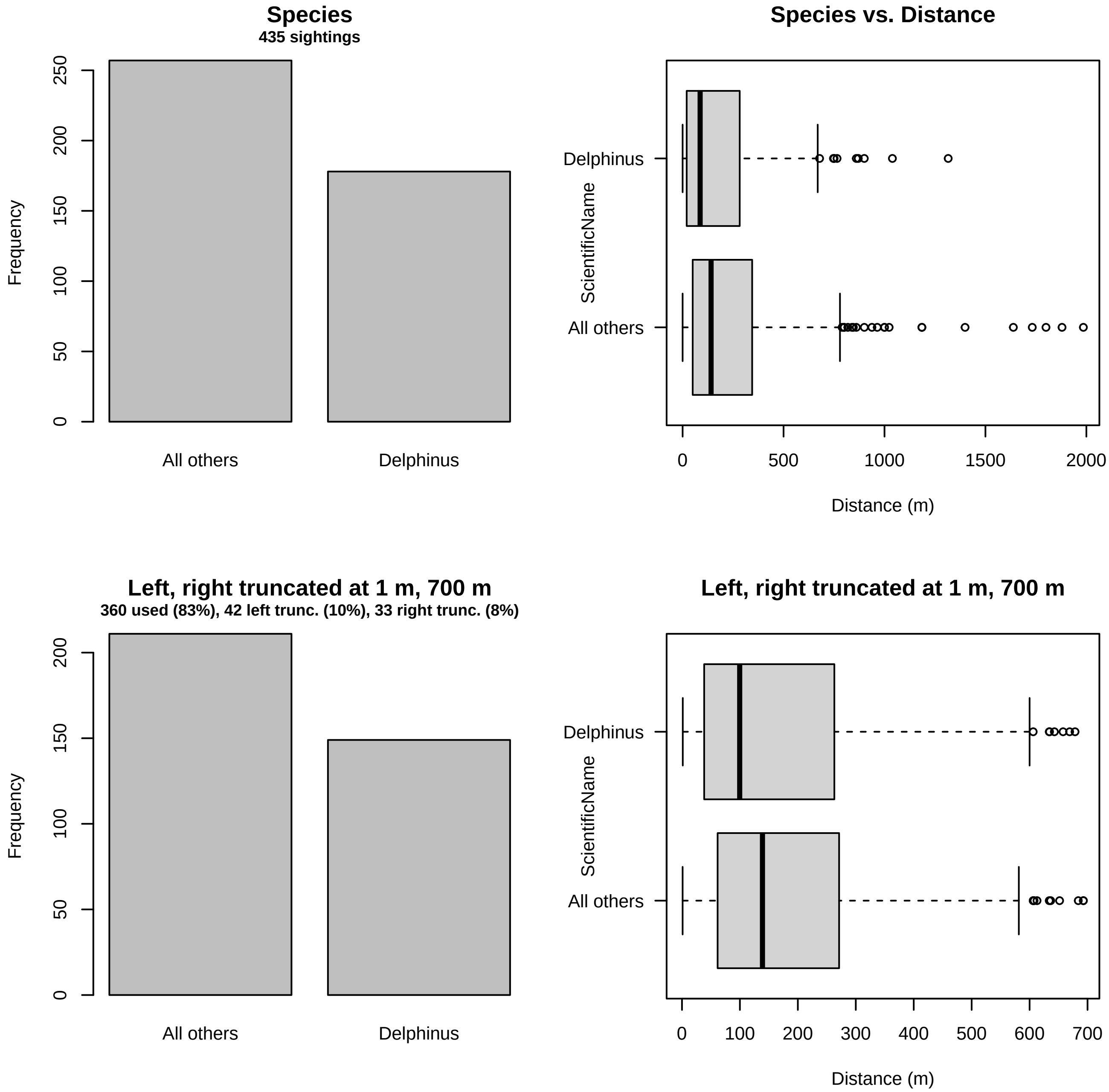

Figure 27: Distribution of the ScientificName covariate before (top row) and after (bottom row) observations were truncated to fit the Song of the Whale detection function.

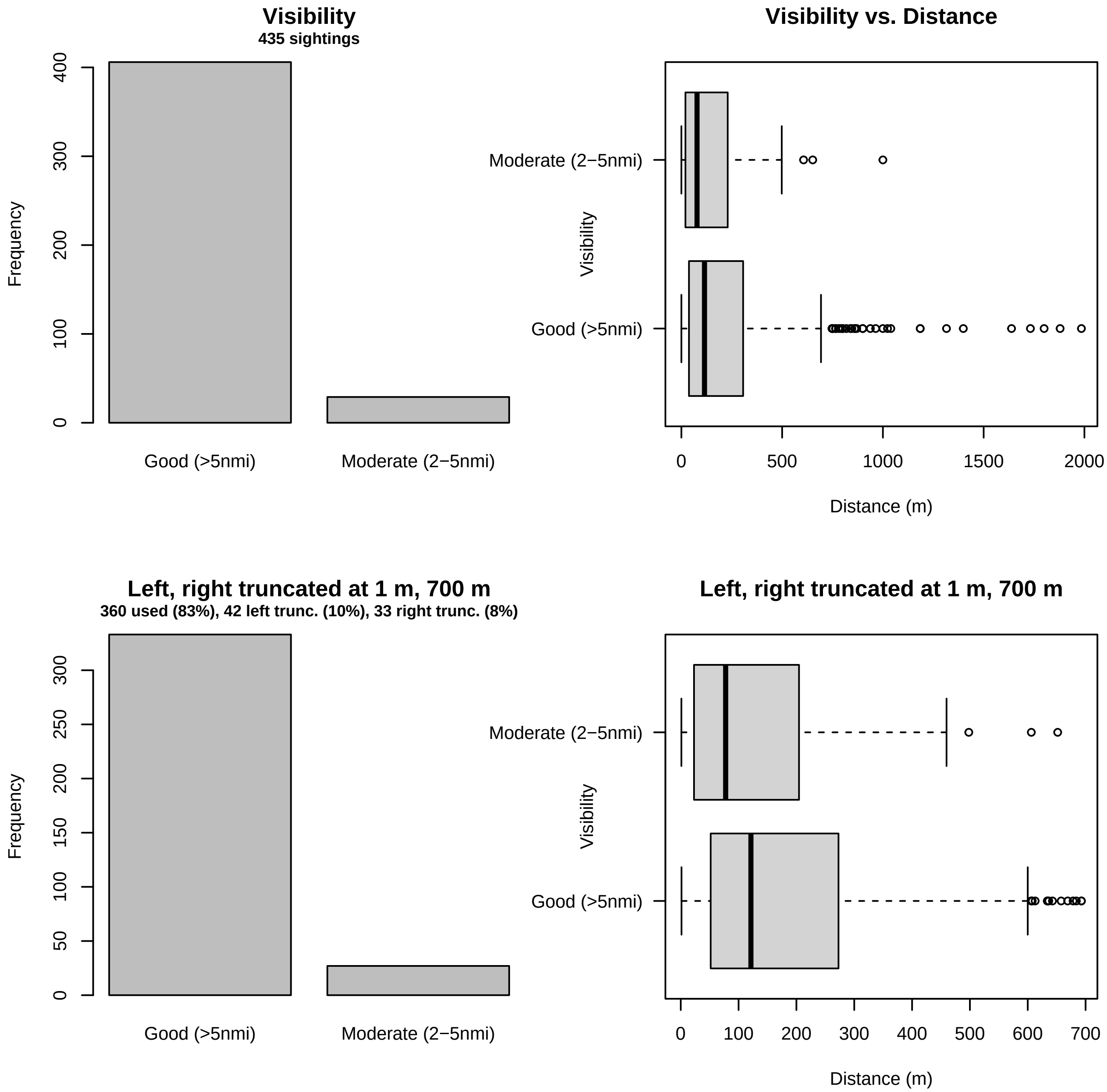

Figure 28: Distribution of the Visibility covariate before (top row) and after (bottom row) observations were truncated to fit the Song of the Whale detection function.

3.2 Without a Taxonomic Covariate

We fitted the detection functions in this section to pools of species with similar detectability characteristics but could not use a taxonomic identification as a covariate to account for differences between them. We usually took this approach after trying the taxonomic covariate and finding it had insufficient statistical power to be retained. We also resorted to it when the focal taxon being modeled had too few observations to be allocated its own taxonomic covariate level and was too poorly known for us to confidently determine which other taxa we could group it with.

3.2.1 Aerial Surveys

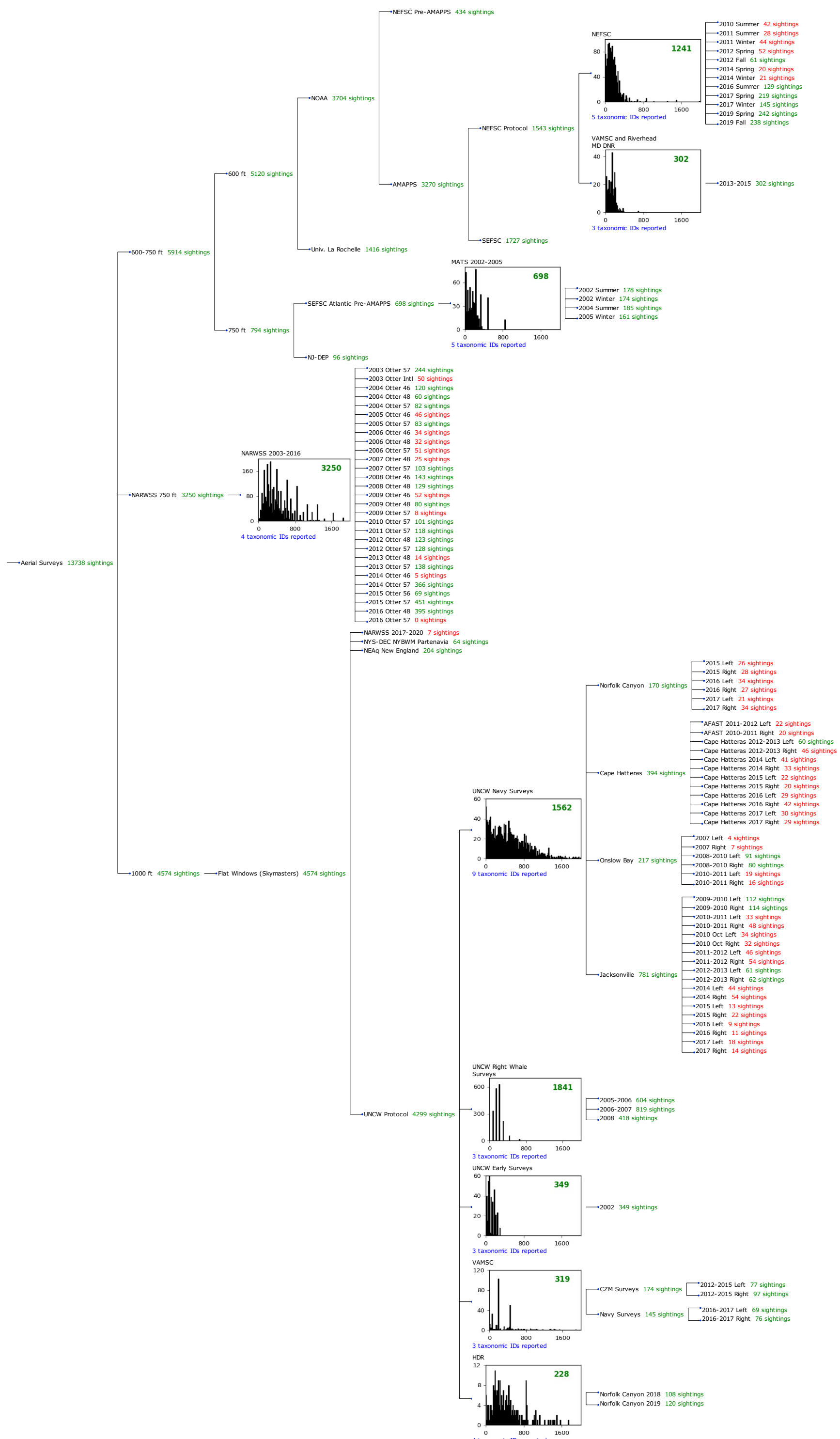

Figure 29: Detection hierarchy for aerial surveys, showing how they were pooled during detectability modeling, for detection functions that pooled multiple taxa but could not use a taxonomic covariate to account for differences between them. Each histogram represents a detection function and summarizes the perpendicular distances of observations that were pooled to fit it, prior to truncation. Observation counts, also prior to truncation, are shown in green when they met the recommendation of Buckland et al. (2001) that detection functions utilize at least 60 sightings, and red otherwise. For rare taxa, it was not always possible to meet this recommendation, yielding higher statistical uncertainty. During the spatial modeling stage of the analysis, effective strip widths were computed for each survey using the closest detection function above it in the hierarchy (i.e. moving from right to left in the figure). Surveys that do not have a detection function above them in this figure were either addressed by a detection function presented in a different section of this report, or were omitted from the analysis.

3.2.1.1 NEFSC AMAPPS

After right-truncating observations greater than 600 m, we fitted the detection function to the 1218 observations that remained (Table 12). The selected detection function (Figure 30) used a hazard rate key function with Season (Figure 31) as a covariate.

Table 12: Observations used to fit the NEFSC AMAPPS detection function.

ScientificName	n
Delphinus delphis	817
Lagenorhynchus acutus	280
Lagenorhynchus albirostris	3
Stenella coeruleoalba	13
Tursiops truncatus	105
Total	**1218**

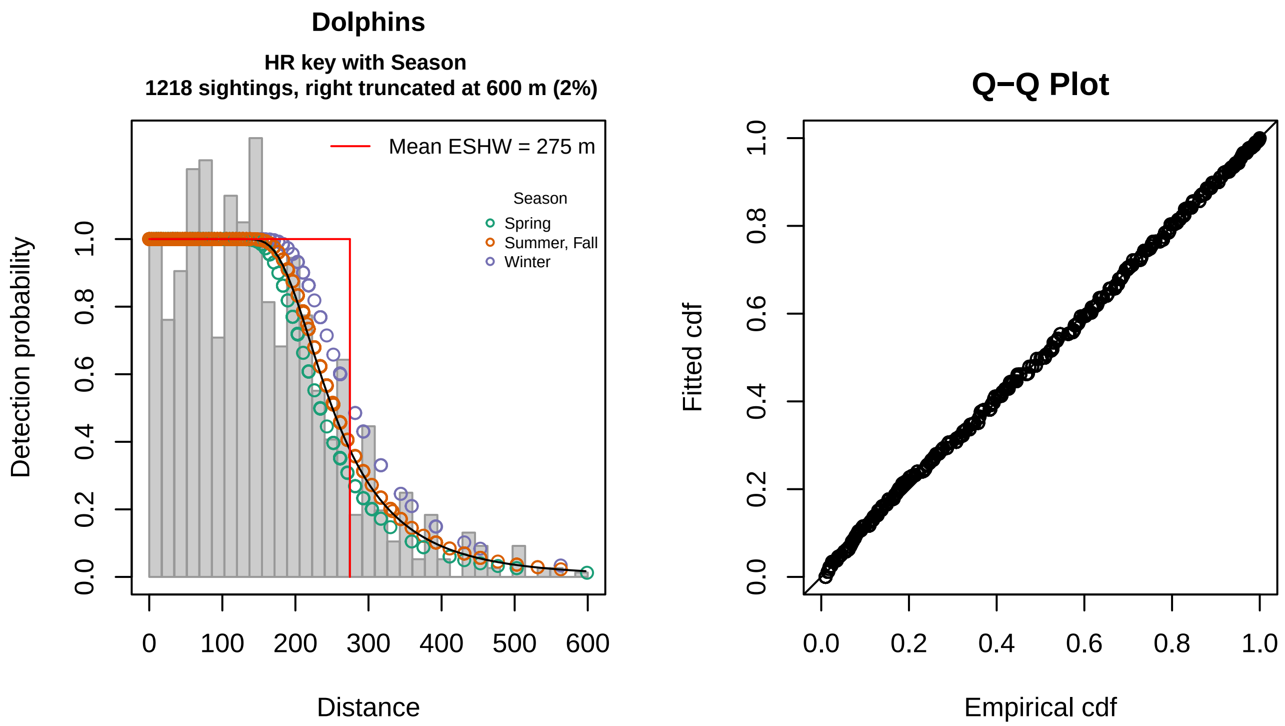

Figure 30: NEFSC AMAPPS detection function and Q-Q plot showing its goodness of fit.

Statistical output for this detection function:

```
Summary for ds object
Number of observations :  1218
Distance range         :  0  -  600
AIC                    :  14460.69

Detection function:
 Hazard-rate key function

Detection function parameters
Scale coefficient(s):
                     estimate         se
(Intercept)        5.36944749 0.04422696
SeasonSummer, Fall 0.08083579 0.04638562
SeasonWinter       0.17600218 0.07702020
```

```
Shape coefficient(s):
            estimate       se
(Intercept) 1.452854 0.065484

                       Estimate          SE         CV
Average p              0.456561  0.00970389 0.02125431
N in covered region 2667.770370 79.97999993 0.02998009

Distance sampling Cramer-von Mises test (unweighted)
Test statistic = 0.126854  p = 0.468488
```

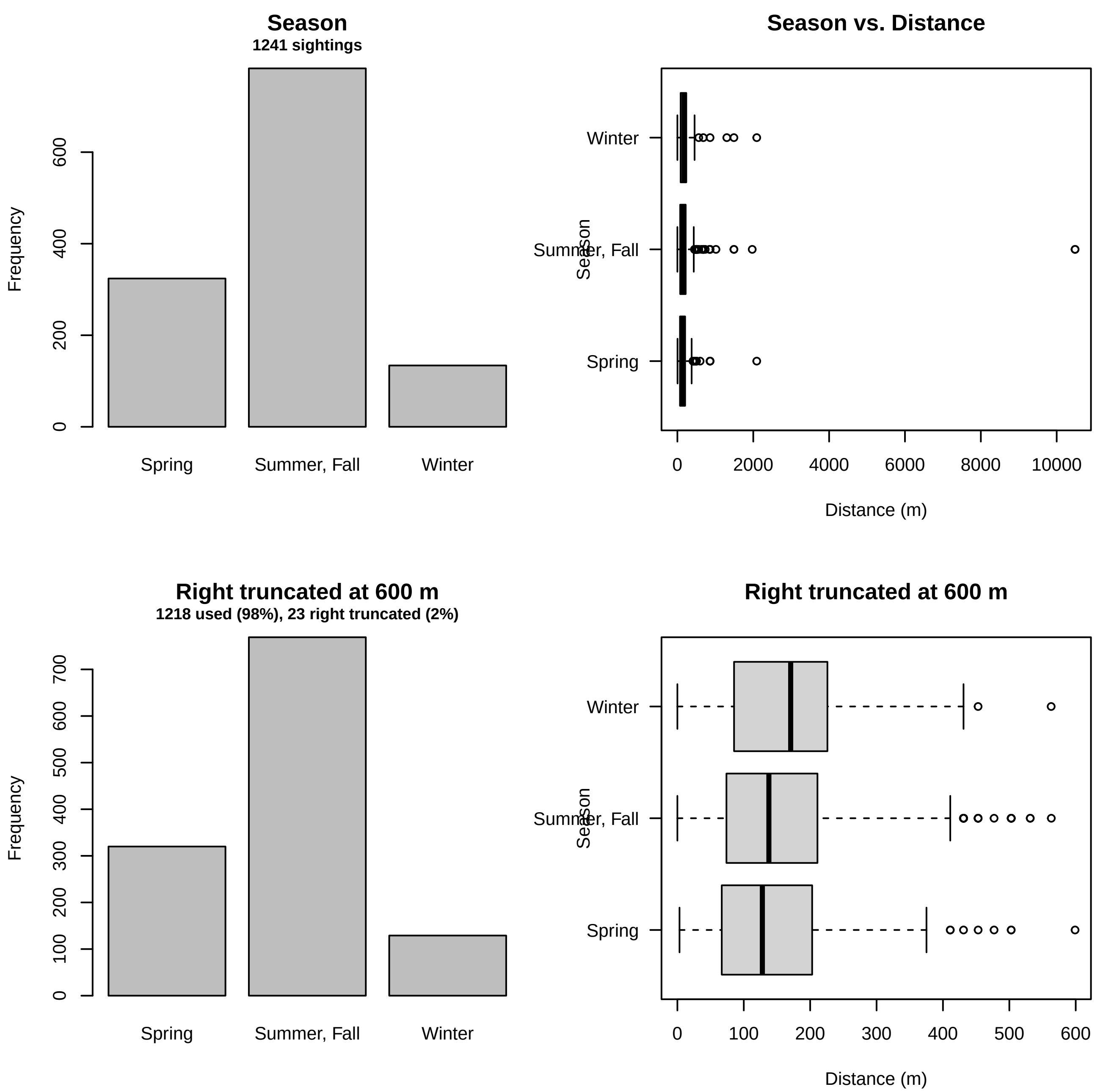

Figure 31: Distribution of the Season covariate before (top row) and after (bottom row) observations were truncated to fit the NEFSC AMAPPS detection function.

3.2.1.2 VAMSC and Riverhead MD DNR

After right-truncating observations greater than 400 m, we fitted the detection function to the 301 observations that remained (Table 13). The selected detection function (Figure 32) used a hazard rate key function with no covariates.

Table 13: Observations used to fit the VAMSC and Riverhead MD DNR detection function.

ScientificName	n
Delphinus delphis	22
Stenella frontalis	1
Tursiops truncatus	278
Total	**301**

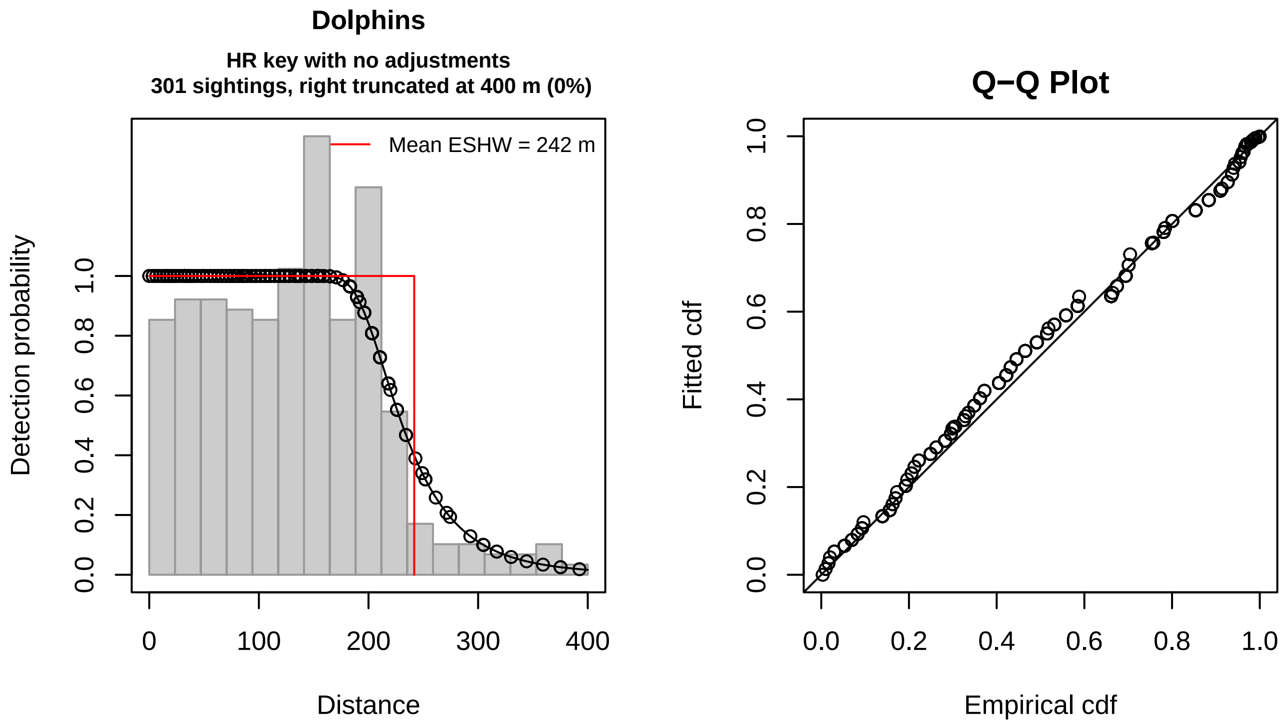

Figure 32: VAMSC and Riverhead MD DNR detection function and Q-Q plot showing its goodness of fit.

Statistical output for this detection function:

```
Summary for ds object
Number of observations :  301
Distance range         :  0  -  400
AIC                    :  3426.124

Detection function:
 Hazard-rate key function

Detection function parameters
Scale coefficient(s):
            estimate         se
(Intercept) 5.388208 0.04209556

Shape coefficient(s):
            estimate        se
(Intercept)  1.91525 0.1331166
```

```
                        Estimate         SE         CV
Average p              0.6042969  0.0203517 0.03367831
N in covered region 498.0995265 24.6489147 0.04948592

Distance sampling Cramer-von Mises test (unweighted)
Test statistic = 0.302011  p = 0.133421
```

3.2.1.3 MATS 2002-2005

After right-truncating observations greater than 629 m, we fitted the detection function to the 684 observations that remained (Table 14). The selected detection function (Figure 33) used a hazard rate key function with Beaufort (Figure 34) as a covariate.

Table 14: Observations used to fit the MATS 2002-2005 detection function.

ScientificName	n
Delphinus delphis	2
Stenella attenuata	2
Stenella frontalis	104
Tursiops truncatus	576
Total	**684**

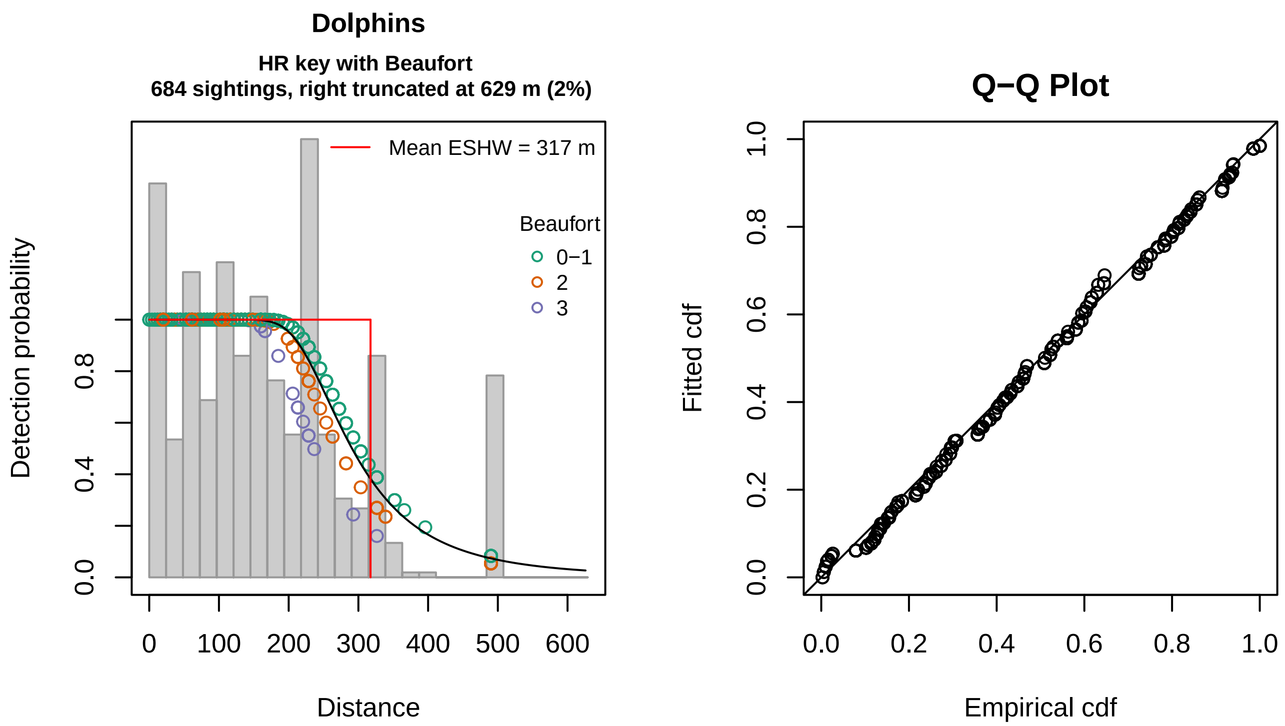

Figure 33: MATS 2002-2005 detection function and Q-Q plot showing its goodness of fit.

Statistical output for this detection function:

```
Summary for ds object
Number of observations :  684
Distance range         :  0  -  629
AIC                    :  8306.088

Detection function:
```

```
 Hazard-rate key function

Detection function parameters
Scale coefficient(s):
              estimate         se
(Intercept)  5.6213531 0.04325709
Beaufort2   -0.1046854 0.06814971
Beaufort3   -0.2421057 0.13060115

Shape coefficient(s):
            estimate         se
(Intercept) 1.449025 0.08965229

                        Estimate         SE         CV
Average p              0.5026836  0.0147185 0.02927984
N in covered region 1360.6968013 54.2106880 0.03984039

Distance sampling Cramer-von Mises test (unweighted)
Test statistic = 0.194502  p = 0.278380
```

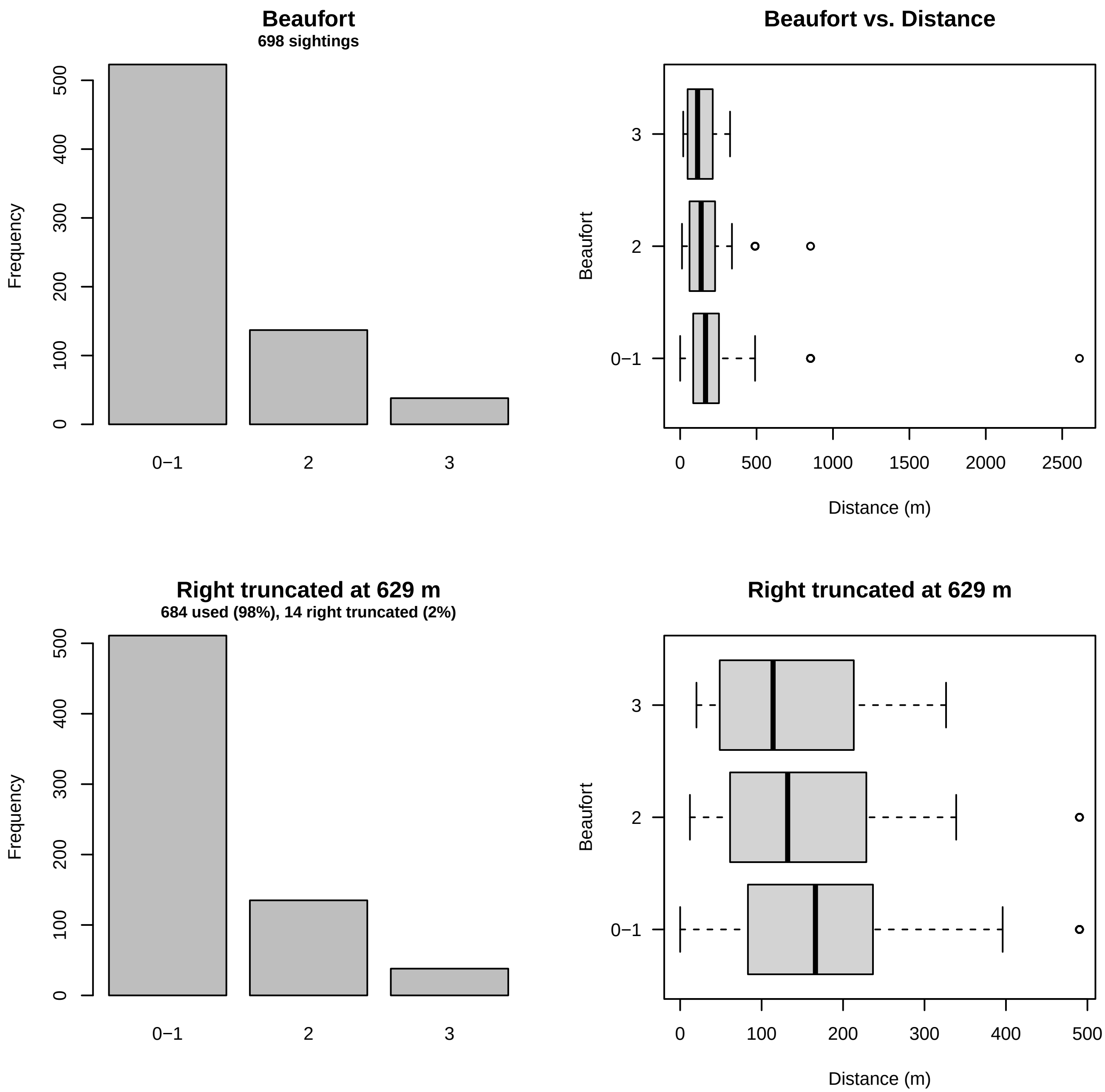

Figure 34: Distribution of the Beaufort covariate before (top row) and after (bottom row) observations were truncated to fit the MATS 2002-2005 detection function.

3.2.1.4 NARWSS 2003-2016

After right-truncating observations greater than 1367 m and left-truncating observations less than 61 m (Figure 36), we fitted the detection function to the 3073 observations that remained (Table 15). The selected detection function (Figure 35) used a hazard rate key function with Beaufort (Figure 37) and Season (Figure 38) as covariates.

Table 15: Observations used to fit the NARWSS 2003-2016 detection function.

ScientificName	n
Delphinus delphis	607
Lagenorhynchus acutus	2404
Lagenorhynchus albirostris	6
Tursiops truncatus	56
Total	**3073**

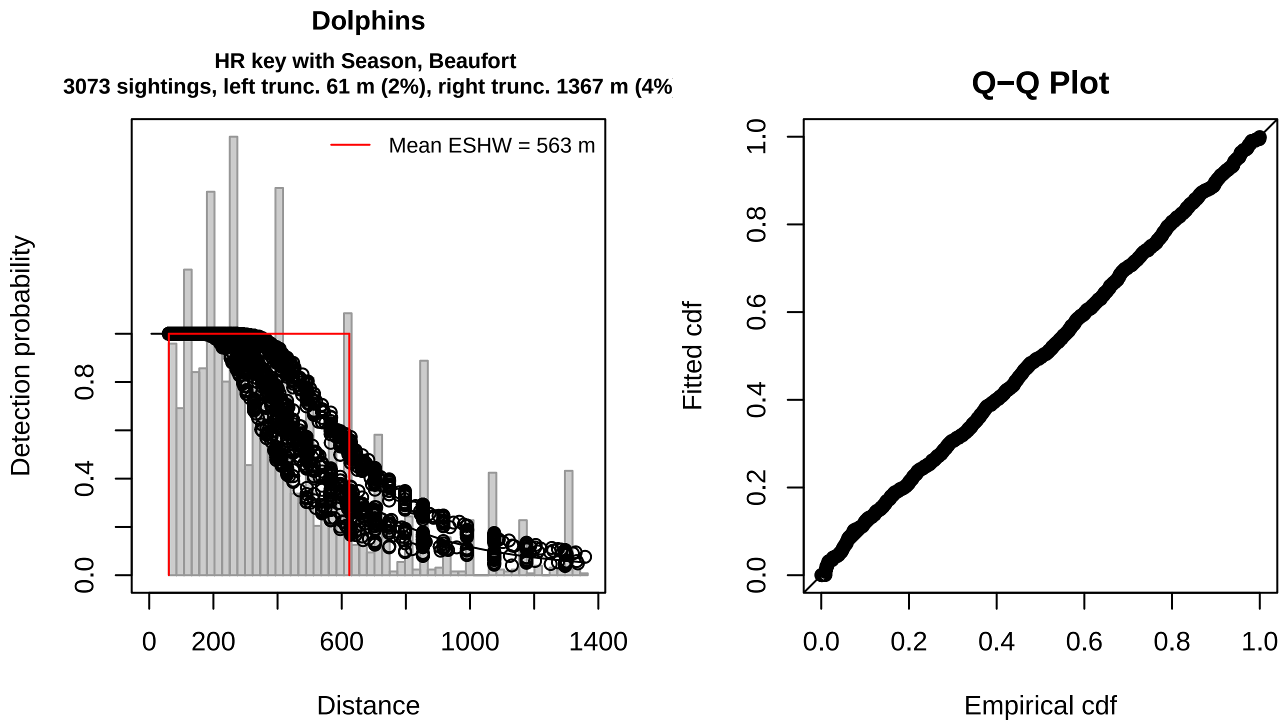

Figure 35: NARWSS 2003-2016 detection function and Q-Q plot showing its goodness of fit.

Statistical output for this detection function:

```
Summary for ds object
Number of observations :  3073
Distance range         :  61  -  1367
AIC                    :  41850.8

Detection function:
 Hazard-rate key function

Detection function parameters
Scale coefficient(s):
                estimate         se
(Intercept)   6.10469263 0.07579397
SeasonSpring  0.06689438 0.05622050
SeasonSummer  0.29278056 0.05383279
SeasonWinter -0.15259970 0.06804643
Beaufort     -0.03572691 0.02383833

Shape coefficient(s):
            estimate        se
(Intercept) 1.009361 0.0398862
```

```
                       Estimate           SE         CV
Average p             0.4196247 8.827249e-03 0.02103606
N in covered region 7323.2113220 1.845410e+02 0.02519946

Distance sampling Cramer-von Mises test (unweighted)
Test statistic = 0.246036  p = 0.193531
```

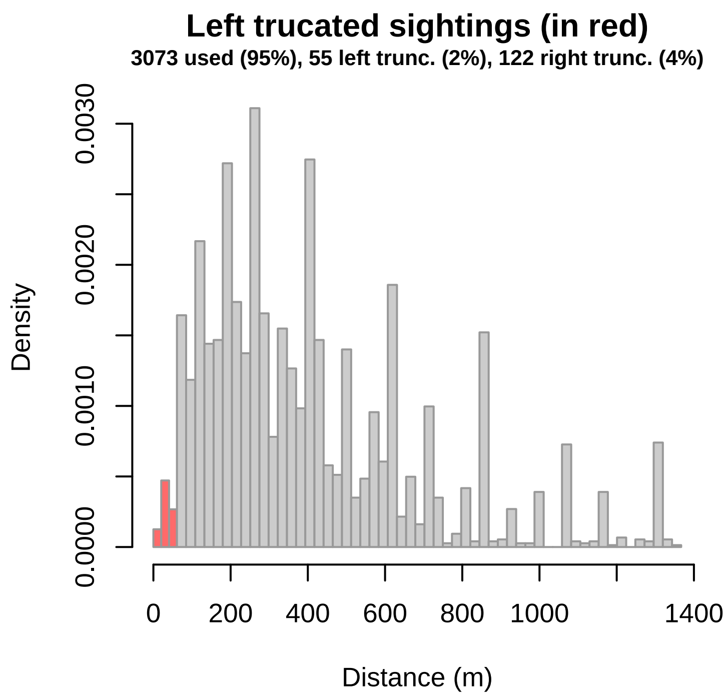

Figure 36: Density histogram of observations used to fit the NARWSS 2003-2016 detection function, with the left-most bar showing observations at distances less than 61 m, which were left-truncated and excluded from the analysis [Buckland et al. (2001)]. (This bar may be very short if there were very few left-truncated sightings, or very narrow if the left truncation distance was very small; in either case it may not appear red.)

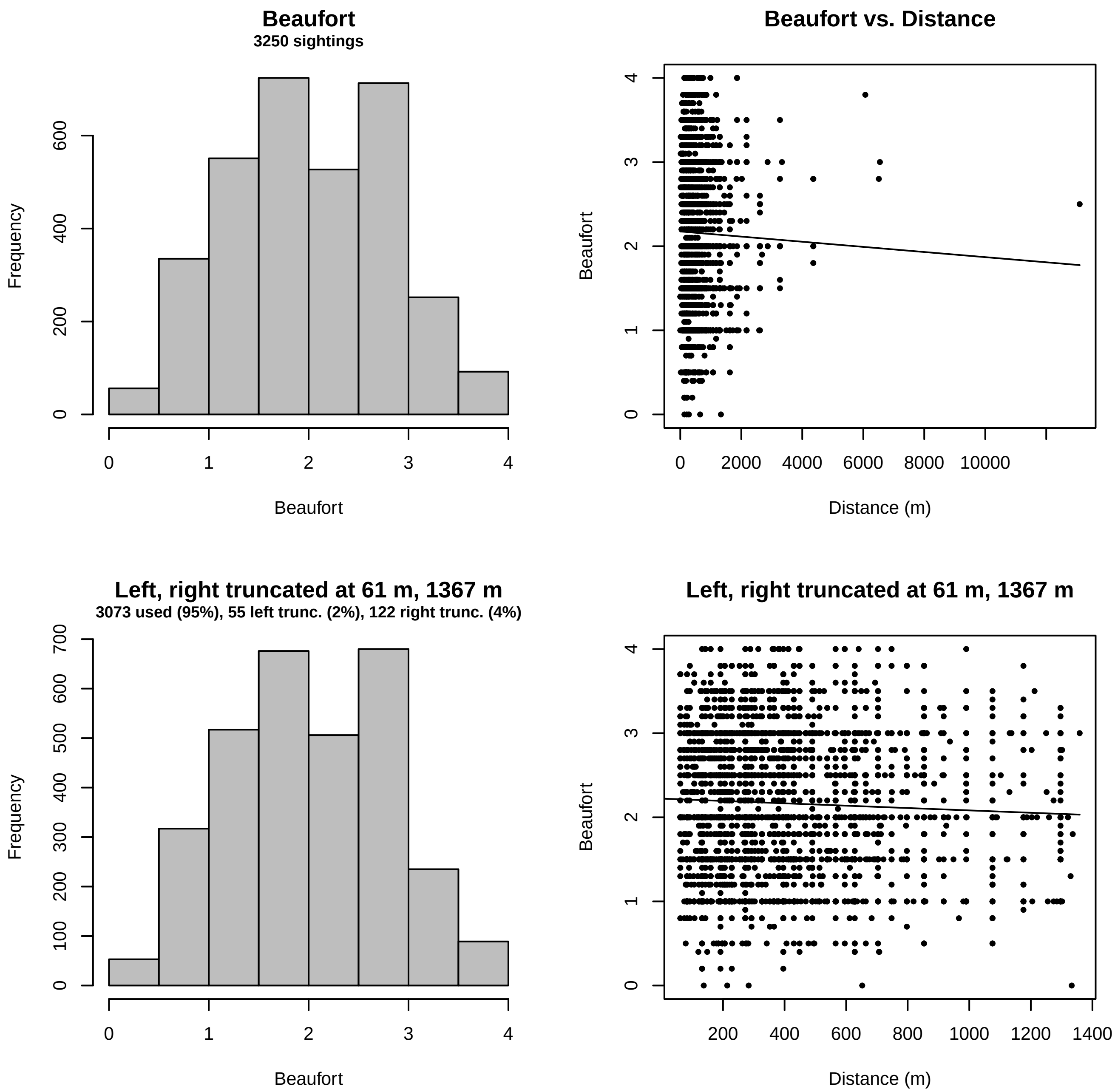

Figure 37: Distribution of the Beaufort covariate before (top row) and after (bottom row) observations were truncated to fit the NARWSS 2003-2016 detection function.

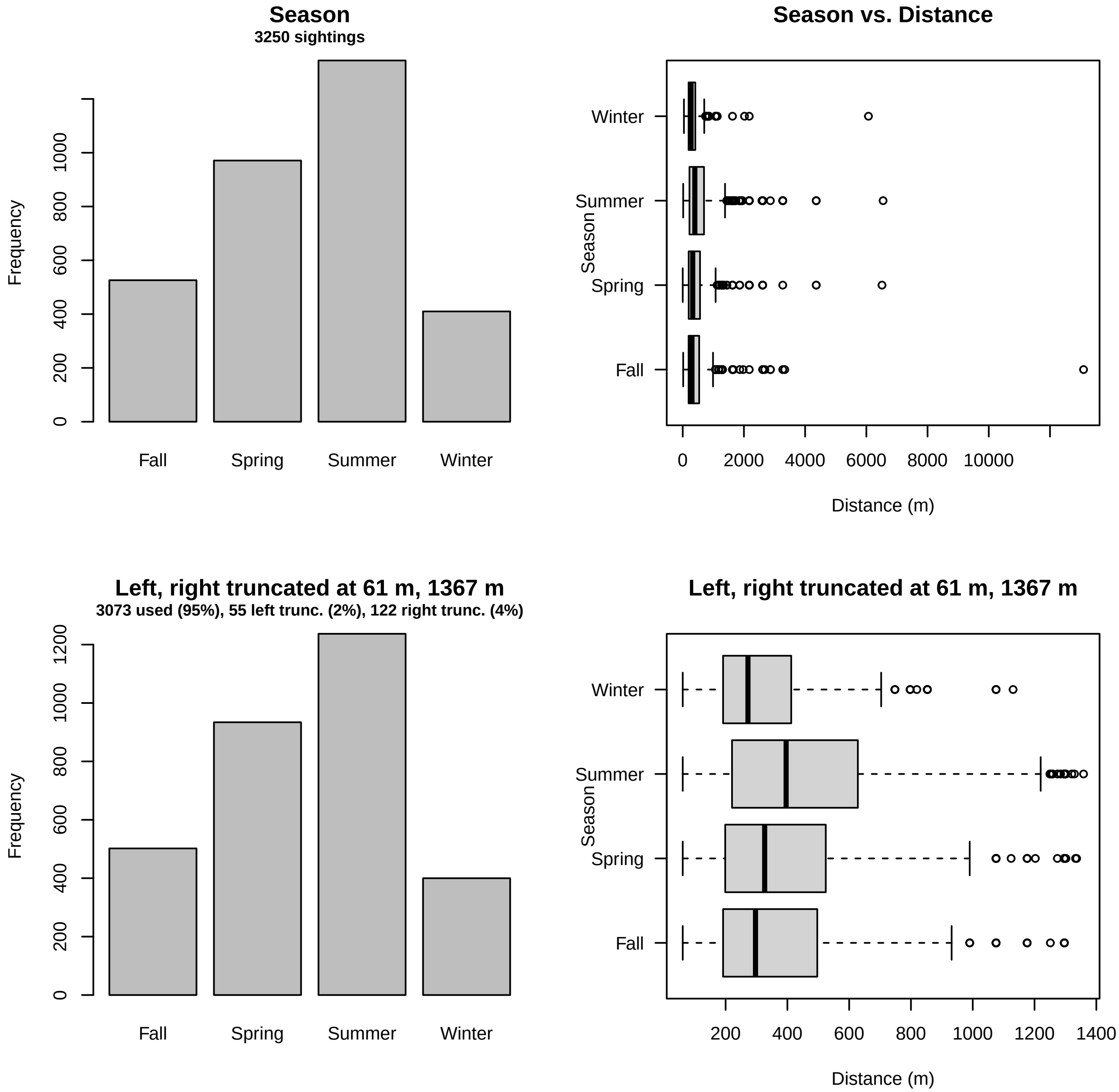

Figure 38: Distribution of the Season covariate before (top row) and after (bottom row) observations were truncated to fit the NARWSS 2003-2016 detection function.

3.2.1.5 UNCW Navy Surveys

After right-truncating observations greater than 1600 m, we fitted the detection function to the 1523 observations that remained (Table 16). The selected detection function (Figure 39) used a half normal key function with Glare (Figure 40) and Visibility (Figure 41) as covariates.

Table 16: Observations used to fit the UNCW Navy Surveys detection function.

ScientificName	n
Delphinus delphis	77
Lagenodelphis hosei	1
Stenella attenuata	2
Stenella clymene	11
Stenella coeruleoalba	19
Stenella frontalis	480
Stenella longirostris	1
Steno bredanensis	14
Tursiops truncatus	918
Total	**1523**

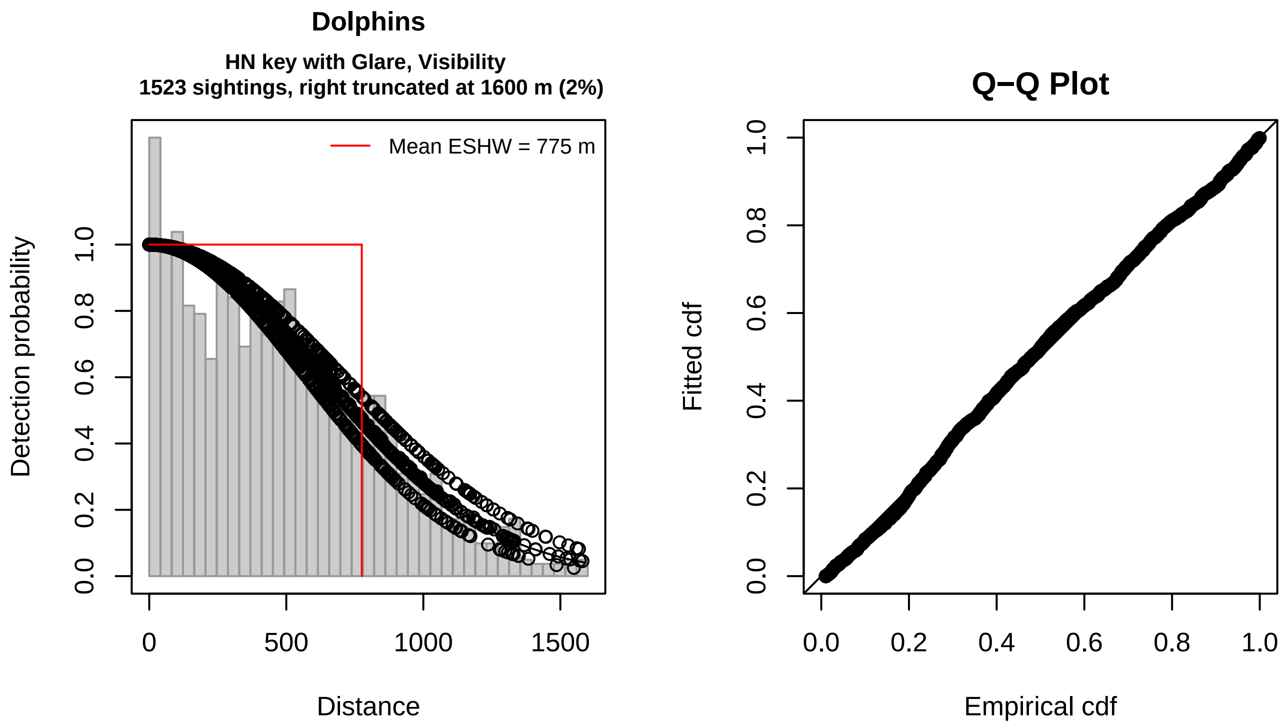

Figure 39: UNCW Navy Surveys detection function and Q-Q plot showing its goodness of fit.

Statistical output for this detection function:

```
Summary for ds object
Number of observations :  1523
Distance range         :  0  -  1600
AIC                    :  21665.78

Detection function:
 Half-normal key function

Detection function parameters
Scale coefficient(s):
                          estimate         se
(Intercept)             6.55223233 0.04798577
GlareNone, 0-25%, Unk. -0.10934970 0.05247015
VisibilityHalf         -0.09759271 0.04601702
```

```
                         Estimate          SE         CV
Average p               0.4827398  0.01003395 0.02078542
N in covered region 3154.9084328 87.71221948 0.02780183

Distance sampling Cramer-von Mises test (unweighted)
Test statistic = 0.331909  p = 0.110182
```

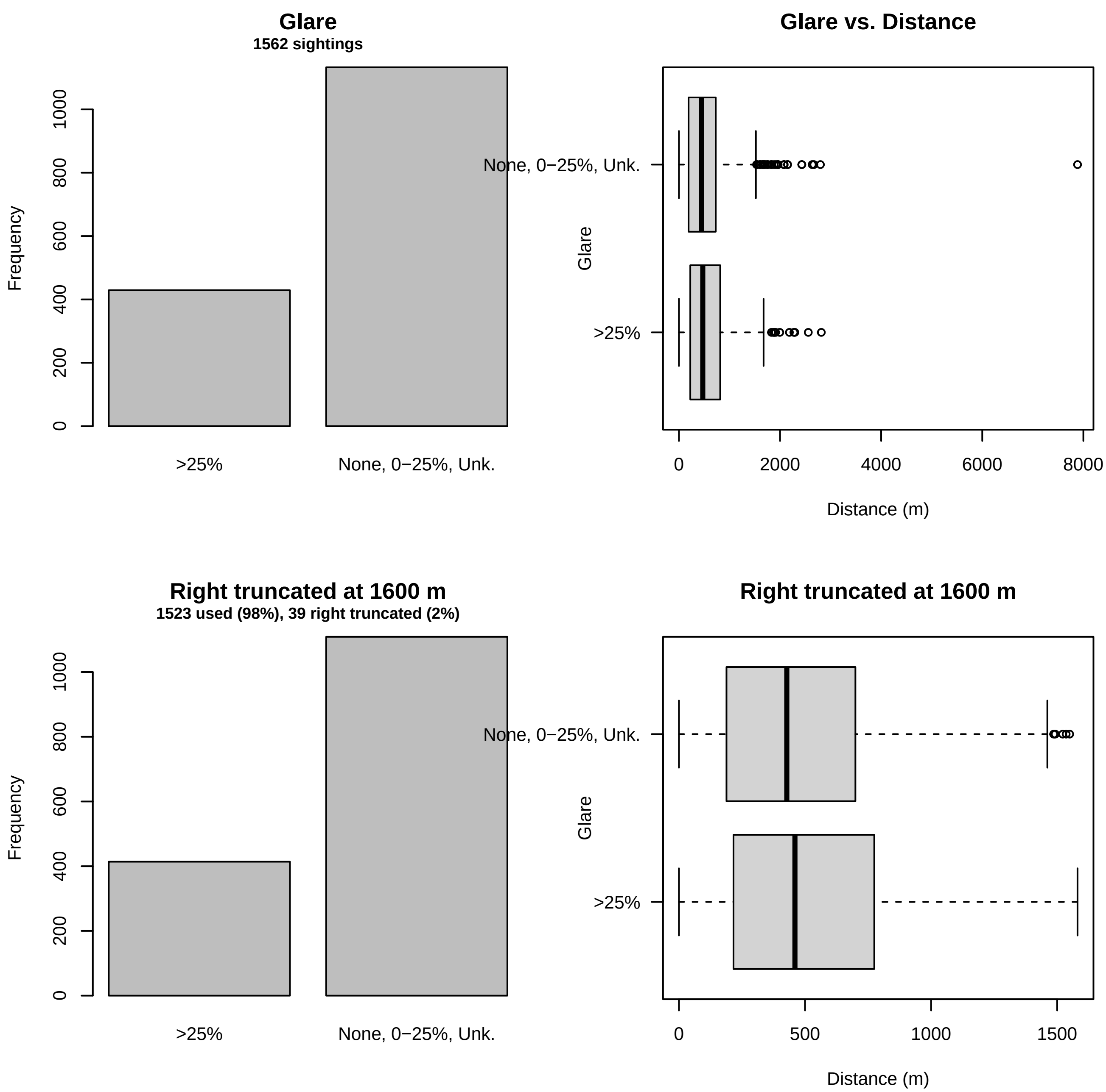

Figure 40: Distribution of the Glare covariate before (top row) and after (bottom row) observations were truncated to fit the UNCW Navy Surveys detection function.

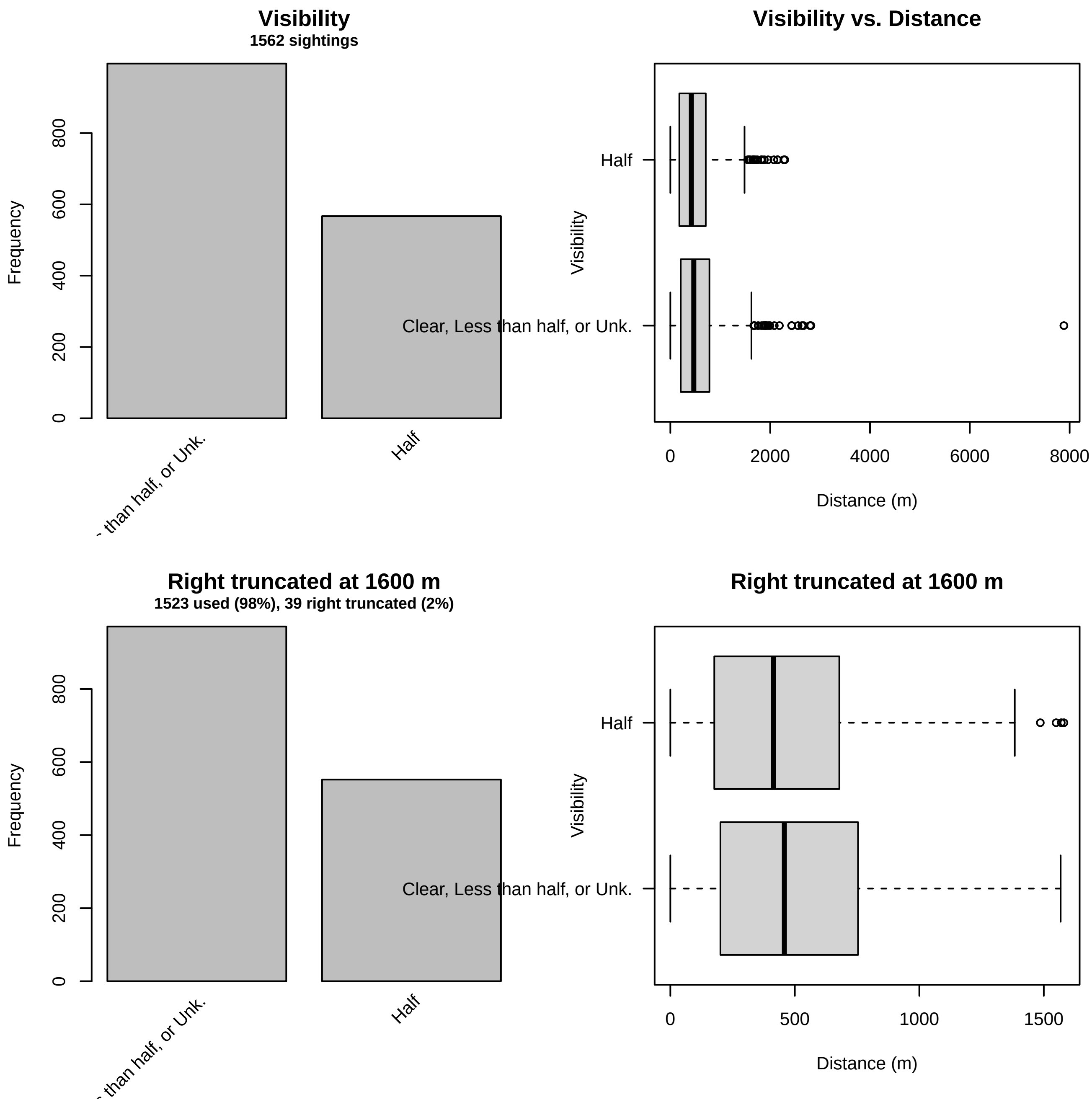

Figure 41: Distribution of the Visibility covariate before (top row) and after (bottom row) observations were truncated to fit the UNCW Navy Surveys detection function.

3.2.1.6 UNCW Right Whale Surveys

After right-truncating observations greater than 528 m and left-truncating observations less than 54 m (Figure 43), we fitted the detection function to the 1821 observations that remained (Table 17). The selected detection function (Figure 42) used a hazard rate key function with no covariates.

Table 17: Observations used to fit the UNCW Right Whale Surveys detection function.

ScientificName	n
Delphinus delphis	26
Stenella frontalis	4
Tursiops truncatus	1791
Total	**1821**

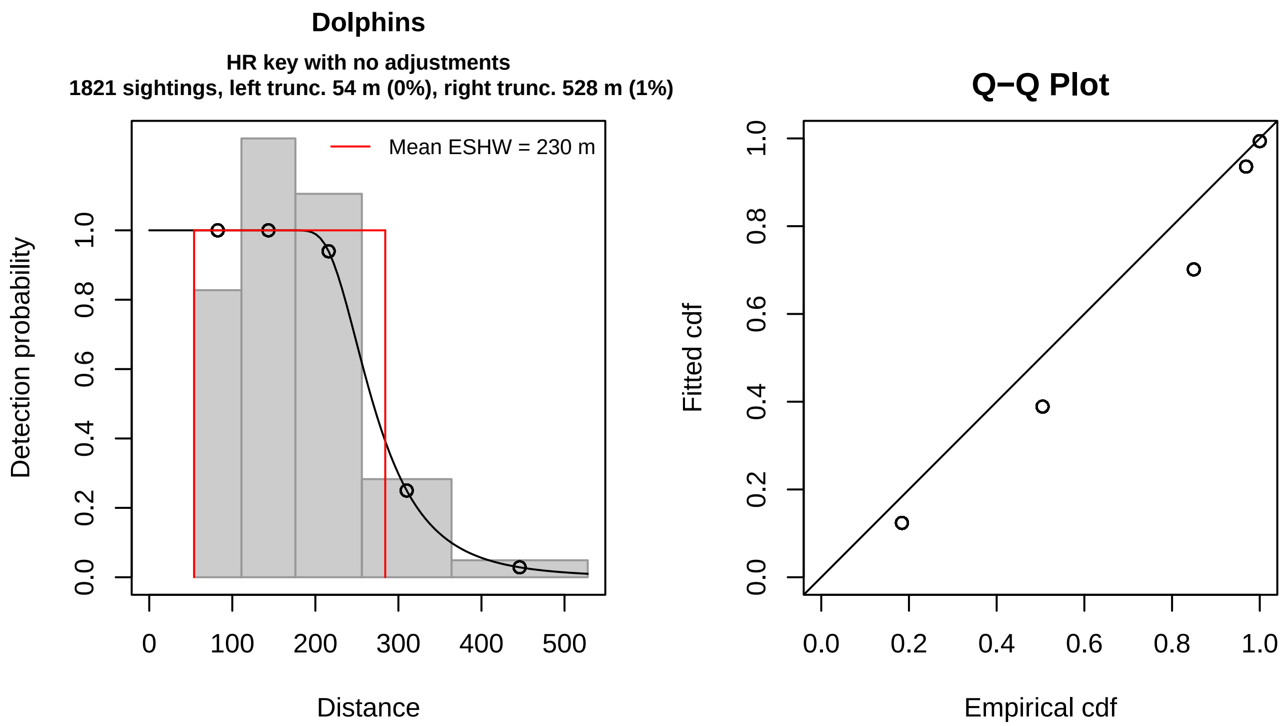

Figure 42: UNCW Right Whale Surveys detection function and Q-Q plot showing its goodness of fit.

Statistical output for this detection function:

```
Summary for ds object
Number of observations :  1821
Distance range         :  54  -  528
AIC                    :  5176.116

Detection function:
 Hazard-rate key function

Detection function parameters
Scale coefficient(s):
            estimate         se
(Intercept) 5.538954 0.02098751

Shape coefficient(s):
            estimate         se
(Intercept) 1.841299 0.06464608

                        Estimate          SE         CV
Average p              0.4855453  0.009233858 0.01901750
N in covered region 3750.4226341 95.188173832 0.02538065
```

```
Distance sampling Cramer-von Mises test (unweighted)
Test statistic = 14.468539  p = 0.010416
```

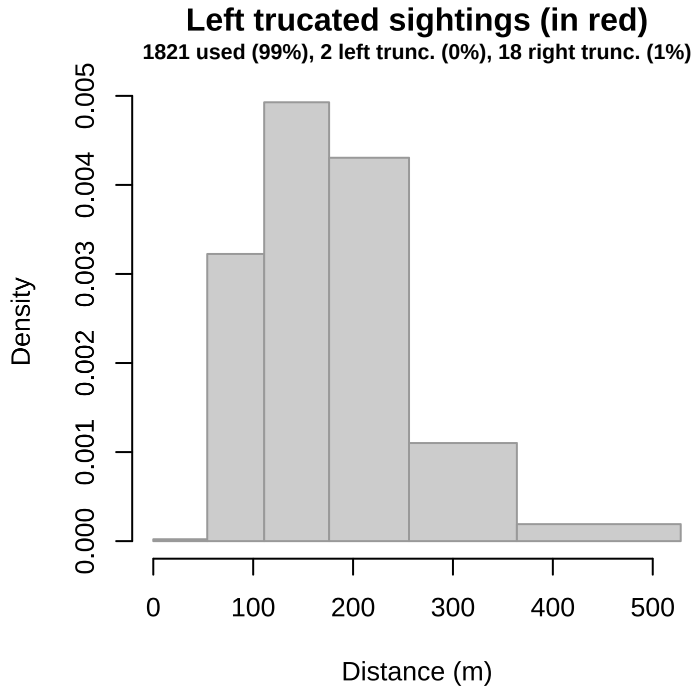

Figure 43: Density histogram of observations used to fit the UNCW Right Whale Surveys detection function, with the left-most bar showing observations at distances less than 54 m, which were left-truncated and excluded from the analysis [Buckland et al. (2001)]. (This bar may be very short if there were very few left-truncated sightings, or very narrow if the left truncation distance was very small; in either case it may not appear red.)

3.2.1.7 UNCW Early Surveys

After right-truncating observations greater than 333 m and left-truncating observations less than 14 m (Figure 45), we fitted the detection function to the 349 observations that remained (Table 18). The selected detection function (Figure 44) used a half normal key function with Beaufort (Figure 46) as a covariate.

Table 18: Observations used to fit the UNCW Early Surveys detection function.

ScientificName	n
Delphinus delphis	5
Stenella frontalis	1
Tursiops truncatus	343
Total	**349**

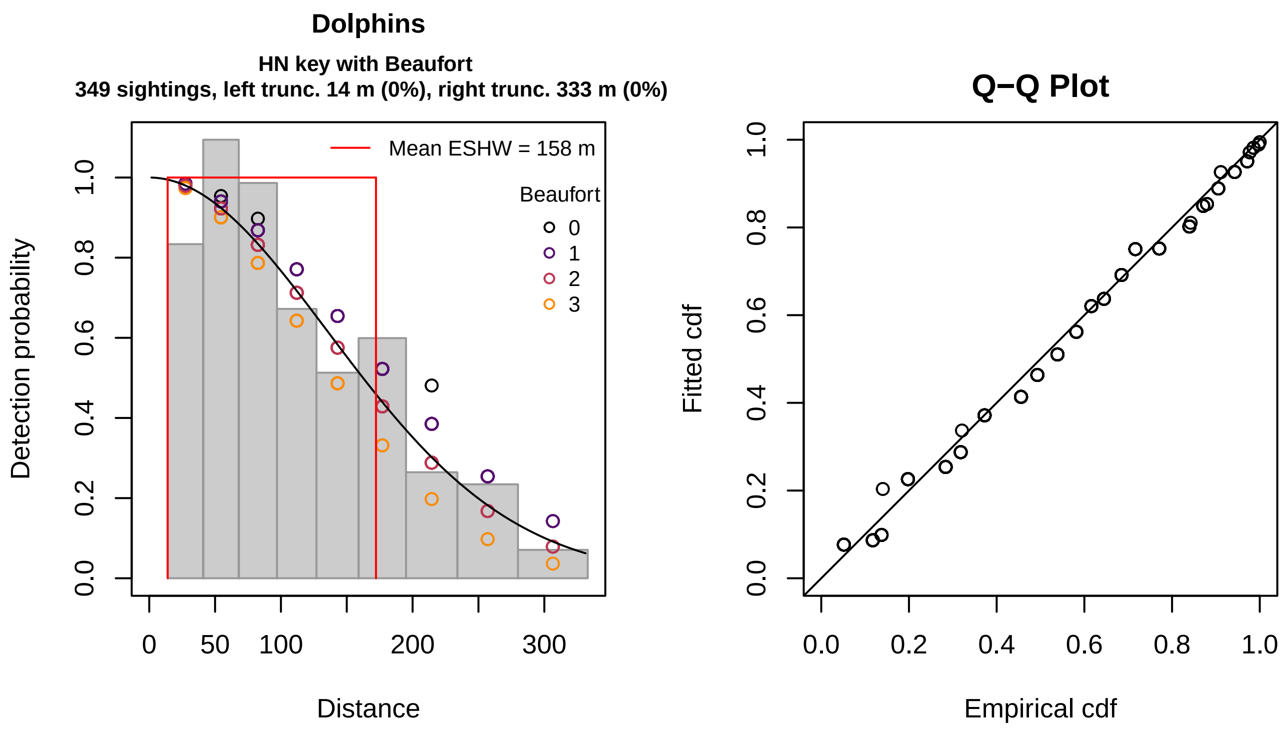

Figure 44: UNCW Early Surveys detection function and Q-Q plot showing its goodness of fit.

Statistical output for this detection function:

```
Summary for ds object
Number of observations :  349
Distance range         :  14  -  333
AIC                    :  1464.597

Detection function:
 Half-normal key function

Detection function parameters
Scale coefficient(s):
              estimate         se
(Intercept)  5.1778911 0.14575211
Beaufort    -0.1325498 0.07066838

                       Estimate          SE         CV
Average p             0.4915207  0.02352103 0.04785360
N in covered region 710.0413079 43.53534195 0.06131382

Distance sampling Cramer-von Mises test (unweighted)
Test statistic = 0.278162  p = 0.155953
```

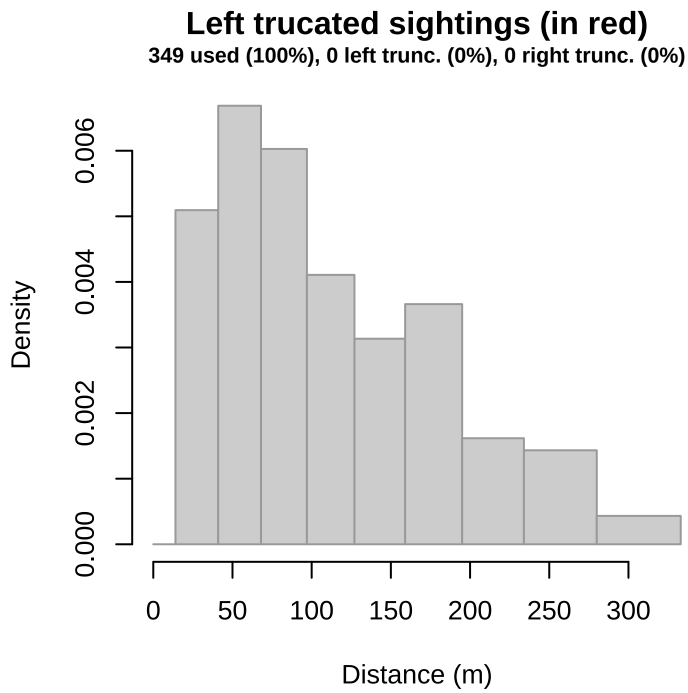

Figure 45: Density histogram of observations used to fit the UNCW Early Surveys detection function, with the left-most bar showing observations at distances less than 14 m, which were left-truncated and excluded from the analysis [Buckland et al. (2001)]. (This bar may be very short if there were very few left-truncated sightings, or very narrow if the left truncation distance was very small; in either case it may not appear red.)

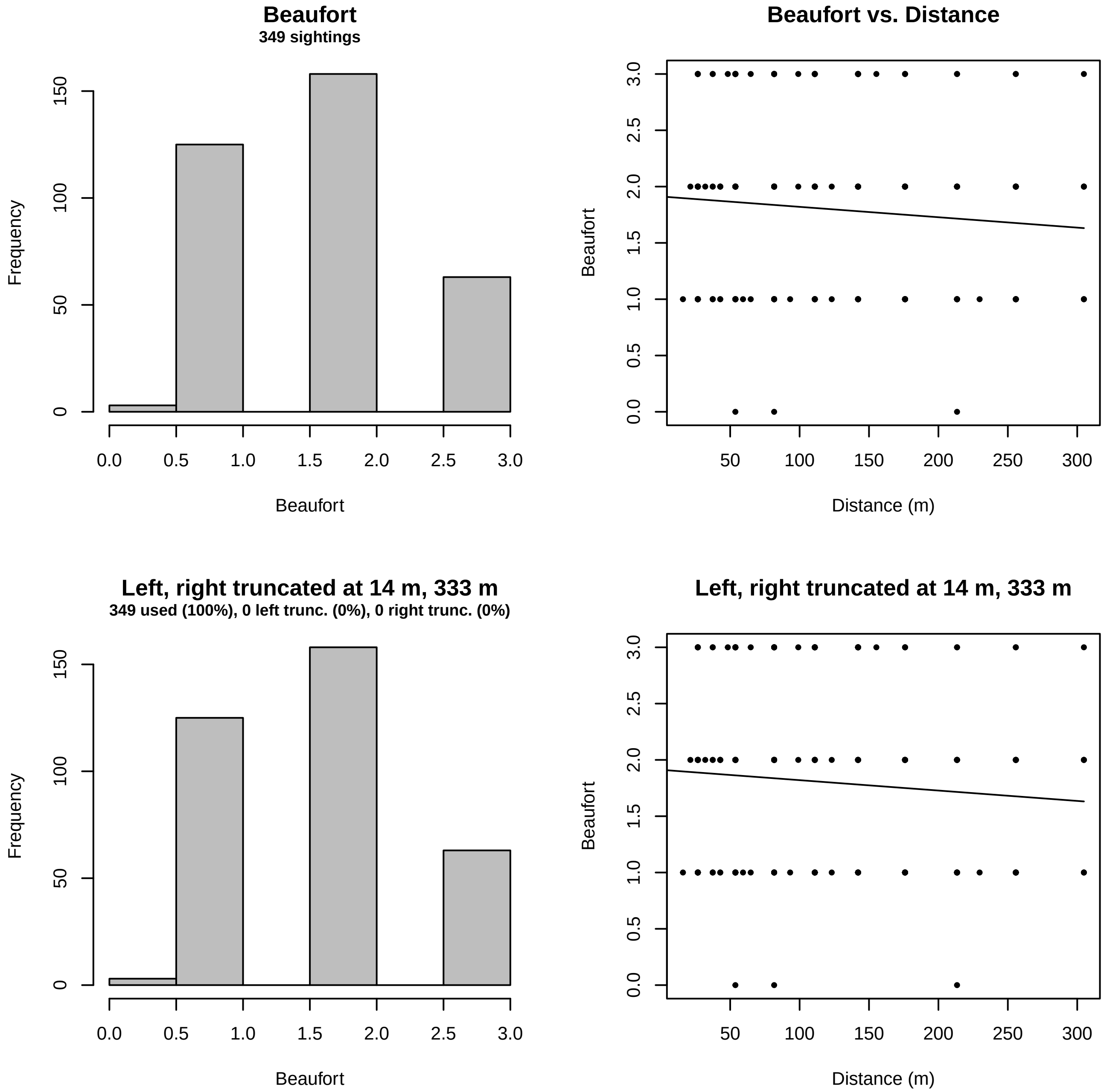

Figure 46: Distribution of the Beaufort covariate before (top row) and after (bottom row) observations were truncated to fit the UNCW Early Surveys detection function.

3.2.1.8 VAMSC

After right-truncating observations greater than 1000 m, we fitted the detection function to the 303 observations that remained (Table 19). The selected detection function (Figure 47) used a hazard rate key function with no covariates.

Table 19: Observations used to fit the VAMSC detection function.

ScientificName	n
Delphinus delphis	30
Stenella frontalis	4
Tursiops truncatus	269
Total	**303**

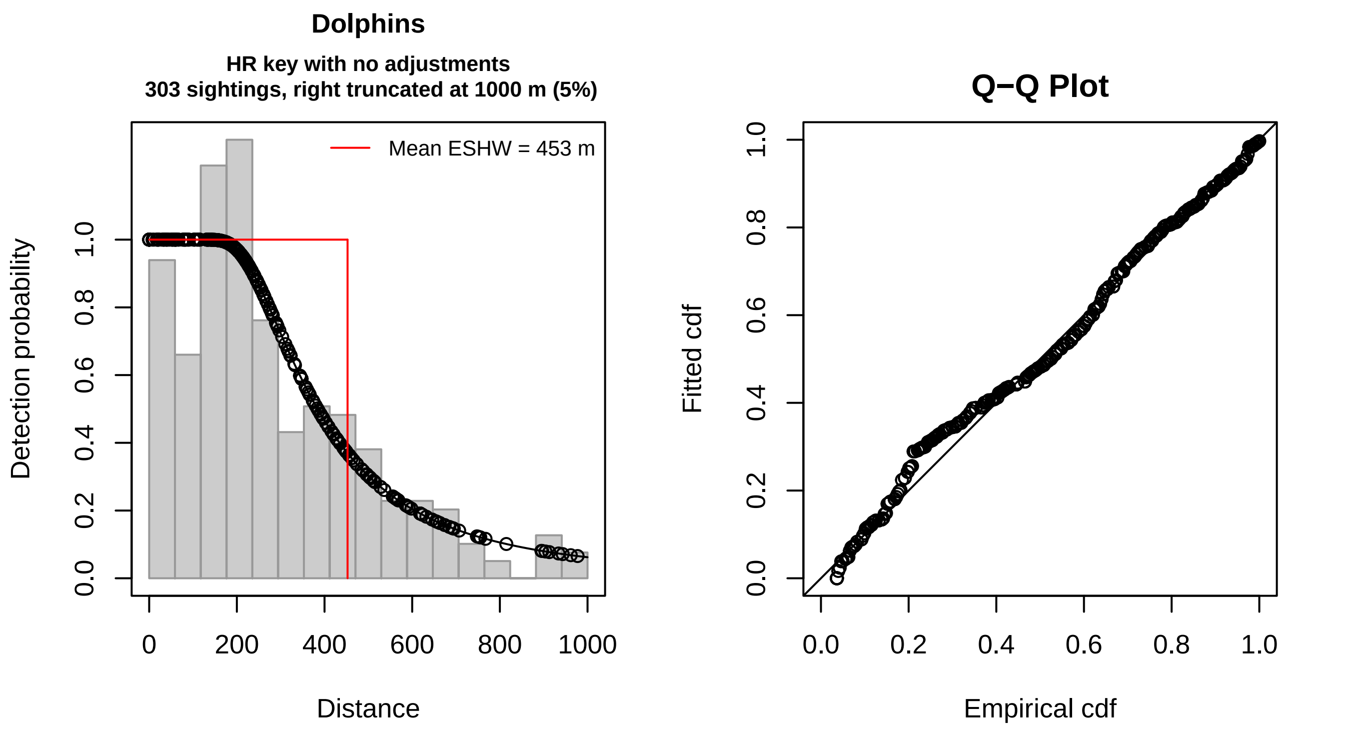

Figure 47: VAMSC detection function and Q-Q plot showing its goodness of fit.

Statistical output for this detection function:

```
Summary for ds object
Number of observations :  303
Distance range         :  0  -  1000
AIC                    :  3992.632

Detection function:
 Hazard-rate key function

Detection function parameters
Scale coefficient(s):
            estimate        se
(Intercept) 5.803823 0.1019737

Shape coefficient(s):
             estimate        se
(Intercept) 0.9119562 0.1438459

                        Estimate          SE         CV
Average p              0.4525805  0.02853931 0.06305908
N in covered region 669.4942067 50.91287837 0.07604678

Distance sampling Cramer-von Mises test (unweighted)
Test statistic = 0.212402  p = 0.244680
```

3.2.1.9 HDR

After right-truncating observations greater than 1500 m and left-truncating observations less than 111 m (Figure 49), we fitted the detection function to the 203 observations that remained (Table 20). The selected detection function (Figure 48) used a hazard rate key function with Season (Figure 50) and Swell (Figure 51) as covariates.

Table 20: Observations used to fit the HDR detection function.

ScientificName	n
Delphinus delphis	47
Stenella coeruleoalba	14
Stenella frontalis	19
Tursiops truncatus	123
Total	**203**

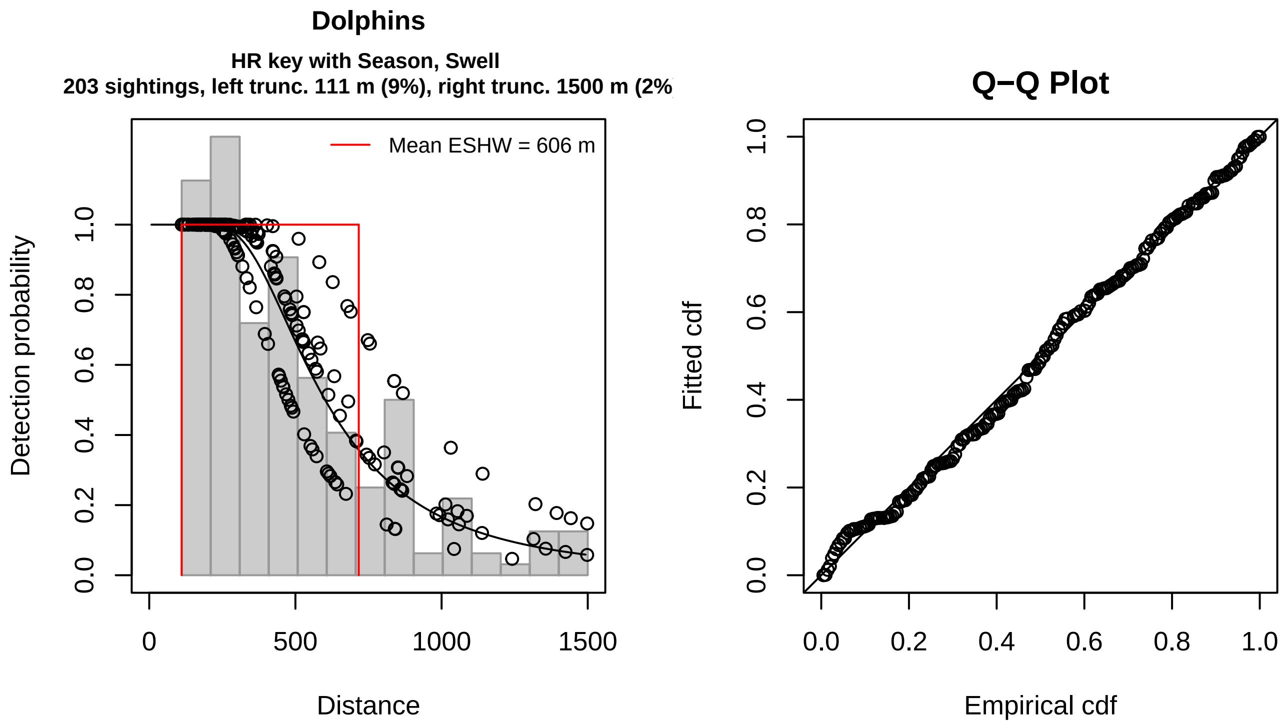

Figure 48: HDR detection function and Q-Q plot showing its goodness of fit.

Statistical output for this detection function:

```
Summary for ds object
Number of observations :  203
Distance range         :  111  -  1500
AIC                    :  2802.845

Detection function:
 Hazard-rate key function

Detection function parameters
Scale coefficient(s):
                      estimate        se
(Intercept)          6.3015171 0.1328018
SeasonWinter, Spring -0.2671651 0.1458664
Swell3-4             0.3527933 0.1530784

Shape coefficient(s):
            estimate        se
(Intercept) 1.026101 0.1620057

                      Estimate          SE         CV
```

```
Average p             0.419883  0.03654238 0.08702991
N in covered region 483.467993 49.56848062 0.10252691

Distance sampling Cramer-von Mises test (unweighted)
Test statistic = 0.059652  p = 0.816171
```

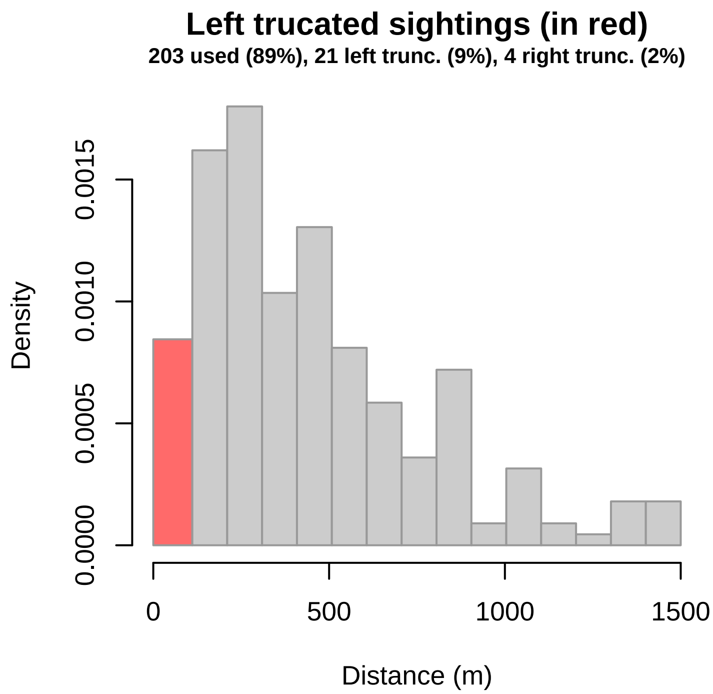

Figure 49: Density histogram of observations used to fit the HDR detection function, with the left-most bar showing observations at distances less than 111 m, which were left-truncated and excluded from the analysis [Buckland et al. (2001)]. (This bar may be very short if there were very few left-truncated sightings, or very narrow if the left truncation distance was very small; in either case it may not appear red.)

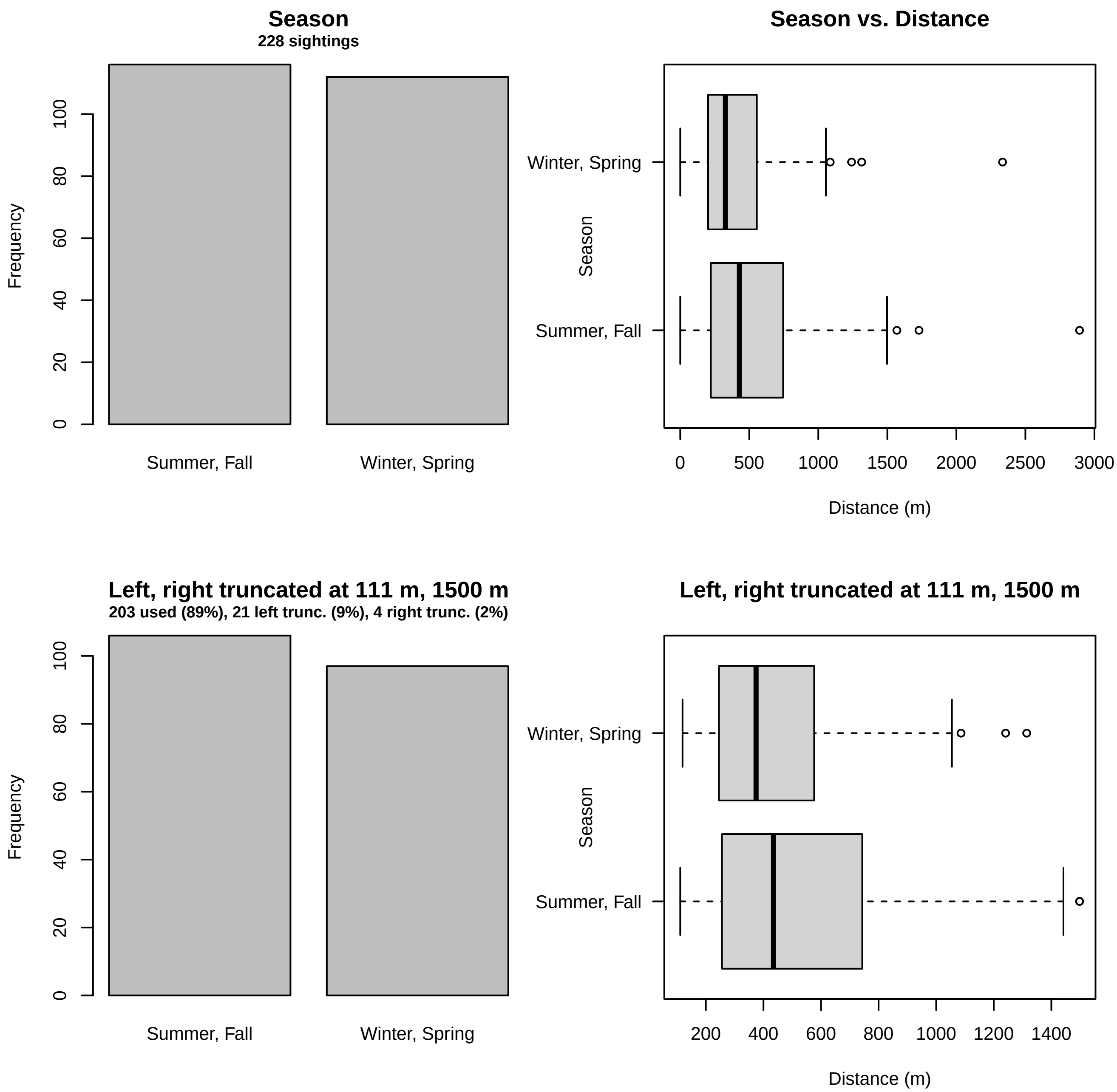

Figure 50: Distribution of the Season covariate before (top row) and after (bottom row) observations were truncated to fit the HDR detection function.

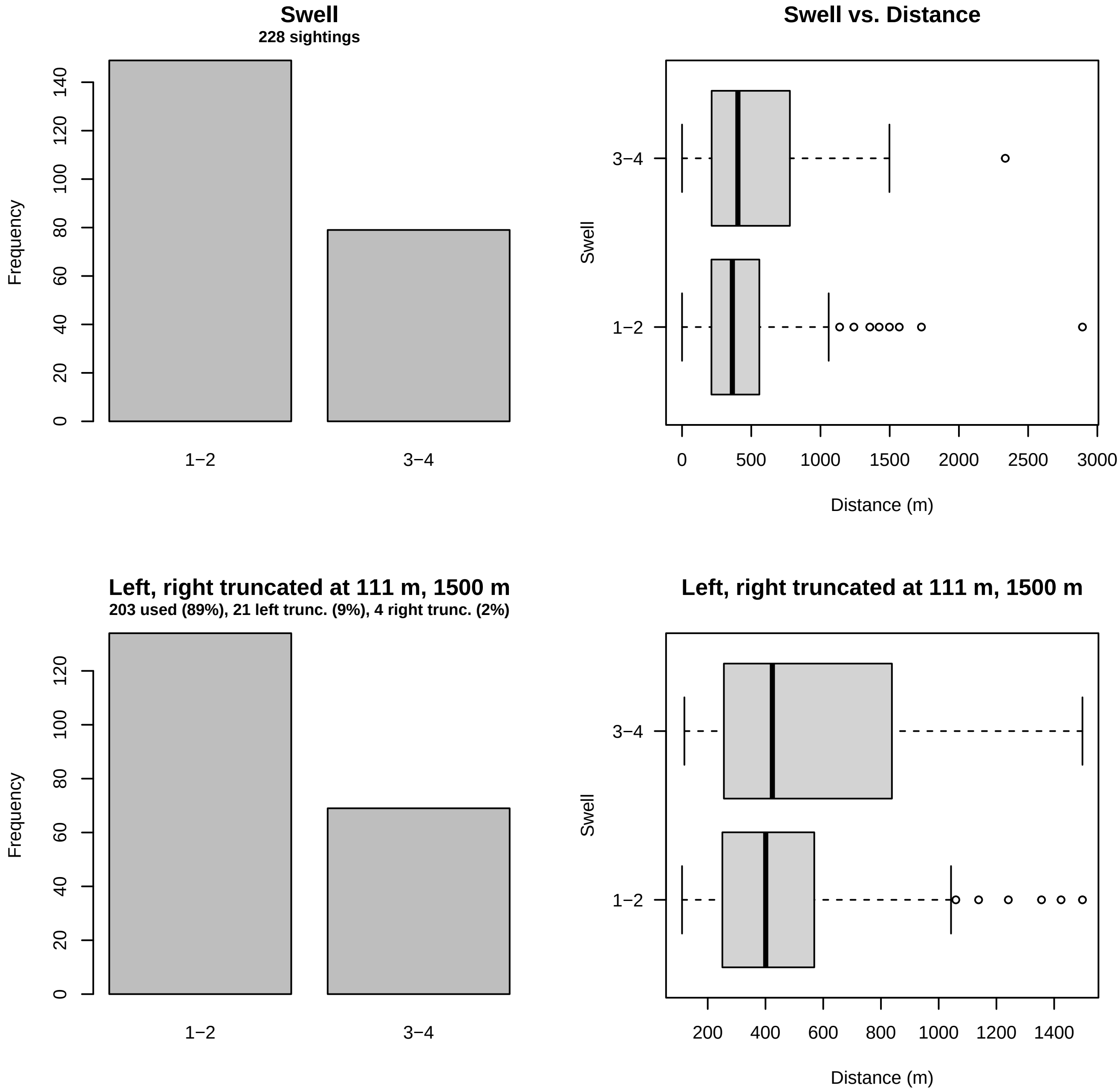

Figure 51: Distribution of the Swell covariate before (top row) and after (bottom row) observations were truncated to fit the HDR detection function.

3.2.2 Shipboard Surveys

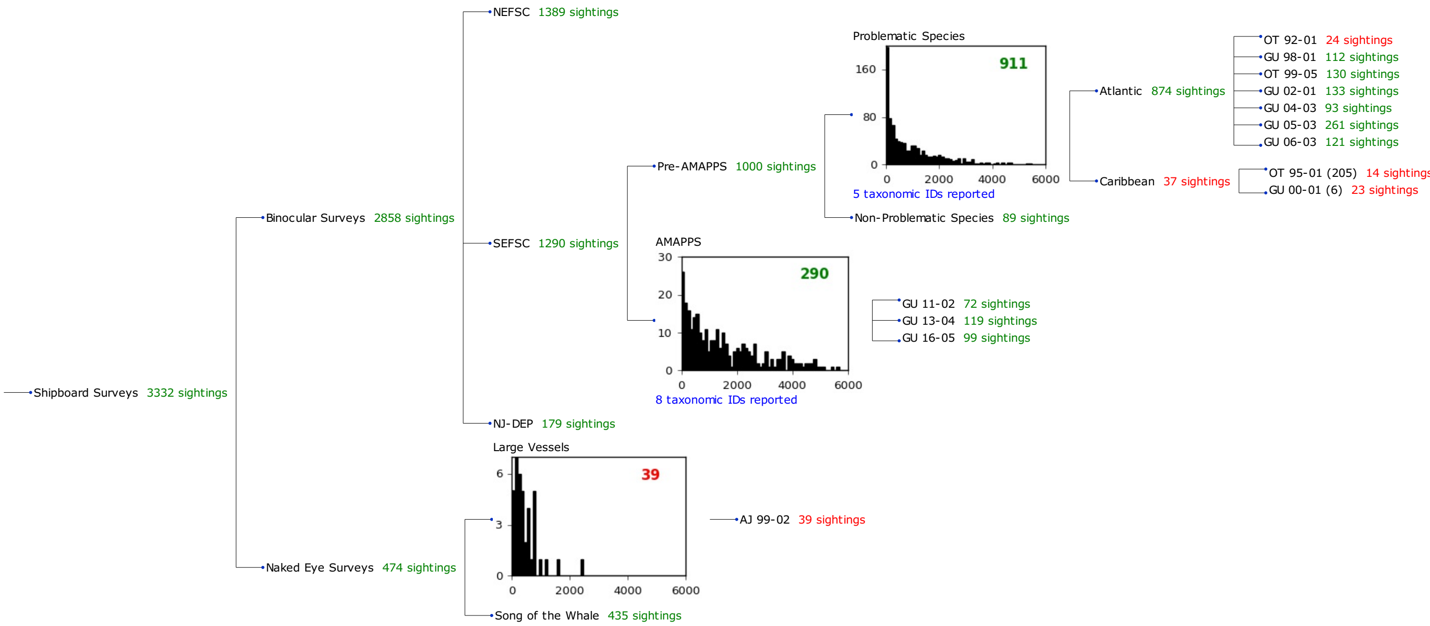

Figure 52: Detection hierarchy for shipboard surveys, showing how they were pooled during detectability modeling, for detection functions that pooled multiple taxa but could not use a taxonomic covariate to account for differences between them. Each histogram represents a detection function and summarizes the perpendicular distances of observations that were pooled to fit it, prior to truncation. Observation counts, also prior to truncation, are shown in green when they met the recommendation of Buckland et al. (2001) that detection functions utilize at least 60 sightings, and red otherwise. For rare taxa, it was not always possible to meet this recommendation, yielding higher statistical uncertainty. During the spatial modeling stage of the analysis, effective strip widths were computed for each survey using the closest detection function above it in the hierarchy (i.e. moving from right to left in the figure). Surveys that do not have a detection function above them in this figure were either addressed by a detection function presented in a different section of this report, or were omitted from the analysis.

3.2.2.1 SEFSC Pre-AMAPPS Problematic Species

After right-truncating observations greater than 4000 m and left-truncating observations less than 200 m (Figure 54), we fitted the detection function to the 616 observations that remained (Table 21). The selected detection function (Figure 53) used a hazard rate key function with Beaufort (Figure 55) and VesselName (Figure 56) as covariates.

Table 21: Observations used to fit the SEFSC Pre-AMAPPS Problematic Species detection function.

ScientificName	n
Delphinus delphis	34
Stenella attenuata	14
Stenella frontalis	262
Steno bredanensis	4
Tursiops truncatus	302
Total	**616**

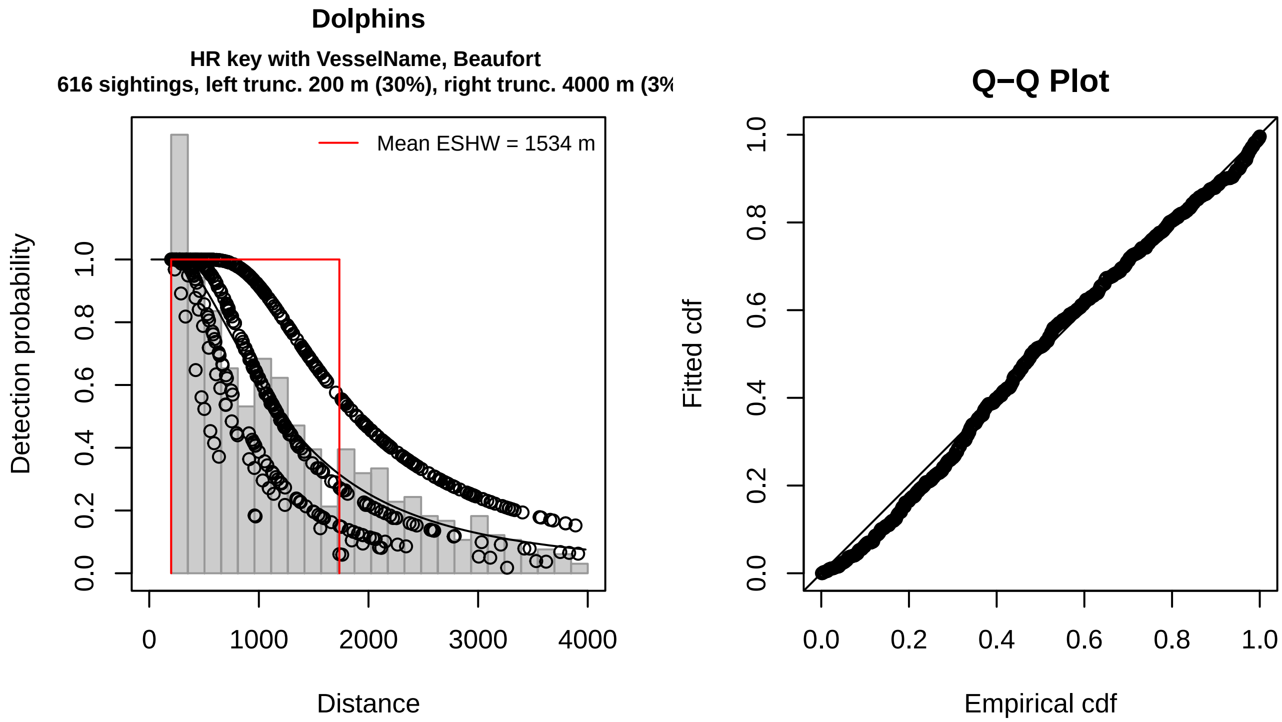

Figure 53: SEFSC Pre-AMAPPS Problematic Species detection function and Q-Q plot showing its goodness of fit.

Statistical output for this detection function:

```
Summary for ds object
Number of observations :  616
Distance range         :  200  -  4000
AIC                    :  9753.004

Detection function:
 Hazard-rate key function

Detection function parameters
Scale coefficient(s):
                      estimate         se
(Intercept)          7.3628462 0.09422017
VesselNameOregon II -0.4793018 0.17480366
Beaufort3           -0.4668391 0.14302976
Beaufort4-5         -0.8137669 0.16103824

Shape coefficient(s):
            estimate         se
(Intercept) 0.689867 0.09372714

                        Estimate           SE         CV
Average p              0.3555714   0.02671315 0.07512737
N in covered region 1732.4228173 142.52885613 0.08227140

Distance sampling Cramer-von Mises test (unweighted)
Test statistic = 0.313292  p = 0.124062
```

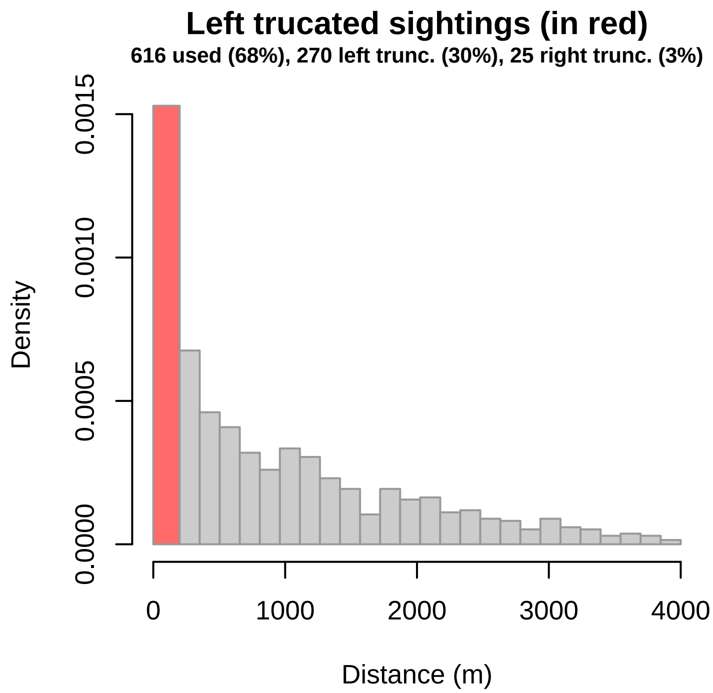

Figure 54: Density histogram of observations used to fit the SEFSC Pre-AMAPPS Problematic Species detection function, with the left-most bar showing observations at distances less than 200 m, which were left-truncated and not used to fit the detection function. (This bar may be very short if there were very few left-truncated sightings, or very narrow if the left truncation distance was very small; in either case it may not appear red.) These were excluded because they formed a problematic "spike" in detections close to the trackline, suggesting that animals approached the vessel (e.g. to bow-ride) prior to being detected. To address this, we fitted the detection function to the observations beyond the spike and assumed that within it, detection probability was 1, effectively treating it like a strip transect. We then added the left-truncated observations back into the analysis as if they occurred in this strip. This treatment may have resulted in an underestimation of detection probability.

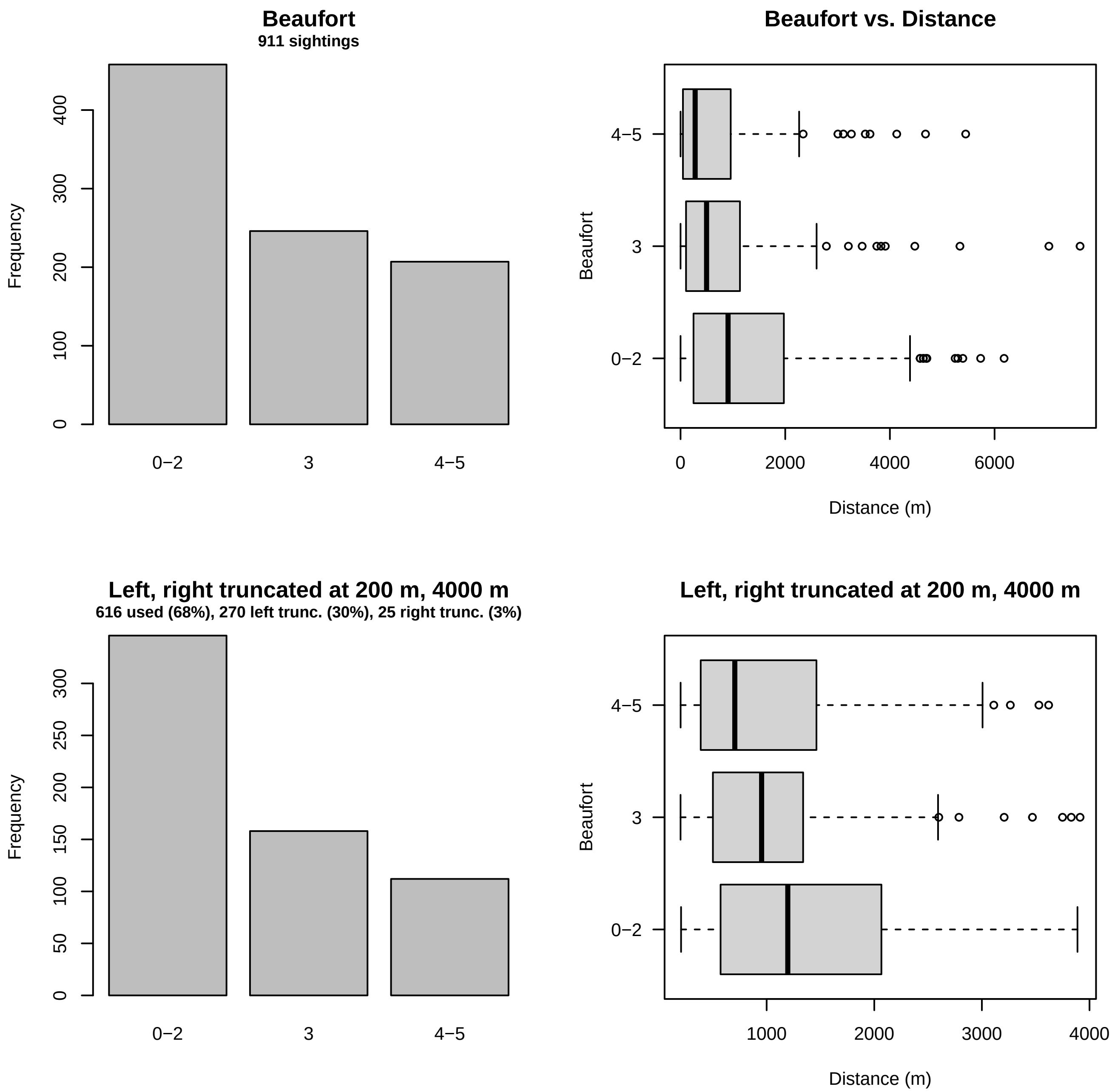

Figure 55: Distribution of the Beaufort covariate before (top row) and after (bottom row) observations were truncated to fit the SEFSC Pre-AMAPPS Problematic Species detection function.

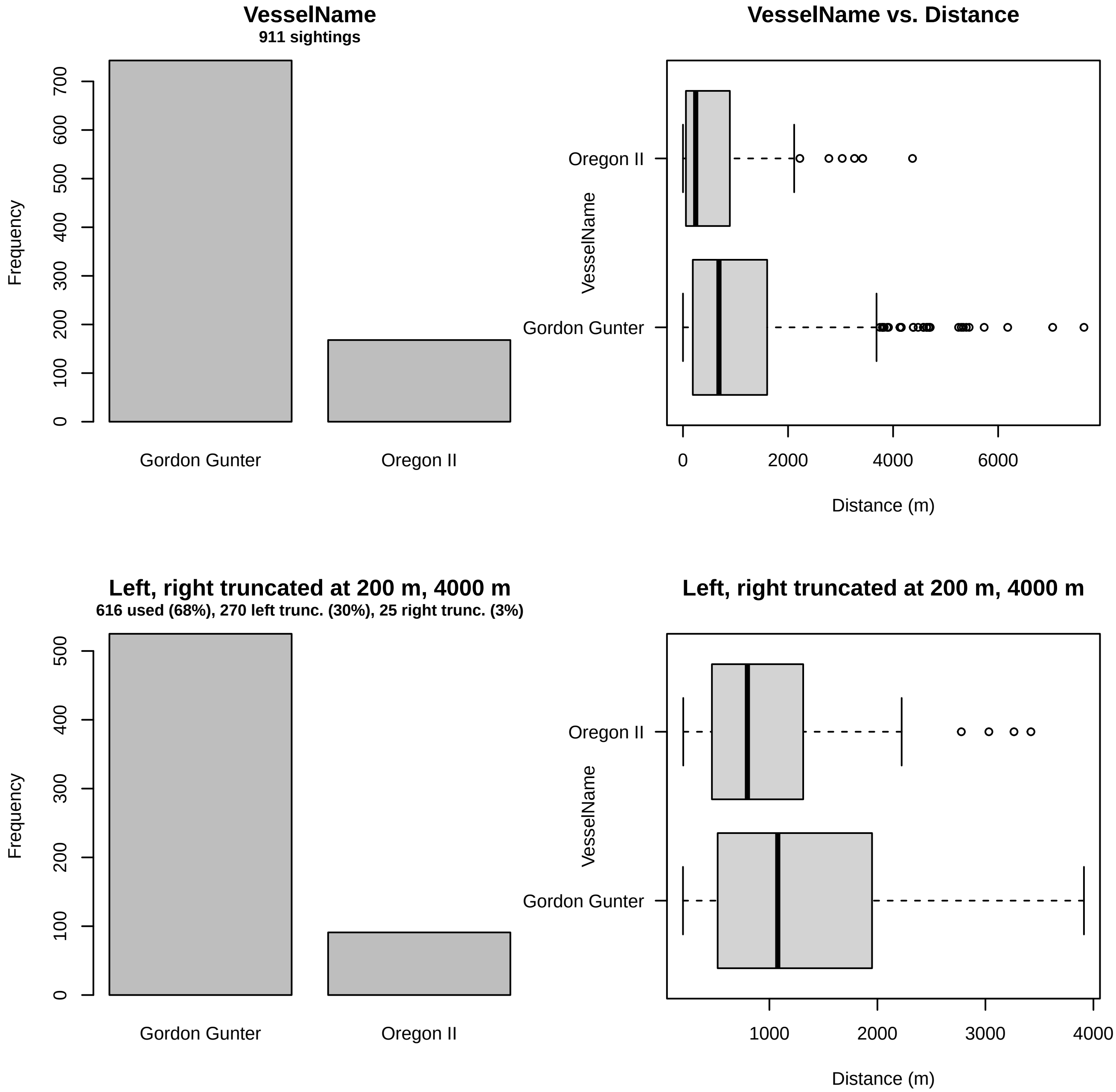

Figure 56: Distribution of the VesselName covariate before (top row) and after (bottom row) observations were truncated to fit the SEFSC Pre-AMAPPS Problematic Species detection function.

3.2.2.2 SEFSC AMAPPS

After right-truncating observations greater than 5000 m, we fitted the detection function to the 284 observations that remained (Table 22). The selected detection function (Figure 57) used a hazard rate key function with Beaufort (Figure 58) as a covariate.

Table 22: Observations used to fit the SEFSC AMAPPS detection function.

ScientificName	n
Delphinus delphis	2
Stenella attenuata	10
Stenella clymene	3
Stenella coeruleoalba	11
Stenella frontalis	84
Stenella longirostris	1
Steno bredanensis	2
Tursiops truncatus	171
Total	**284**

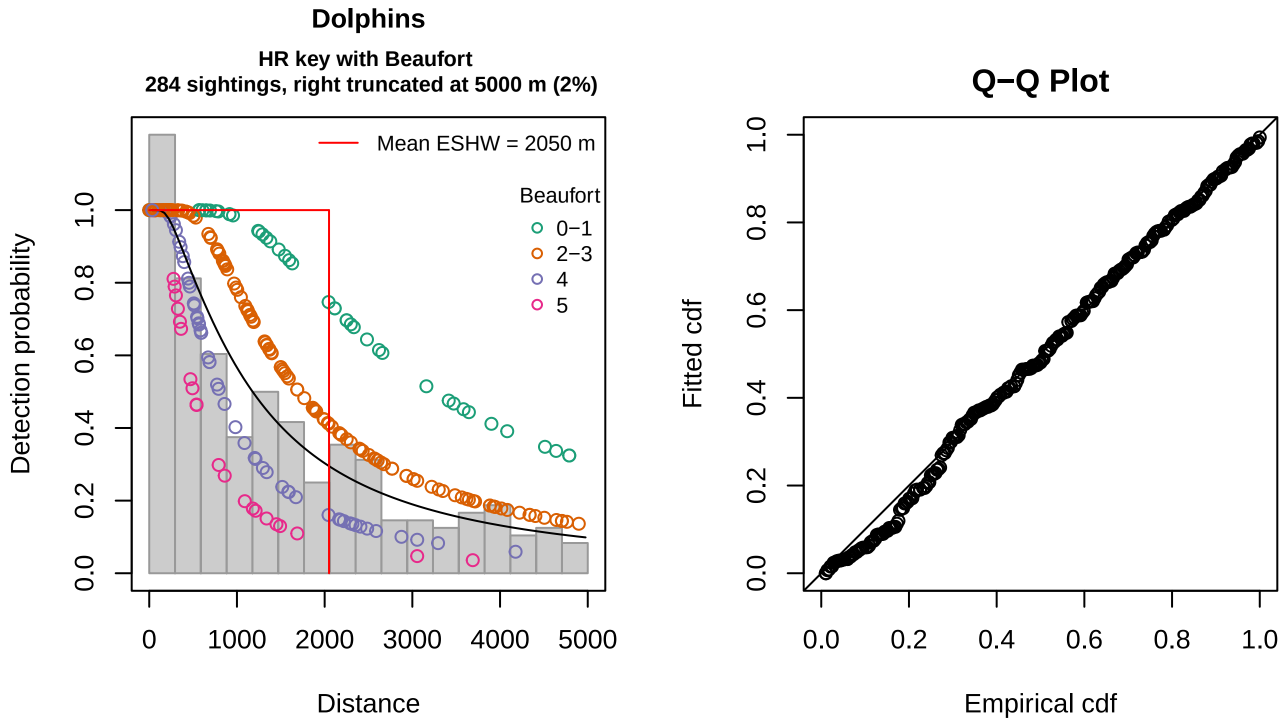

Figure 57: SEFSC AMAPPS detection function and Q-Q plot showing its goodness of fit.

Statistical output for this detection function:

```
Summary for ds object
Number of observations :  284
Distance range         :  0  -  5000
AIC                    :  4678.464

Detection function:
 Hazard-rate key function

Detection function parameters
Scale coefficient(s):
              estimate        se
(Intercept)  7.8386611 0.3487749
Beaufort2-3 -0.6450433 0.3816484
Beaufort4   -1.3990617 0.4441169
Beaufort5   -1.8689041 0.5186901
```

```
Shape coefficient(s):
             estimate        se
(Intercept) 0.3878689 0.1380351

                        Estimate           SE        CV
Average p              0.3478259   0.03965009 0.1139941
N in covered region 816.5004271 101.68622285 0.1245391

Distance sampling Cramer-von Mises test (unweighted)
Test statistic = 0.107898  p = 0.547527
```

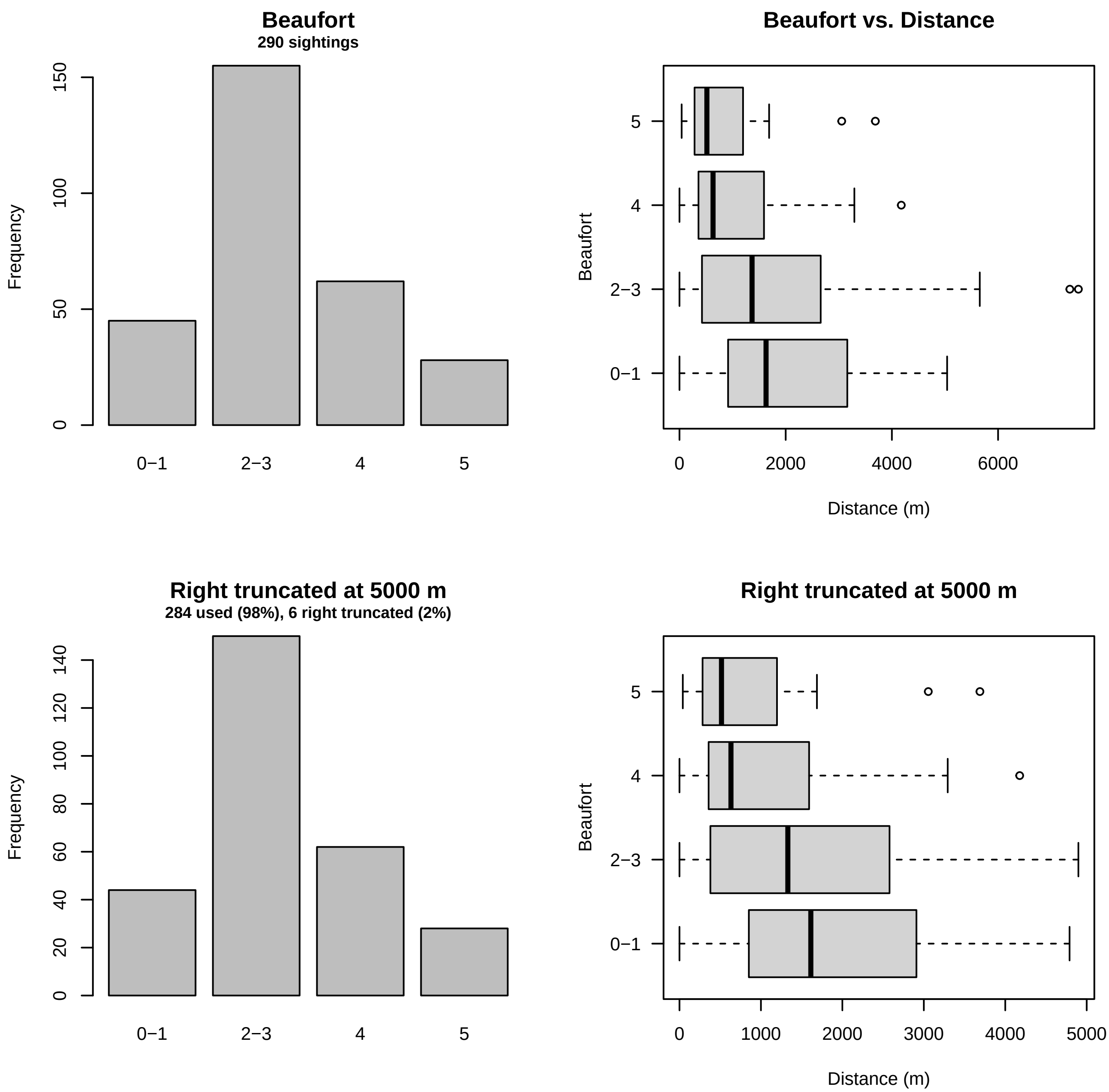

Figure 58: Distribution of the Beaufort covariate before (top row) and after (bottom row) observations were truncated to fit the SEFSC AMAPPS detection function.

3.2.2.3 Large Vessels

After right-truncating observations greater than 1100 m, we fitted the detection function to the 36 observations that remained (Table 23). The selected detection function (Figure 59) used a half normal key function with no covariates.

Table 23: Observations used to fit the Large Vessels detection function.

ScientificName	n
Lagenorhynchus acutus	36
Total	**36**

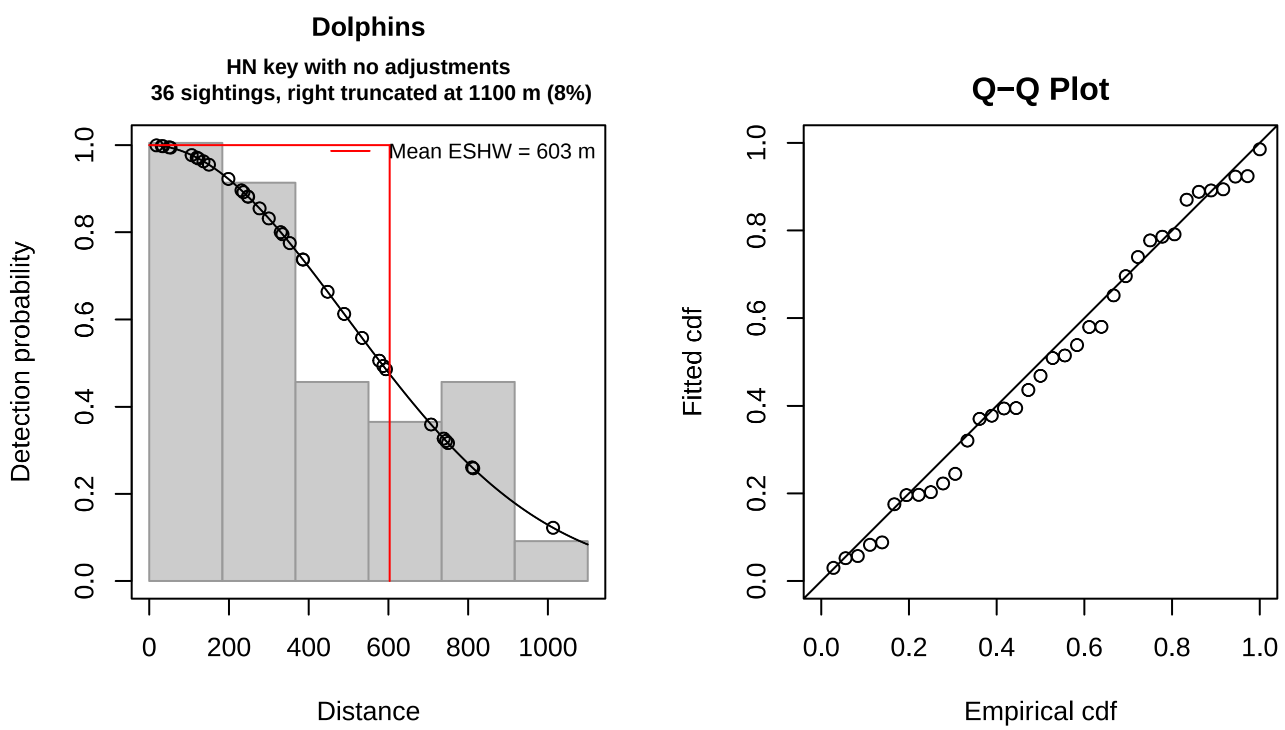

Figure 59: Large Vessels detection function and Q-Q plot showing its goodness of fit.

Statistical output for this detection function:

```
Summary for ds object
Number of observations :  36
Distance range         :  0  -  1100
AIC                    :  493.4472

Detection function:
 Half-normal key function

Detection function parameters
Scale coefficient(s):
            estimate        se
(Intercept) 6.202683 0.1646341

                      Estimate          SE        CV
Average p            0.5483057  0.07646146 0.1394504
N in covered region 65.6568085 11.74385160 0.1788672

Distance sampling Cramer-von Mises test (unweighted)
Test statistic = 0.026241  p = 0.986825
```

4 Bias Corrections

Density surface modeling methodology uses *distance sampling* (Buckland et al. 2001) to model the probability that an observer on a line transect survey will detect an animal given the perpendicular distance to it from the transect line. Distance sampling assumes that detection probability is 1 when perpendicular distance is 0. When this assumption is not met, detection probability is biased high, leading to an underestimation of density and abundance. This is known as the $g_0 < 1$ problem, where g_0 refers to the detection probability at distance 0. Modelers often try to address this problem by estimating g_0 empirically and dividing it into estimated density or abundance, thereby correcting those estimates to account for the animals that were presumed missed.

Two important sources of bias for visual surveys are known as *availability bias*, in which an animal was present on the transect line but impossible to detect, e.g. because it was under water, and *perception bias*, in which an animal was present and available but not noticed, e.g. because of its small size or cryptic coloration or behavior (Marsh and Sinclair 1989). Modelers often estimate the influence of these two sources of bias on detection probability independently, yielding two estimates of g_0, hereafter referred to as g_{0A} and g_{0P}, and multiply them together to obtain a final, combined estimate: $g_0 = g_{0A} \cdot g_{0P}$.

Our overall approach was to perform this correction on a per-observation basis, to have the flexibility to account for many factors such as platform type, surveyor institution, group size, group composition (e.g. singleton, mother-calf pair, or surface active group), and geographic location (e.g. feeding grounds vs. calving grounds). The level of complexity of the corrections varied by species according to the amount of information available, with North Atlantic right whale having the most elaborate corrections, derived from a substantial set of publications documenting its behavior, and various lesser known odontocetes having corrections based only on platform type (aerial or shipboard), derived from comparatively sparse information. Here we document the corrections used for short-beaked common dolphin.

4.1 Aerial Surveys

Palka et al. (2021) developed perception bias corrections using two team, mark recapture distance sampling (MRDS) methodology (Burt et al. 2014) for aerial surveys conducted in 2010-2017 by NOAA NEFSC and SEFSC during the AMAPPS program. These were the only extant perception bias estimates developed from aerial surveys used in our analysis, aside from estimates developed earlier by Palka and colleagues (Palka 2006; Palka et al. 2017). Those earlier efforts utilized older methods and less data than their 2021 analysis, so we applied the Palka et al. (2021) estimates to all aerial survey programs (Table 24).

We applied Palka's estimate for SEFSC to all programs other than NEFSC, as those programs mainly occurred to the south of NEFSC's study area, and overlapped more with SEFSC's. Also, short-beaked common dolphin group sizes were larger in the southerly programs, better matching SEFSC's group sizes than NEFSC's (Table 1). Given that larger groups are easier to detect than smaller groups, it was appropriate to apply SEFSC's weaker correction. However, for all surveys, to account for the influence of large group sizes on perception bias, we followed Carretta et al. (2000) and set the perception bias correction factor for sightings of more than 25 animals to $g_{0P} = 0.994$.

We caution that it is possible that perception bias was different on the other aerial programs, as they often used different aircraft, flew at different altitudes, and were staffed by different personnel. Of particular concern are that many programs flew Cessna 337 Skymasters, which had flat windows, while NOAA flew de Havilland Twin Otters, which had bubble windows, which likely afforded a better view of the transect line and therefore might have required less of a correction than the Skymasters. Correcting the other programs using NOAA's estimate as we have done is likely to yield less bias than leaving them uncorrected, but we urge all programs to undertake their own efforts to estimate perception bias, as resources allow.

We estimated availability bias corrections using the Laake et al. (1997) estimator and dive intervals reported by Palka et al. (2017) (Table 25). To estimate time in view, needed by the Laake estimator, we used results reported by Robertson et al. (2015), rescaled linearly for each survey program according to its target altitude and speed. We caution that Robertson's analysis was done for a de Havilland Twin Otter, which may have a different field of view than that of the other aircraft used here, which mainly comprised Cessna 337 Skymasters with flat windows. However, we note that McLellan et al. (2018) conducted a sensitivity analysis on the influence of the length of the "window of opportunity" to view beaked whales from a Cessna Skymaster on their final density estimates and found that they varied by only a few thousandths of an animal per kilometer when the window of opportunity more than doubled. Still, we urge additional program-specific research into estimation of availability bias.

To address the influence of group size on availability bias, we applied the group availability estimator of McLellan et al. (2018) on a per-observation basis. Following Palka et al. (2021), who also used that method, we assumed that individuals in the group dived asynchronously. The resulting g_{0A} corrections ranged from about 0.6 to 1.0 (Figure 60), with the large majority of observations having a correction of 0.95 or higher, owing to large group sizes. We caution that the assumption of asynchronous diving can lead to an underestimation of density and abundance if diving is actually synchronous; see McLellan et al. (2018) for an exploration of this effect. However, if future research finds that this species conducts synchronous dives and characterizes the degree of synchronicity, the model can be updated to account for this knowledge.

Table 24: Perception bias corrections for short-beaked common dolphin applied to aerial surveys.

Surveys	Group Size	g_{0P}	g_{0P} Source
NEFSC	≤ 25	0.560	Palka et al. (2021): NEFSC
All others	≤ 25	0.780	Palka et al. (2021): SEFSC
All	> 25	0.994	Carretta et al. (2000)

Table 25: Surface and dive intervals for short-beaked common dolphin used to estimate availability bias corrections.

Surface Interval (s)	Dive Interval (s)	Source
44	59.4	Palka et al. (2017)

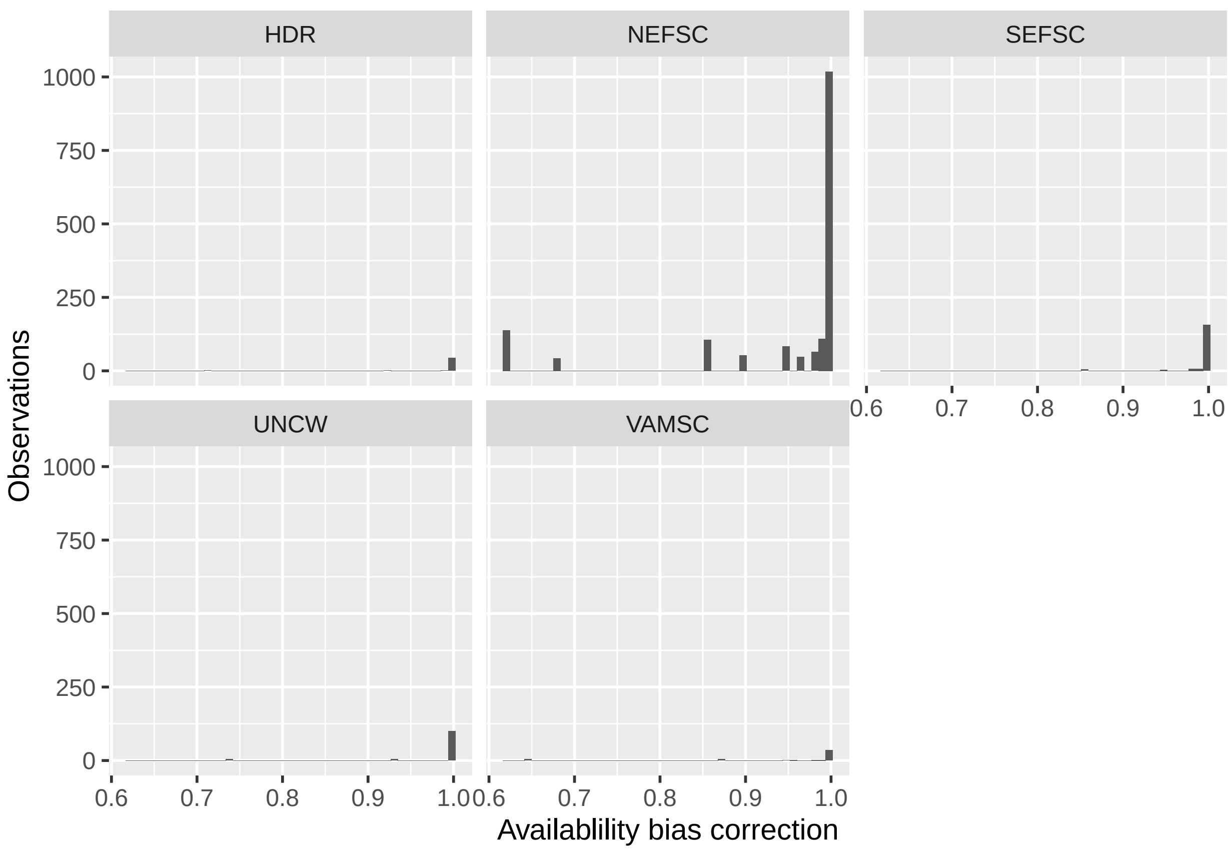

Figure 60: Availability bias corrections for short-beaked common dolphin for aerial surveys, by institution.

4.2 Shipboard Surveys

Most of the shipboard surveys in our analysis used high-power (25x150), pedestal-mounted binoculars. Similar to aerial surveys, Palka et al. (2021) developed perception bias corrections using two team, MRDS methodology (Burt et al. 2014) for high-power binocular surveys conducted in 2010-2017 by NOAA NEFSC and SEFSC during the AMAPPS program. These were the only extant perception bias estimates developed from high-power binocular surveys used in our analysis, aside from estimates developed earlier by Palka and colleagues (Palka 2006; Palka et al. 2017). Those earlier efforts utilized older methods and less data than their 2021 analysis, so we applied the Palka et al. (2021) estimates to all shipboard surveys that searched with high-power binoculars (Table 26).

A few surveys used naked eyes rather than high-power binoculars, but none of these programs prepared perception bias estimates for short-beaked common dolphin. The best compatible estimate we located in the literature was from Cañadas et al. (2004), which was for a 36m modified long-liner fishing vessel that surveyed in the vicinity of the Faroese Islands. We applied this to all shipboard surveys that searched by naked eye (Table 26).

For all surveys, to account for the influence of large group sizes on perception bias, we followed Barlow and Forney (2007) and set the perception bias correction factor for sightings of more than 20 animals to $g_{0P} = 0.97$. Given that the dive interval of this species (Table 25) was short relative to the amount of time a given patch of water remained in view to shipboard observers, we assumed that no availability bias correction was needed ($g_{0A} = 1$), following Palka et al. (2021).

Table 26: Perception and availability bias corrections for short-beaked common dolphin applied to shipboard surveys.

Surveys	Searching Method	Group Size	g_{0P}	g_{0P} Source	g_{0A}	g_{0A} Source
NEFSC, NJDEP	Binoculars	≤ 20	0.520	Palka et al. (2021): NEFSC	1	Assumed
SEFSC	Binoculars	≤ 20	0.620	Palka et al. (2021): SEFSC	1	Assumed
NEFSC, MCR	Naked eye	≤ 20	0.796	Cañadas et al. (2004)	1	Assumed
All	All	> 20	0.970	Barlow and Forney (2007)	1	Assumed

5 Density Model

Short-beaked common dolphins are widely distributed in temperate and sub-tropical waters (Hayes et al. 2022). Jefferson et al. (2009) conducted a comprehensive review of the species' distribution in the western North Atlantic. According to this study, in recent decades off the North American east coast, short-beaked common dolphins were found mainly in cooler waters, ranging between the 200m and 2000m isobaths from at least Cape Hatteras north to 47-50 N off the Canadian coast. The authors reported that this may be a change from the first half of the 20th century, in which short-beaked common dolphins were believed to be more common in the waters of the southeast U.S. as far south as Florida, and speculated that the shift may be related to changes in water temperature, prey distributions resulting from oceanographic changes, or displacement by Stenella species.

Jefferson et al. (2009) described seasonal movements in our study area as follows. From January to May, short-beaked common dolphins regularly range north only as far as Georges Bank, then shift northwards in summer as waters warm into the Gulf of Maine, Scotian Shelf, and prominent bottom escarpments such as the Flemish Cap. They are extremely rare in the Bay of Fundy at all times but are common in slope waters of Nova Scotia in late summer and autumn and are frequently seen near the Gully Canyon at this time.

The surveys incorporated into our model, spanning 1998-2019 (see Section 1), reported sightings largely consistent with this description. Over 2500 sightings were reported (Figure 61), most between Cape Hatteras and Canada and concentrated along the continental shelf break, with numerous sightings over the shelf but very few beyond the upper continental slope. Although the described seasonal shift in sightings was apparent in monthly aggregate maps of surveys and sightings (see figures in Section 6.1), we could find no description in the literature that indicated a clear seasonal switch in the species' relationship to environmental covariates (as with certain baleen whales migrating between cold feeding grounds and warm calving grounds). Given that, we fitted a single year-round model that incorporated all available survey data.

The model selection procedure was straightforward. When ranked by REML score (Wood 2011), the highest ranked models with contemporaneous covariates outranked those with climatological covariates, and explained more than 2% more deviance. We selected the highest ranked model, which included seven covariates (Table 27). Relationships with bathymetric covariates indicated the highest marginal boosts to density at seafloor depths around 100m, close to submarine canyons, and at high seafloor slopes, all conditions that predominate along the continental shelf break (Figure 64). For sea surface temperature (SST), a positive effect on density was indicated for temperatures between 9-21 °C, roughly consistent with but slightly cooler than the range of 10.5-22.8 °C observed across 83 common dolphin sightings recorded by Gowans and Whitehead (1995) at the Gully. A positive effect was also indicated for bottom temperatures cooler than 16 °C, consistent with shelf waters north of Cape Hatteras and waters offshore, for locations close to SST fronts (and also far from them, but the confidence intervals enclosed zero), and for zooplankton biomass values that were neither extremely low nor extremely high.

5.1 Final Model

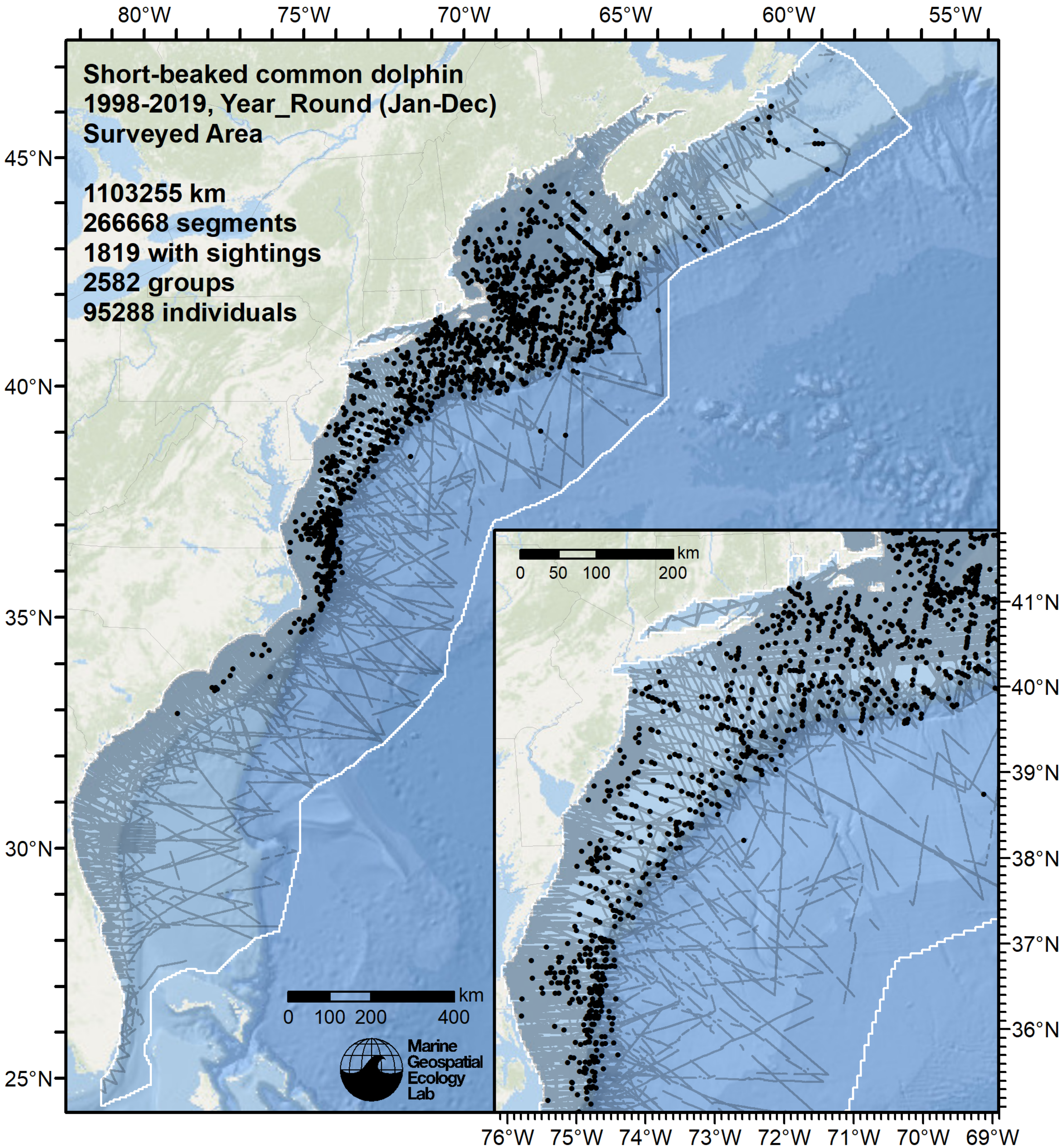

Figure 61: Survey segments used to fit the model. Black points indicate segments with observations.

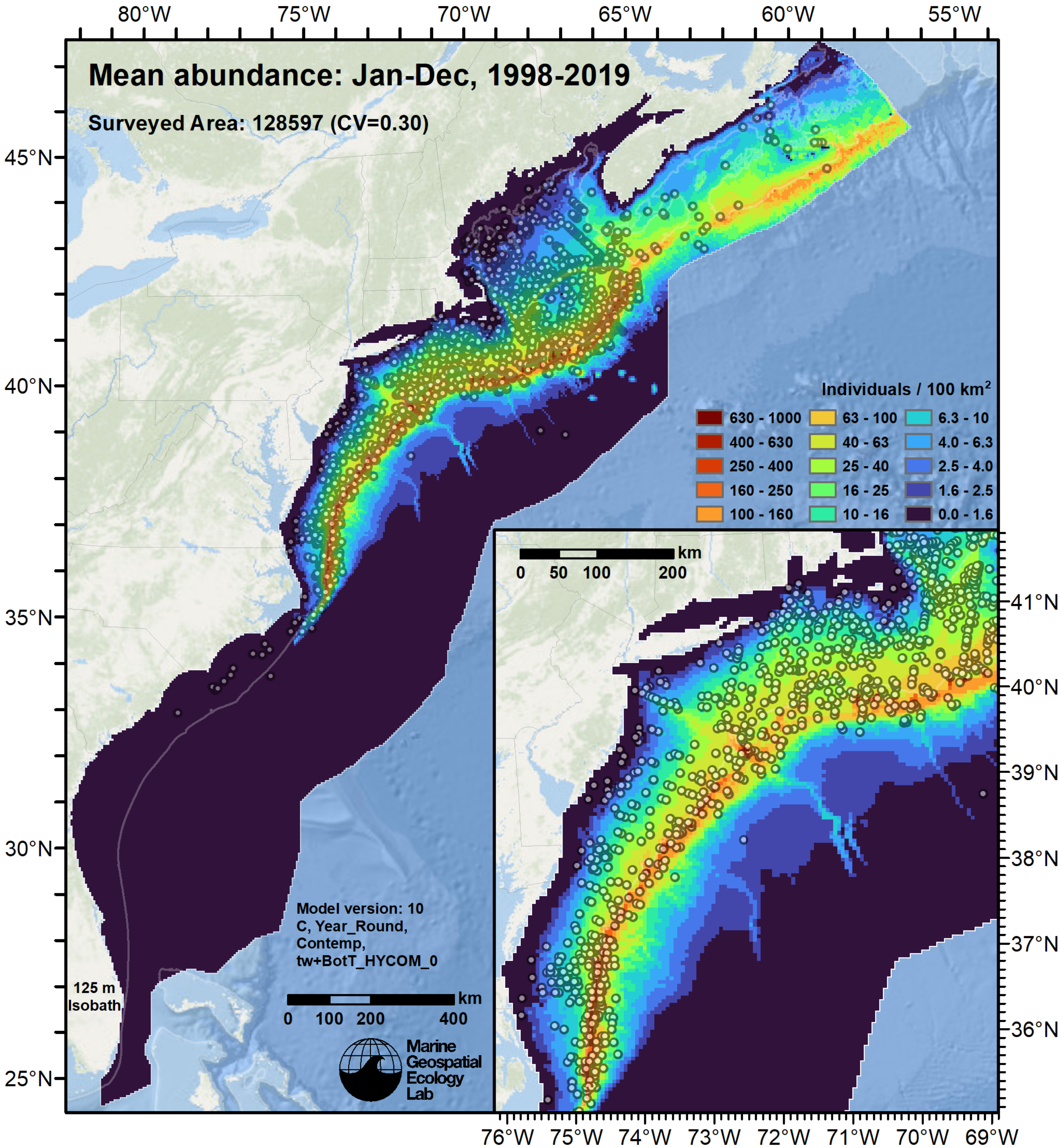

Figure 62: Short-beaked common dolphin mean density for the indicated period, as predicted by the model. Open circles indicate segments with observations. Mean total abundance and its coefficient of variation (CV) are given in the subtitle. Variance was estimated with the analytic approach given by Miller et al. (2022), Appendix S1, and accounts both for uncertainty in model parameter estimates and for seasonal and interannual variability in dynamic covariates.

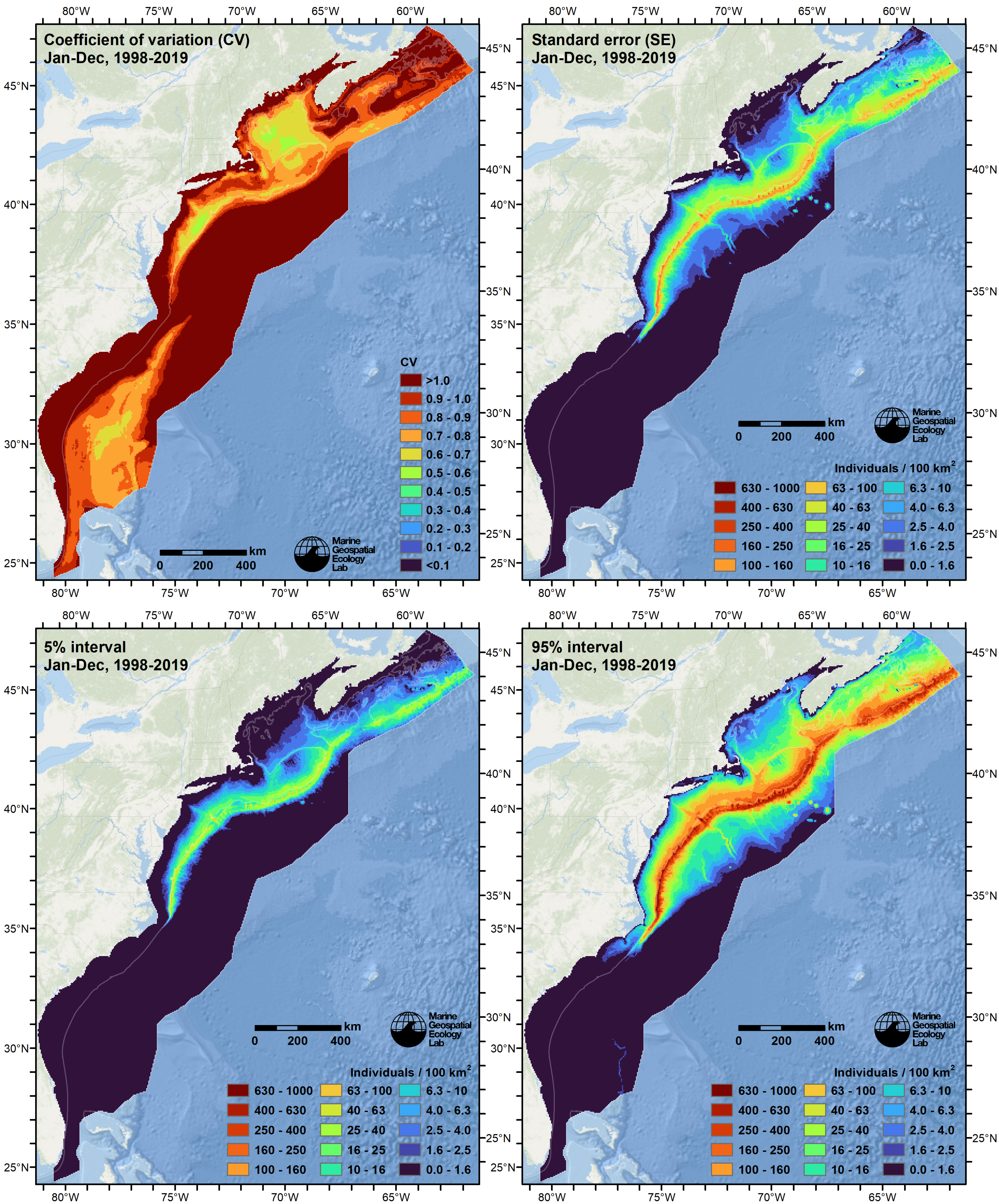

Figure 63: Uncertainty statistics for the short-beaked common dolphin mean density surface (Figure 62) predicted by the model. Variance was estimated with the analytic approach given by Miller et al. (2022), Appendix S1, and accounts both for uncertainty in model parameter estimates and for seasonal and interannual variability in dynamic covariates.

Statistical output for this model:

```
Family: Tweedie(p=1.485)
Link function: log

Formula:
IndividualsCorrected ~ offset(log(SegmentArea)) + s(log10(pmax(10,
    pmin(Depth, 4000))), bs = "ts") + s(pmin(I(DistToCan/1000),
    400), bs = "ts") + s(log10(pmax(0.03, pmin(Slope, 12))),
    bs = "ts") + s(pmax(3, pmin(SST_CMC, 30)), bs = "ts") + s(pmax(3,
    pmin(BotT_HYCOM, 27)), bs = "ts") + s(pmin(I(DistToFront105/1000),
    75), bs = "ts") + s(pmax(0.2, pmin(Zoo_SEAPODYM, 11)), bs = "ts")

Parametric coefficients:
            Estimate Std. Error t value Pr(>|t|)
(Intercept) -20.3879     0.2129  -95.74   <2e-16 ***
---
Signif. codes:  0 '***' 0.001 '**' 0.01 '*' 0.05 '.' 0.1 ' ' 1

Approximate significance of smooth terms:
                                        edf Ref.df      F  p-value
s(log10(pmax(10, pmin(Depth, 4000)))) 7.717      9 23.512  < 2e-16 ***
s(pmin(I(DistToCan/1000), 400))       1.787      9 32.224  < 2e-16 ***
s(log10(pmax(0.03, pmin(Slope, 12)))) 4.392      9  7.469  < 2e-16 ***
s(pmax(3, pmin(SST_CMC, 30)))         8.188      9 23.495  < 2e-16 ***
s(pmax(3, pmin(BotT_HYCOM, 27)))      5.995      9 26.148  < 2e-16 ***
s(pmin(I(DistToFront105/1000), 75))   2.976      9  2.736 4.03e-06 ***
s(pmax(0.2, pmin(Zoo_SEAPODYM, 11)))  7.386      9 38.073  < 2e-16 ***
---
Signif. codes:  0 '***' 0.001 '**' 0.01 '*' 0.05 '.' 0.1 ' ' 1

R-sq.(adj) =  0.0169   Deviance explained = 47.1%
-REML =  17961  Scale est. = 95.872    n = 266668

Method: REML   Optimizer: outer newton
full convergence after 13 iterations.
Gradient range [-7.790599e-05,3.913145e-05]
(score 17960.79 & scale 95.87226).
Hessian positive definite, eigenvalue range [0.4944907,5734.636].
Model rank =  64 / 64

Basis dimension (k) checking results. Low p-value (k-index<1) may
indicate that k is too low, especially if edf is close to k'.

                                        k'  edf k-index p-value
s(log10(pmax(10, pmin(Depth, 4000)))) 9.00 7.72    0.61  <2e-16 ***
s(pmin(I(DistToCan/1000), 400))       9.00 1.79    0.61  <2e-16 ***
s(log10(pmax(0.03, pmin(Slope, 12)))) 9.00 4.39    0.62   0.015 *
s(pmax(3, pmin(SST_CMC, 30)))         9.00 8.19    0.62   0.005 **
s(pmax(3, pmin(BotT_HYCOM, 27)))      9.00 5.99    0.60  <2e-16 ***
s(pmin(I(DistToFront105/1000), 75))   9.00 2.98    0.69   0.865
s(pmax(0.2, pmin(Zoo_SEAPODYM, 11)))  9.00 7.39    0.61  <2e-16 ***
---
Signif. codes:  0 '***' 0.001 '**' 0.01 '*' 0.05 '.' 0.1 ' ' 1
```

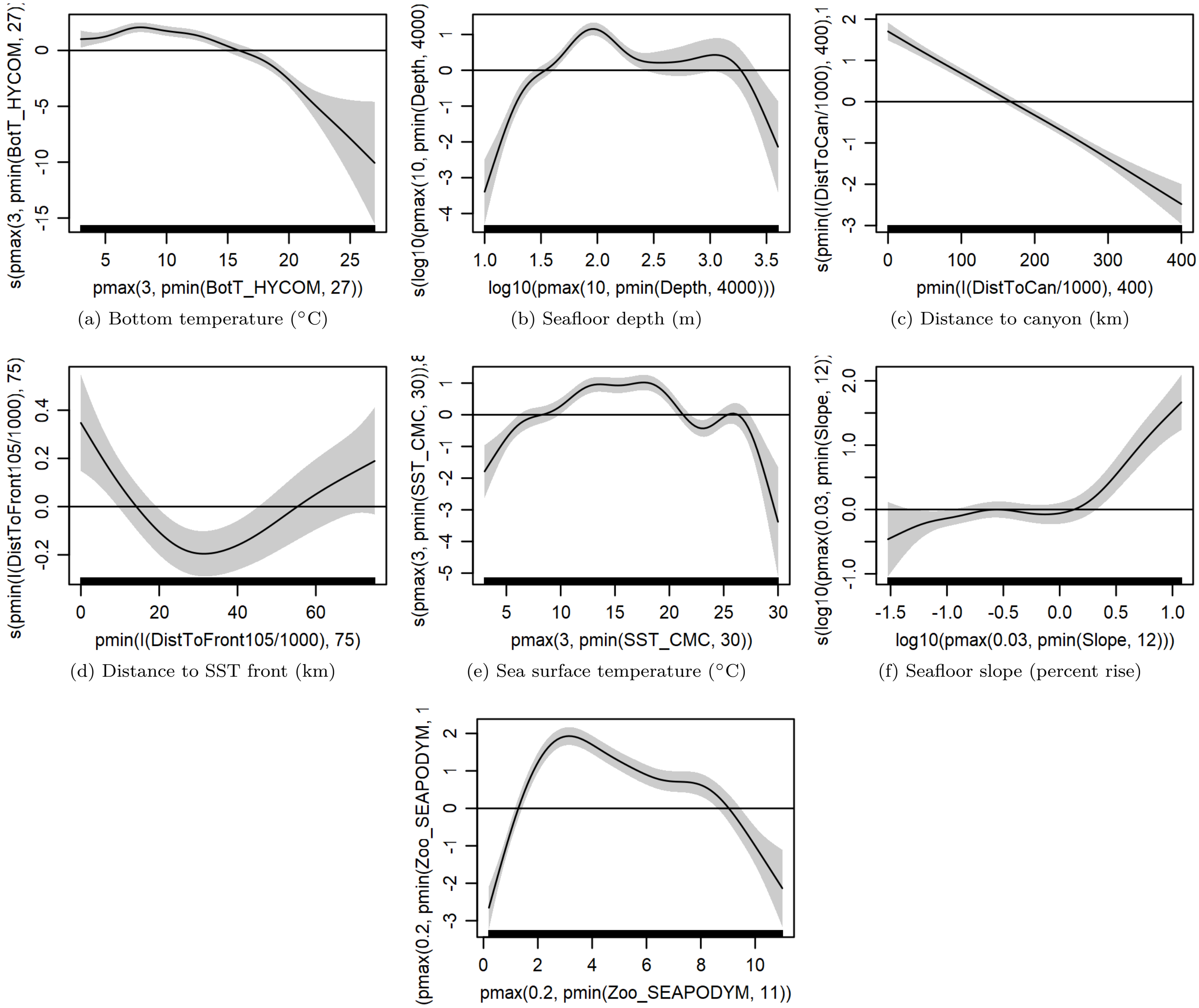

(a) Bottom temperature (°C)

(b) Seafloor depth (m)

(c) Distance to canyon (km)

(d) Distance to SST front (km)

(e) Sea surface temperature (°C)

(f) Seafloor slope (percent rise)

(g) Zooplankton biomass (g C m^{-2})

Figure 64: Functional plots for the final model. Transforms and other treatments are indicated in axis labels. *log10* indicates the covariate was $\log_{10}$ transformed. *pmax* and *pmin* indicate the covariate's minimum and maximum values, respectively, were Winsorized to the values shown. Winsorization was used to prevent runaway extrapolations during prediction when covariates exceeded sampled ranges, or for ecological reasons, depending on the covariate. */1000* indicates meters were transformed to kilometers for interpretation convenience.

Table 27: Covariates used in the final model.

Covariate	Description
BotT_HYCOM	Monthly mean bottom temperature (°C) from the HYCOM GOFS 3.1 1/12° ocean model (Chassignet et al. (2009))
Depth	Depth (m) of the seafloor, from SRTM30_PLUS (Becker et al. (2009))
DistToCan	Distance (km) to the closest submarine canyon, derived from the Harris et al. (2014) geomorphology

Table 27: Covariates used in the final model. *(continued)*

Covariate	Description
DistToFront105	Monthly mean distance (km) to the closest sea surface temperature front detected in daily GHRSST Level 4 CMC0.2deg and CMC0.1deg images (Brasnett (2008); Canada Meteorological Center (2012); Meissner et al. (2016); Canada Meteorological Center (2016)) with MGET's implementation of the Canny edge detector (Roberts et al. (2010); Canny (1986))
SST_CMC	Monthly mean sea surface temperature (°C) from GHRSST Level 4 CMC0.2deg and CMC0.1deg (Brasnett (2008); Canada Meteorological Center (2012); Meissner et al. (2016); Canada Meteorological Center (2016))
Slope	Slope (percent rise) of the seafloor, derived from SRTM30_PLUS (Becker et al. (2009))
Zoo_SEAPODYM	Monthly mean zooplankton biomass expressed in carbon (g C m^{-2}) from SEAPODYM (Lehodey et al. (2008); Lehodey et al. (2015)), provided by E.U. Copernicus Marine Service. doi: 10.48670/moi-00020

5.2 Diagnostic Plots

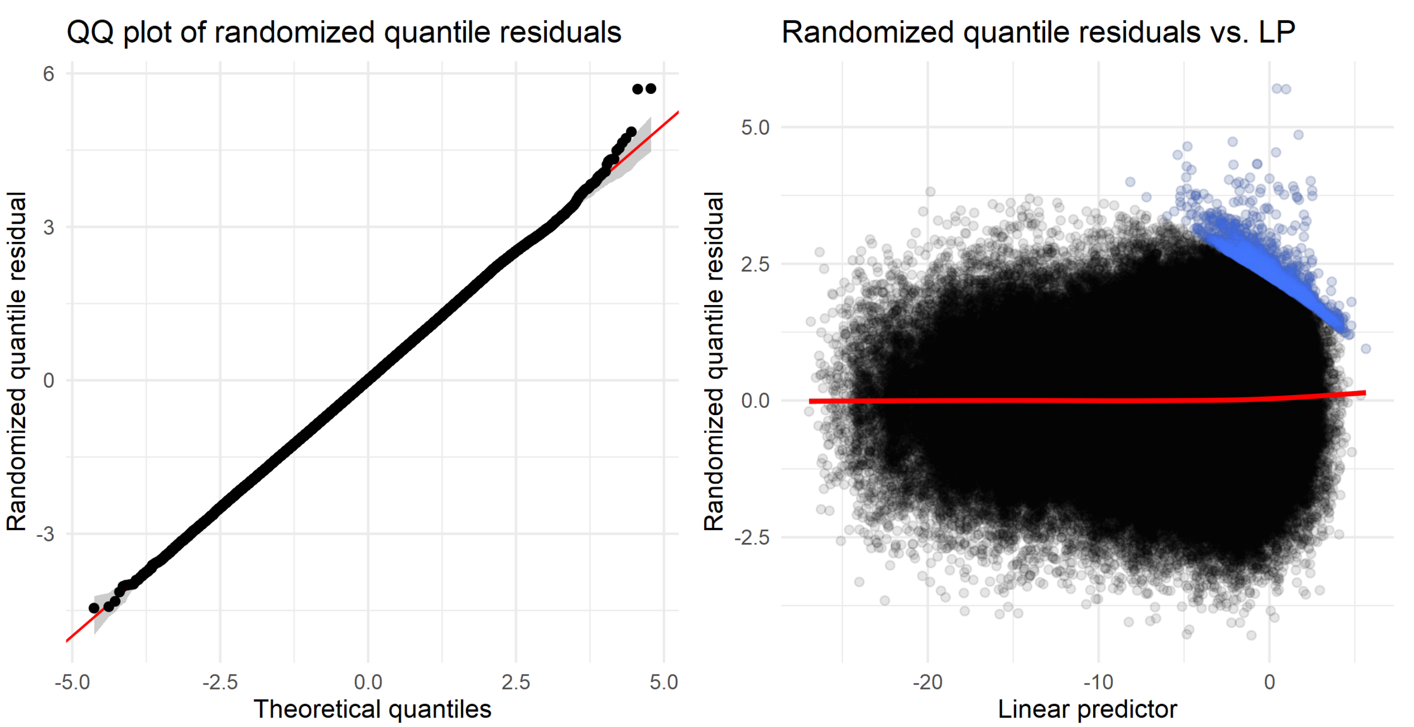

Figure 65: Residual plots for the final model.

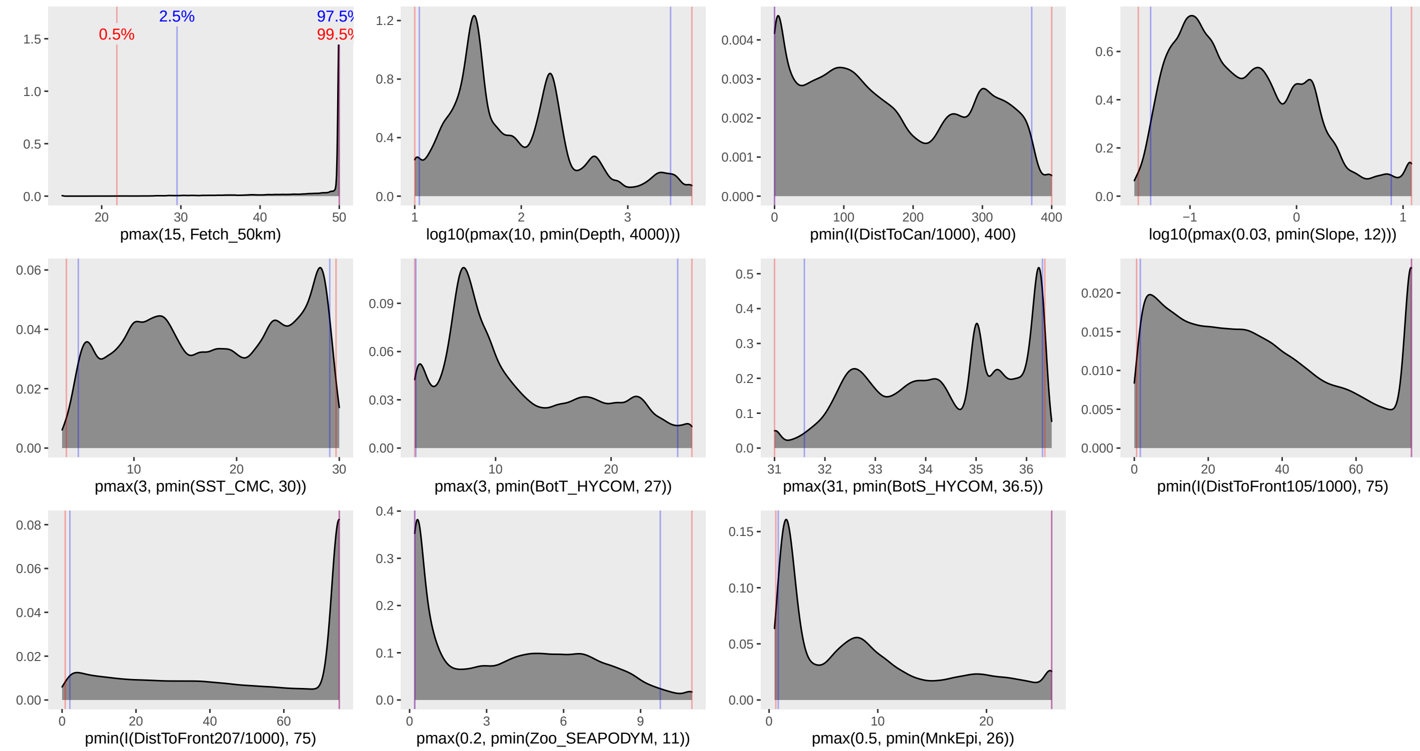

Figure 66: Density histograms showing the distributions of the covariates considered during the final model selection step. The final model may have included only a subset of the covariates shown here (see Figure 64), and additional covariates may have been considered in preceding selection steps. Red and blue lines enclose 99% and 95% of the distributions, respectively. Transforms and other treatments are indicated in axis labels. *log10* indicates the covariate was $\log_{10}$ transformed. *pmax* and *pmin* indicate the covariate's minimum and maximum values, respectively, were Winsorized to the values shown. Winsorization was used to prevent runaway extrapolations during prediction when covariates exceeded sampled ranges, or for ecological reasons, depending on the covariate. */1000* indicates meters were transformed to kilometers for interpretation convenience.

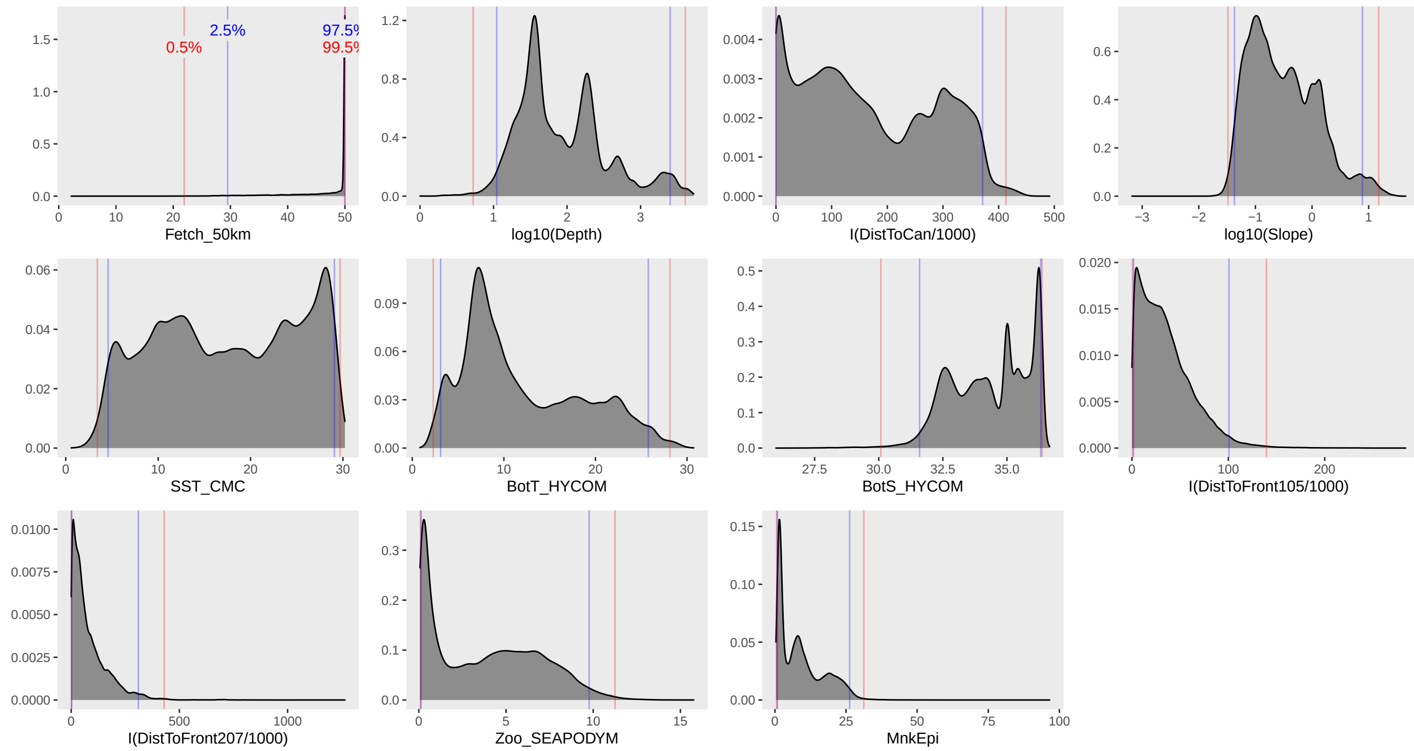

Figure 67: Density histograms shown in Figure 66 replotted without Winsorization, to show the full range of sampling represented by survey segments.

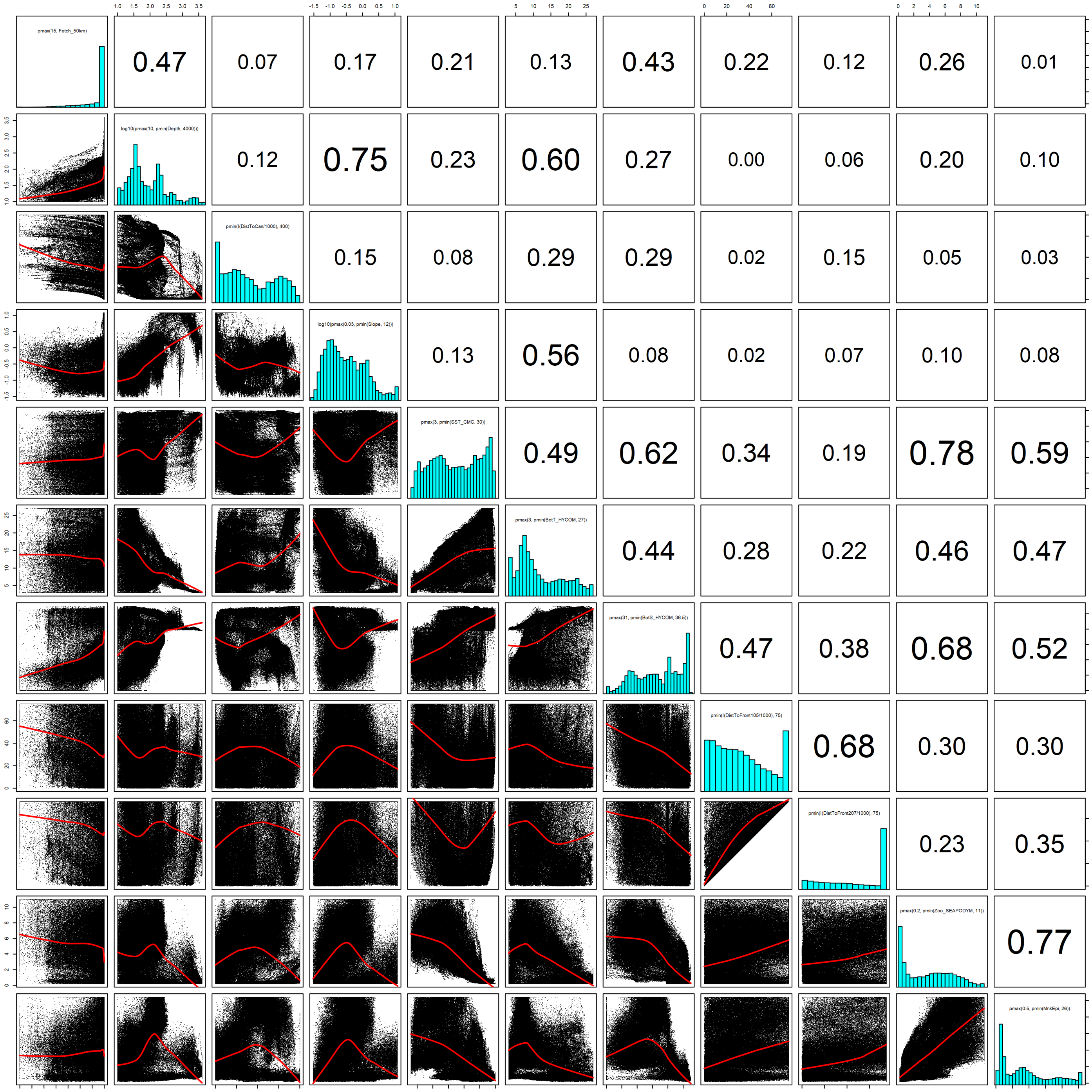

Figure 68: Scatterplot matrix of the covariates considered during the final model selection step. The final model may have included only a subset of the covariates shown here (see Figure 64), and additional covariates may have been considered in preceding selection steps. Covariates are transformed and Winsorized as shown in Figure 66. This plot is used to check simple correlations between covariates (via pairwise Pearson coefficients above the diagonal) and visually inspect for concurvity (via scatterplots and red lowess curves below the diagonal).

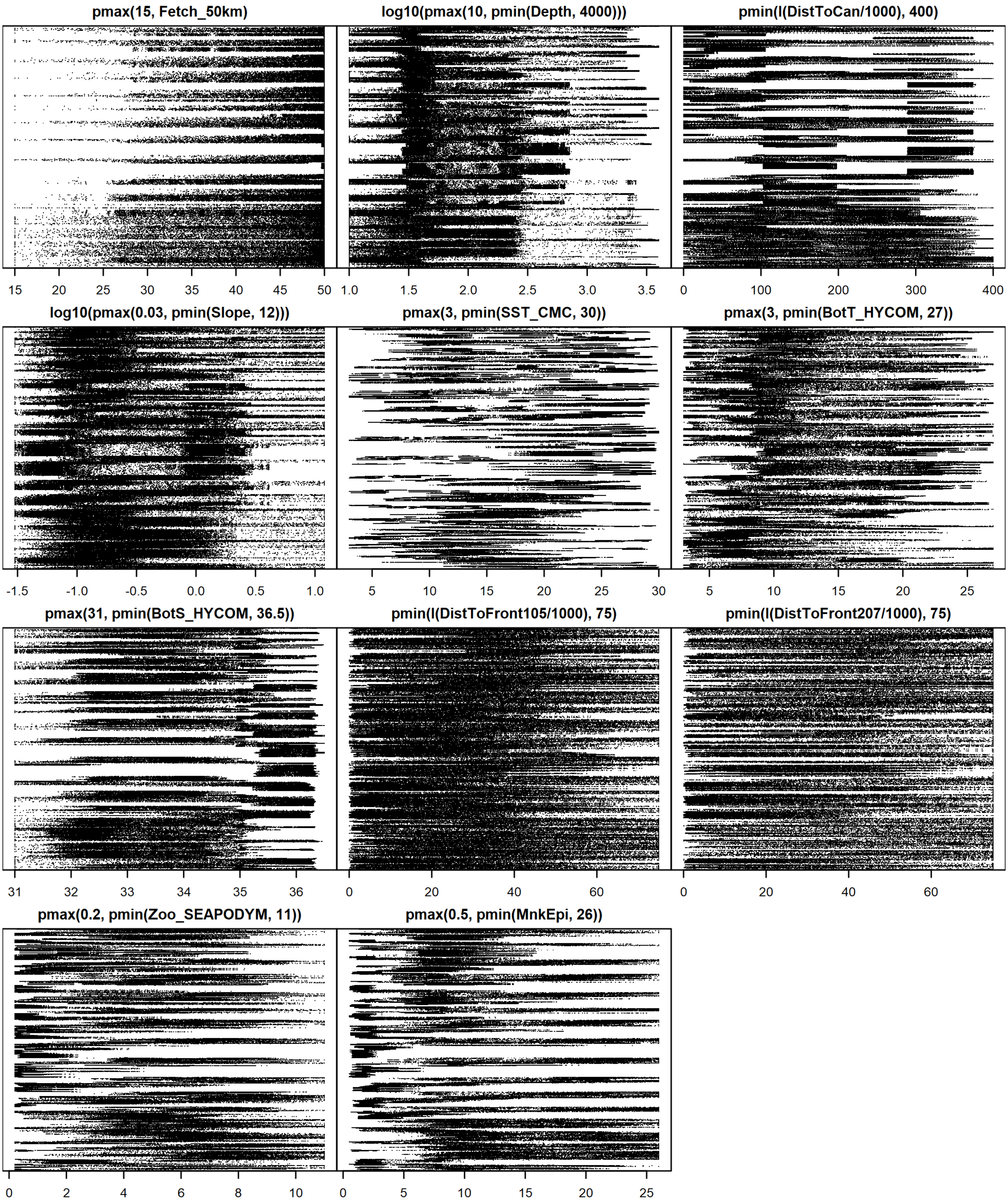

Figure 69: Dotplot of the covariates considered during the final model selection step. The final model may have included only a subset of the covariates shown here (see Figure 64), and additional covariates may have been considered in preceding selection steps. Covariates are transformed and Winsorized as shown in Figure 66. This plot is used to check for suspicious patterns and outliers in the data. Points are ordered vertically by segment ID, sequentially in time.

5.3 Extrapolation Diagnostics

5.3.1 Univariate Extrapolation

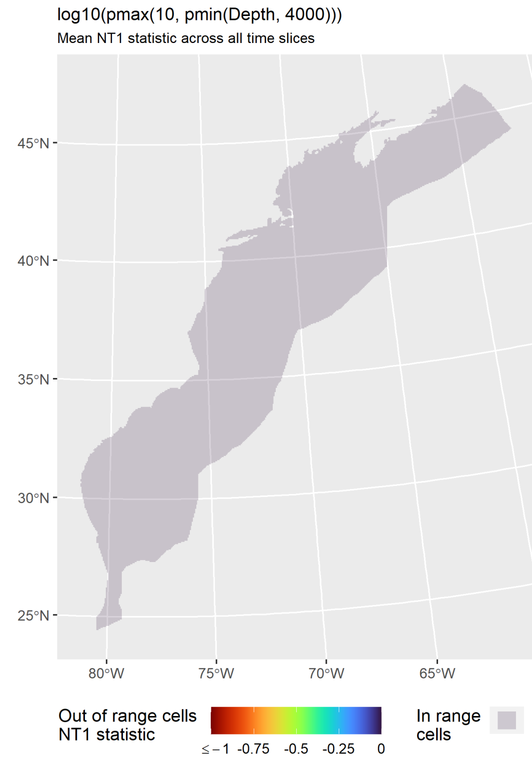

(a) Depth covariate

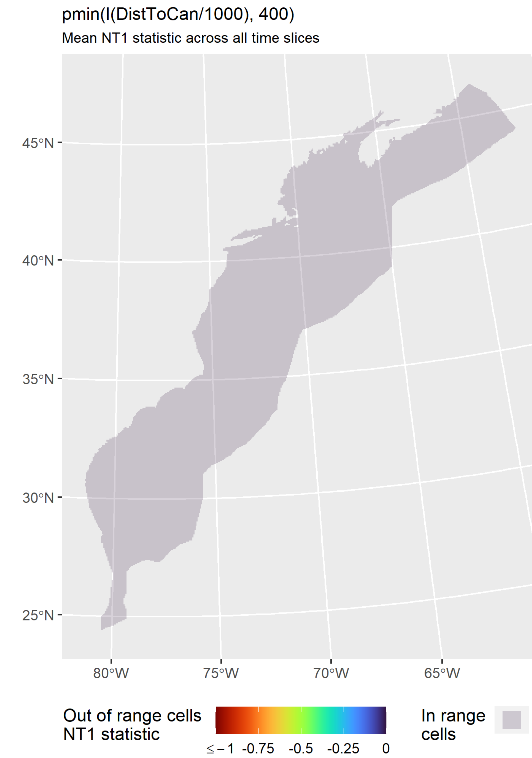

(b) DistToCan covariate

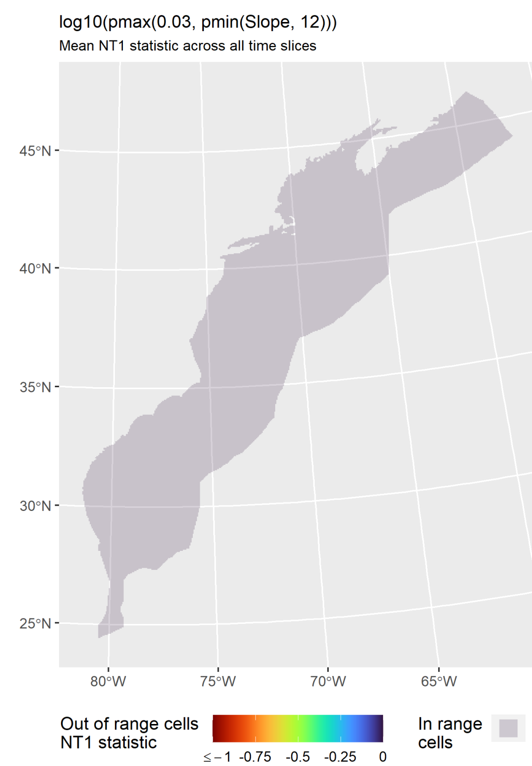

(c) Slope covariate

Figure 70: NT1 statistic (Mesgaran et al. (2014)) for static covariates used in the model. Areas outside the sampled range of a covariate appear in color, indicating univariate extrapolation of that covariate occurred there. Areas within the sampled range appear in gray, indicating it did not occur.

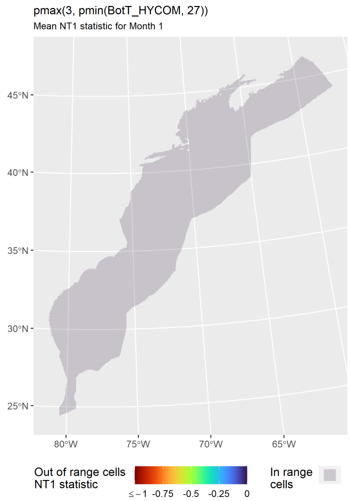

(a) January

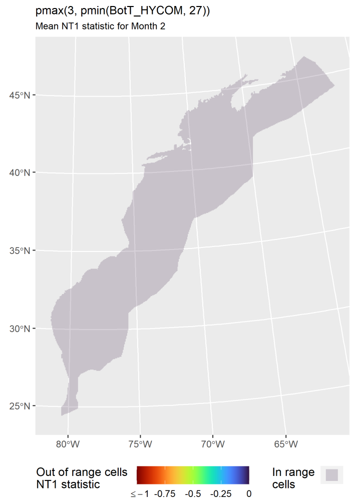

(b) February

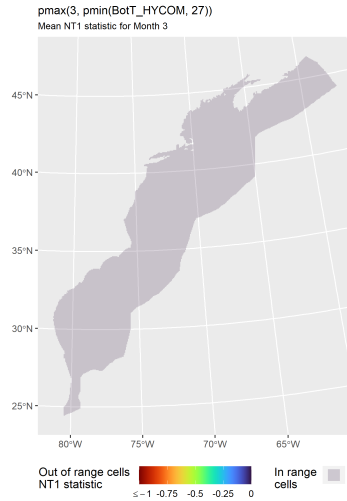

(c) March

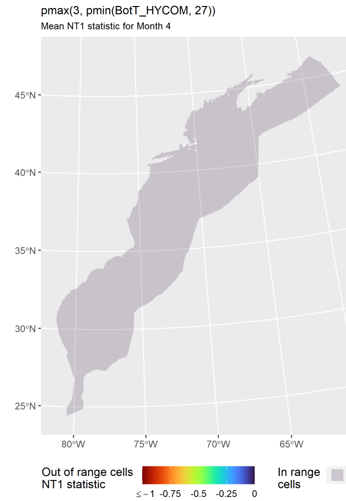

(d) April

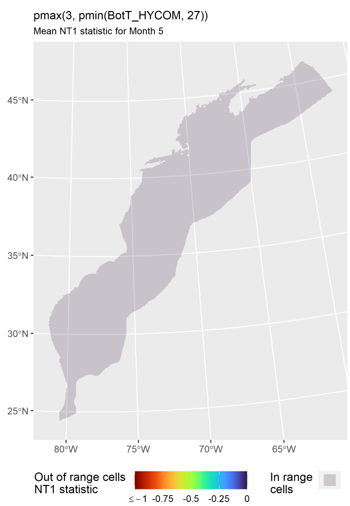

(e) May

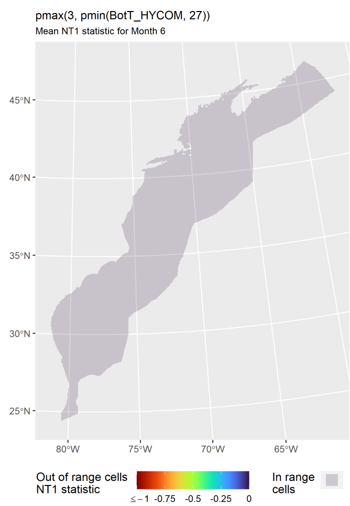

(f) June

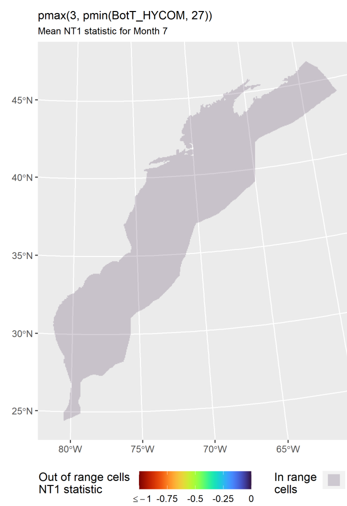

(g) July

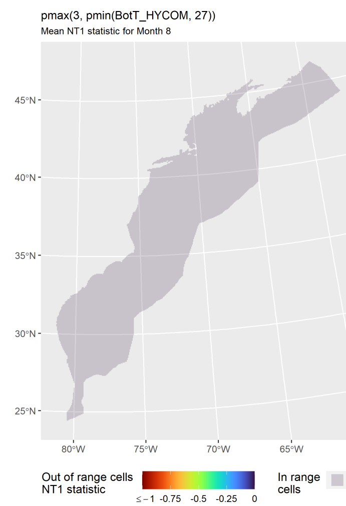

(h) August

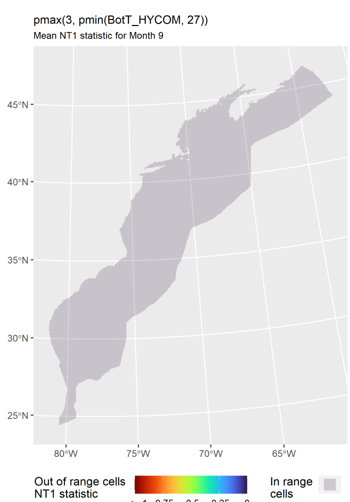

(i) September

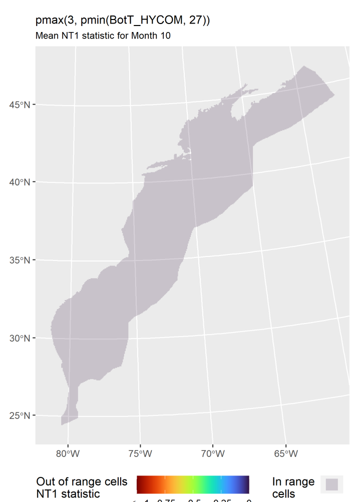

(j) October

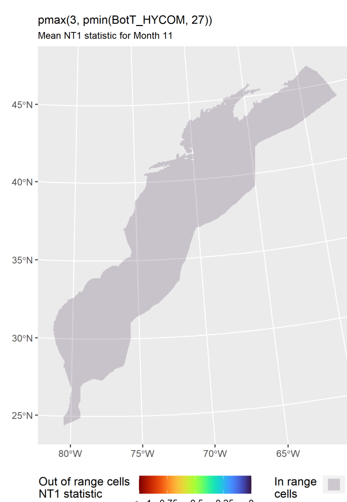

(k) November

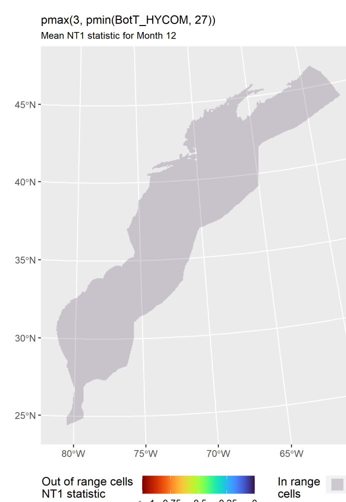

(l) December

Figure 71: NT1 statistic (Mesgaran et al. (2014)) for the BotT_HYCOM covariate in the model. Areas outside the sampled range of a covariate appear in color, indicating univariate extrapolation of that covariate occurred there during the month. Areas within the sampled range appear in gray, indicating it did not occur.

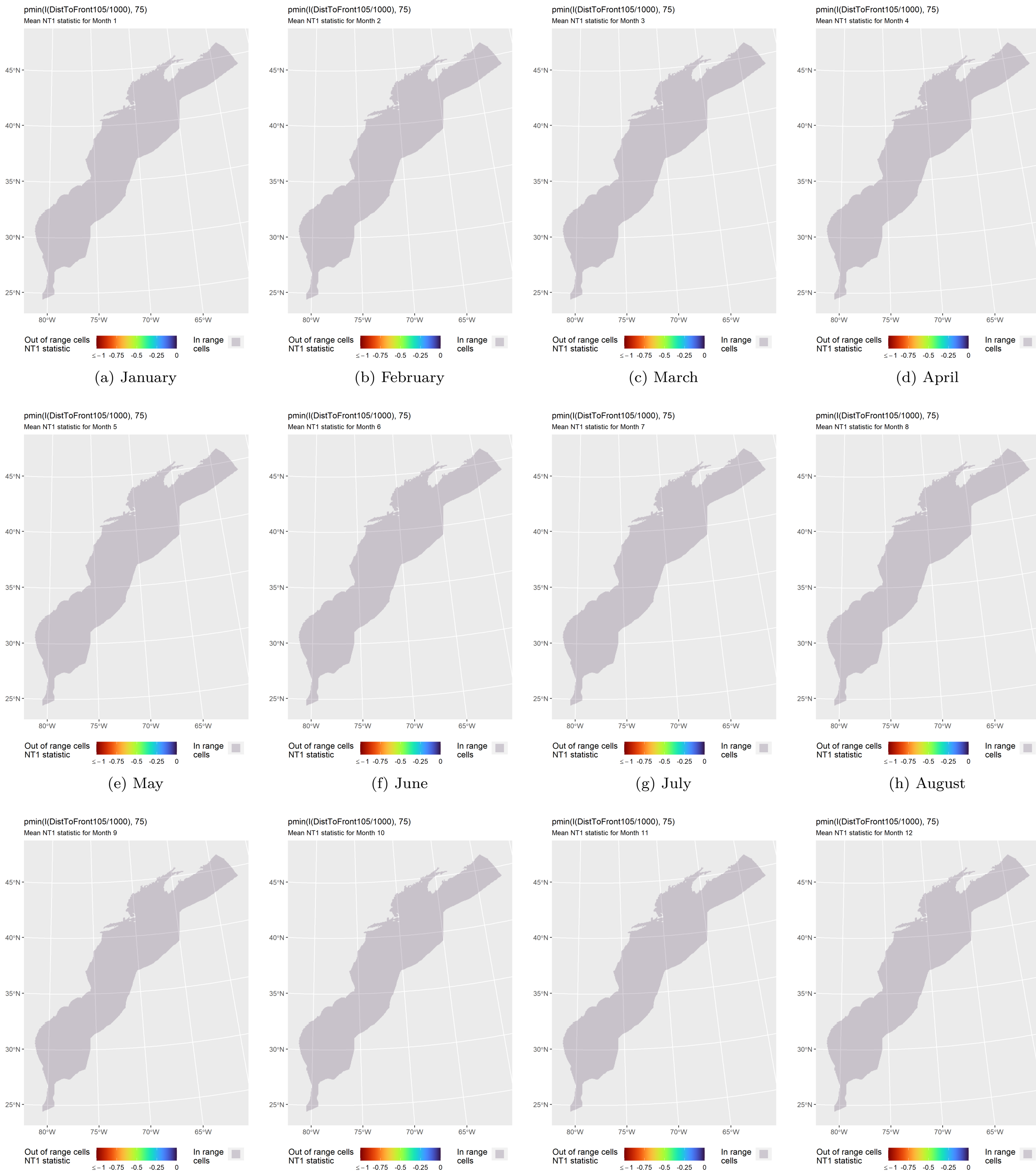

(a) January (b) February (c) March (d) April

(e) May (f) June (g) July (h) August

(i) September (j) October (k) November (l) December

Figure 72: NT1 statistic (Mesgaran et al. (2014)) for the DistToFront105 covariate in the model. Areas outside the sampled range of a covariate appear in color, indicating univariate extrapolation of that covariate occurred there during the month. Areas within the sampled range appear in gray, indicating it did not occur.

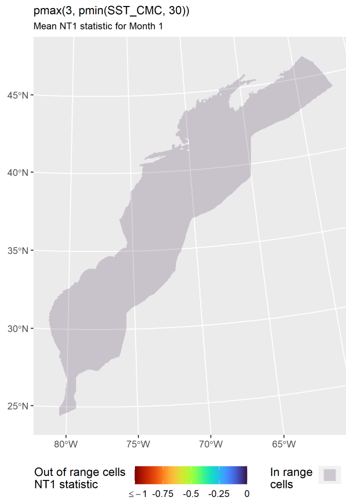

(a) January

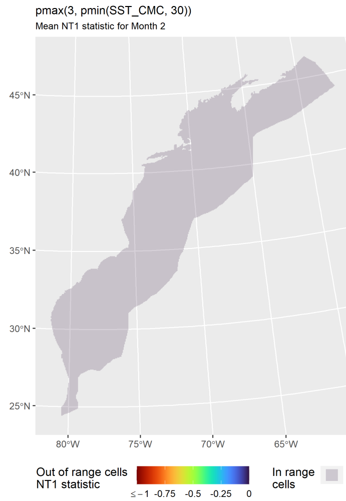

(b) February

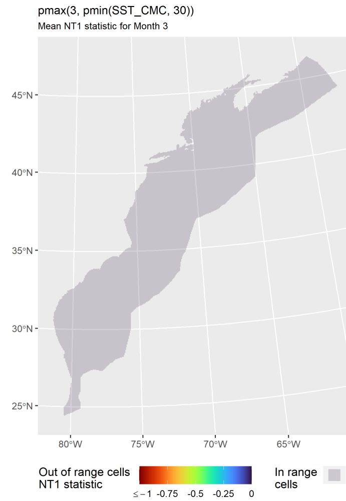

(c) March

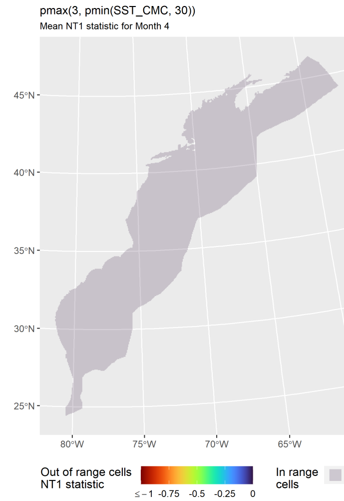

(d) April

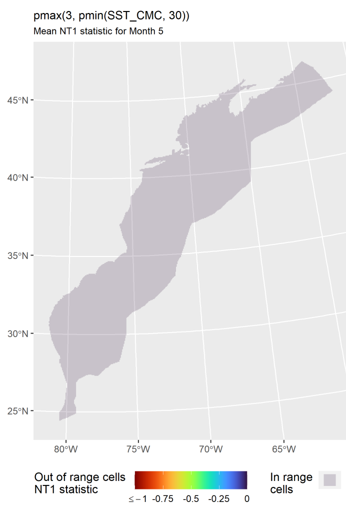

(e) May

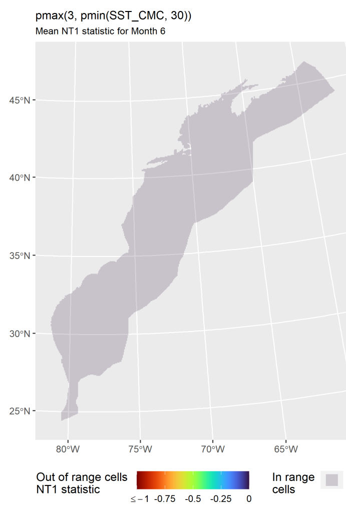

(f) June

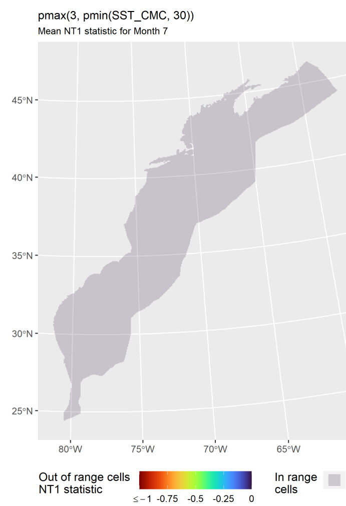

(g) July

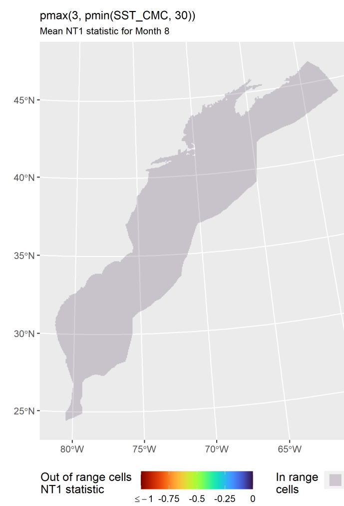

(h) August

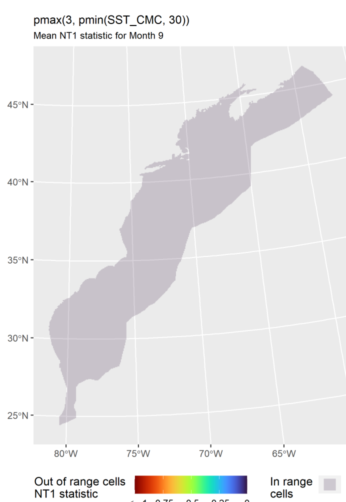

(i) September

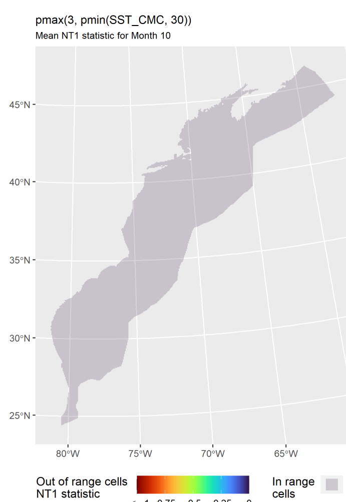

(j) October

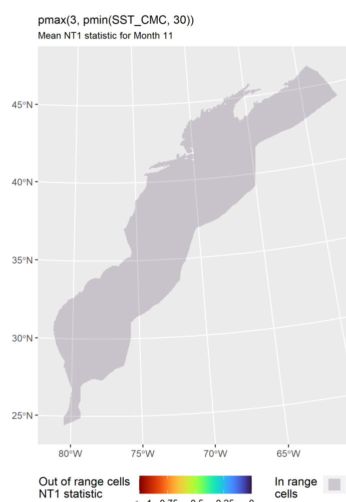

(k) November

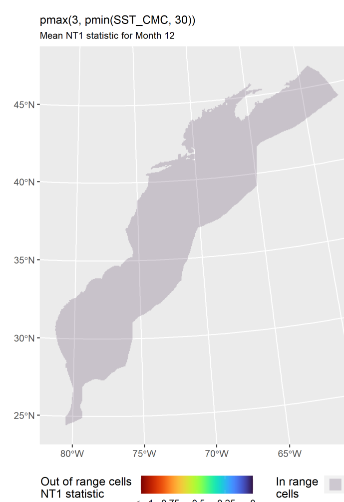

(l) December

Figure 73: NT1 statistic (Mesgaran et al. (2014)) for the SST_CMC covariate in the model. Areas outside the sampled range of a covariate appear in color, indicating univariate extrapolation of that covariate occurred there during the month. Areas within the sampled range appear in gray, indicating it did not occur.

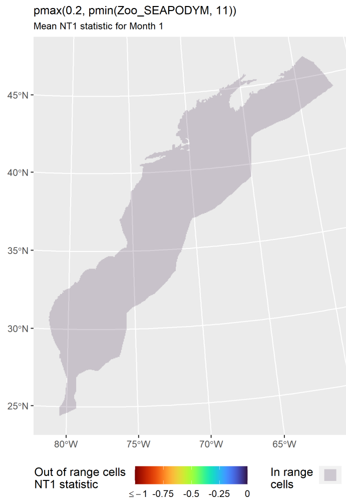

(a) January

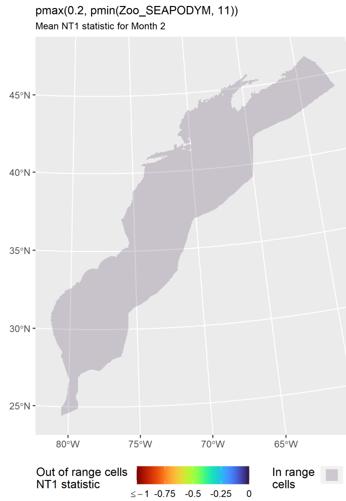

(b) February

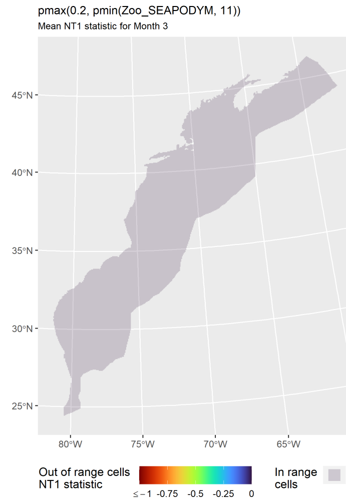

(c) March

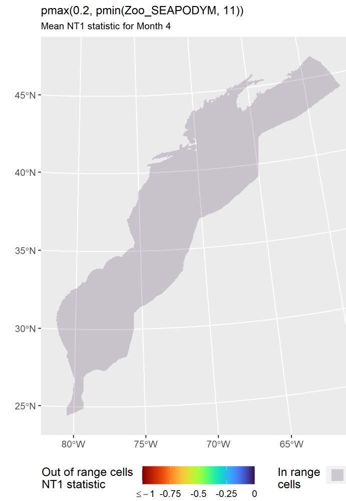

(d) April

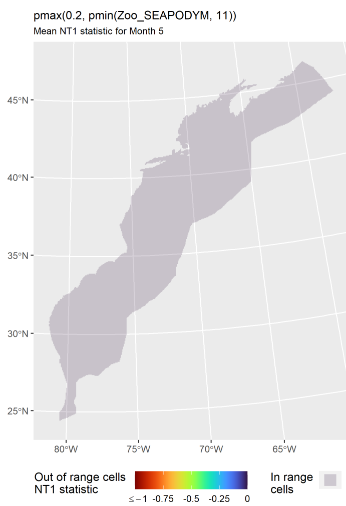

(e) May

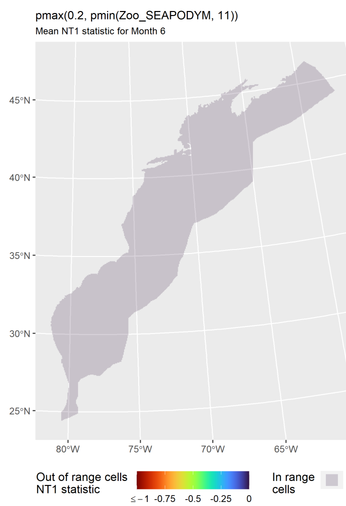

(f) June

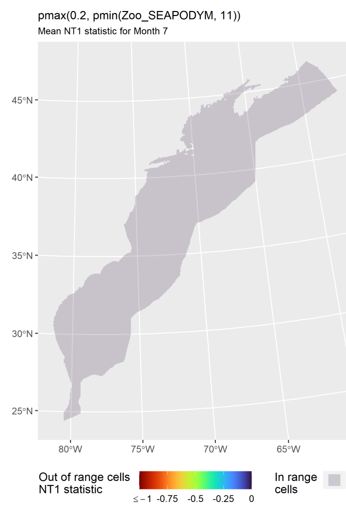

(g) July

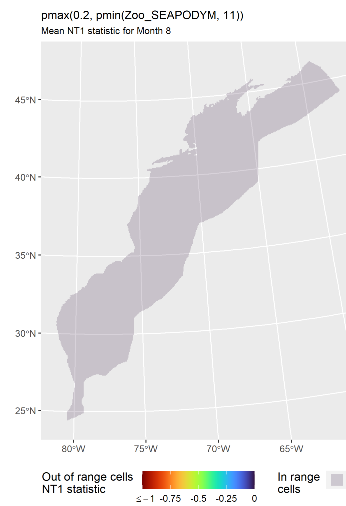

(h) August

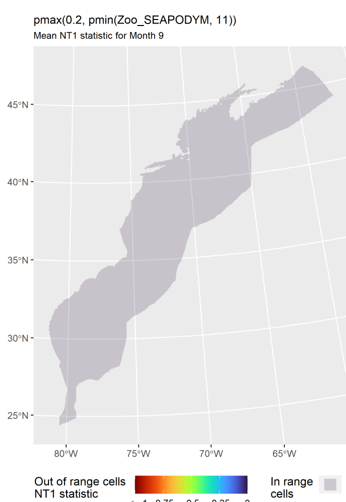

(i) September

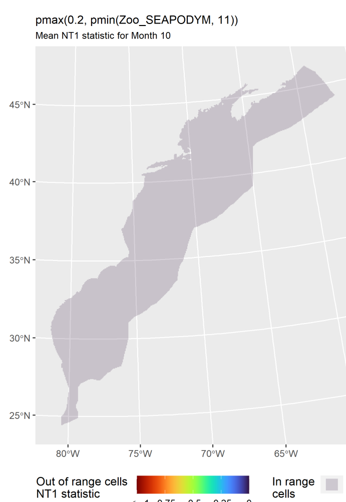

(j) October

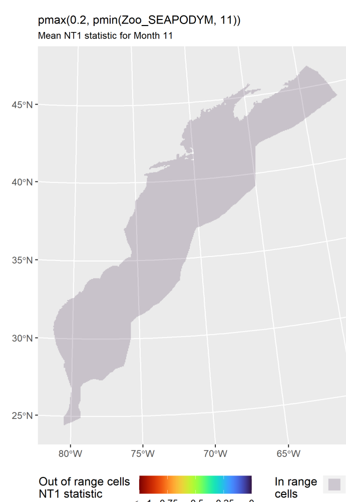

(k) November

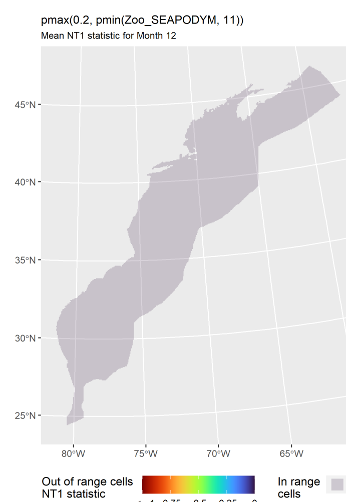

(l) December

Figure 74: NT1 statistic (Mesgaran et al. (2014)) for the Zoo_SEAPODYM covariate in the model. Areas outside the sampled range of a covariate appear in color, indicating univariate extrapolation of that covariate occurred there during the month. Areas within the sampled range appear in gray, indicating it did not occur.

5.3.2 Multivariate Extrapolation

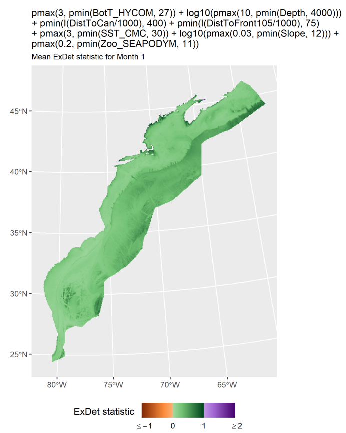

(a) January

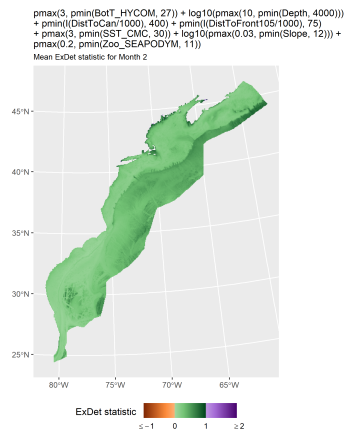

(b) February

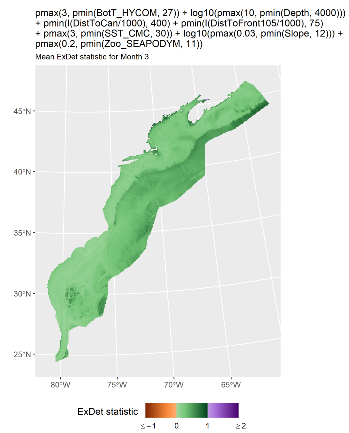

(c) March

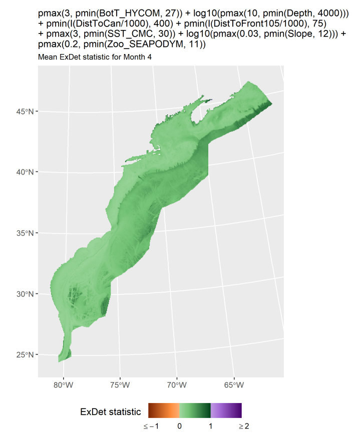

(d) April

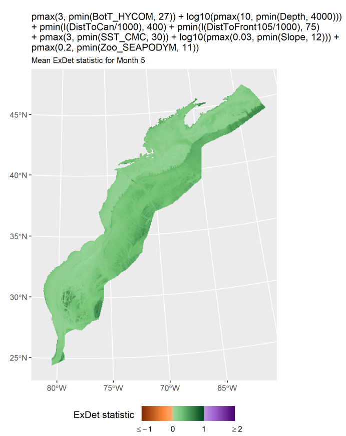

(e) May

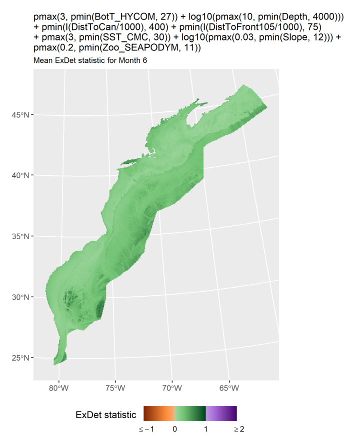

(f) June

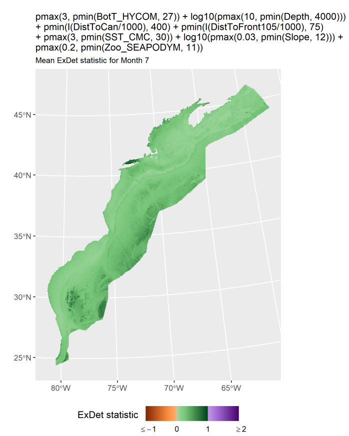

(g) July

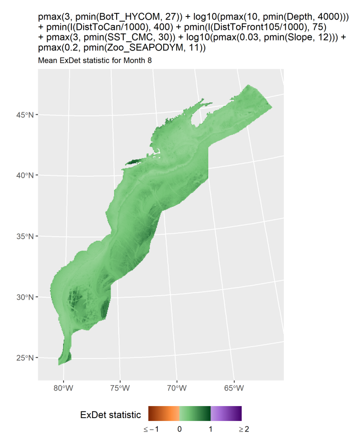

(h) August

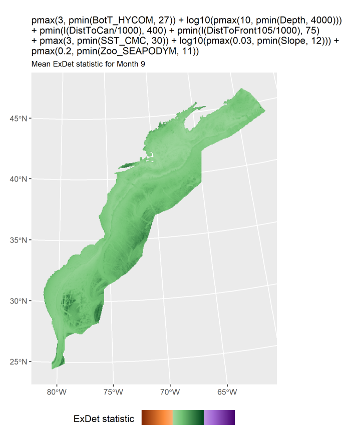

(i) September

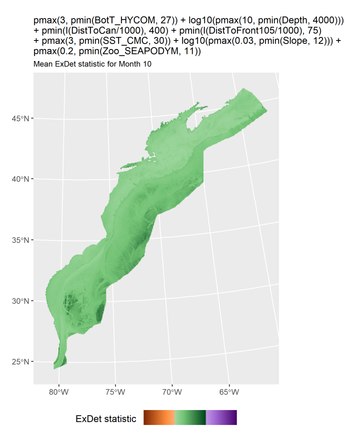

(j) October

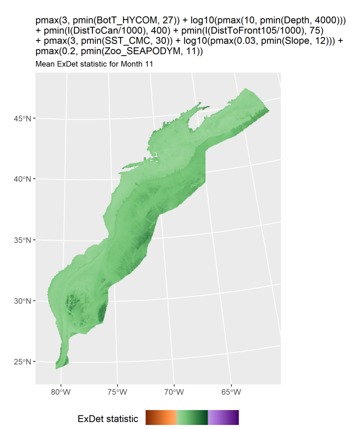

(k) November

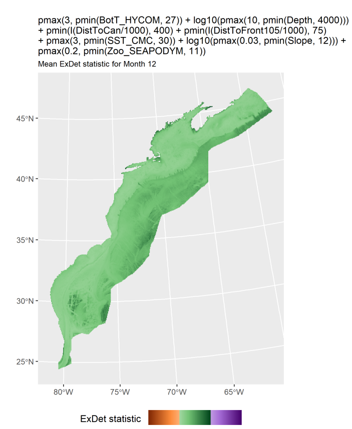

(l) December

Figure 75: ExDet statistic (Mesgaran et al. (2014)) for all of the covariates used in the model. Areas in orange (ExDet < 0) required univariate extrapolation of one or more covariates (see previous section). Areas in purple (ExDet > 1), did not require univariate extrapolation but did require multivariate extrapolation, by virtue of having novel combinations of covariates not represented in the survey data, according to the NT2 statistic (Mesgaran et al. (2014)). Areas in green ($0 \geq$ ExDet ≤ 1) did not require either type of extrapolation.

6 Predictions

Based on our evaluation of this model in the context of what is known of this species (see Section 7), we summarized its predictions into monthly climatological density and uncertainty surfaces, shown in the maps below.

6.1 Summarized Predictions

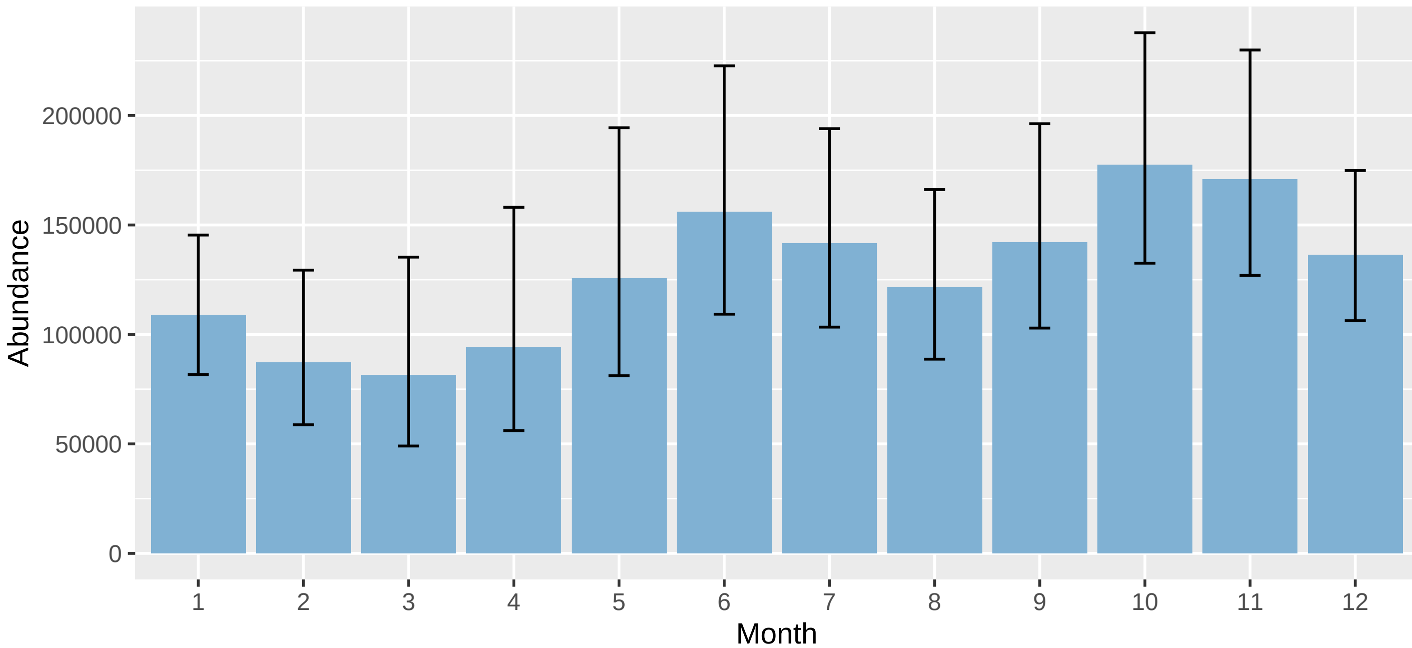

Figure 76: Mean monthly abundance for the prediction area for 1998-2019. Error bars are a 95% interval, made with a log-normal approximation using the prediction's CV. The CV was estimated with the analytic approach given by Miller et al. (2022), Appendix S1, and accounts both for uncertainty in model parameter estimates and for temporal variability in dynamic covariates.

Table 28: Mean monthly abundance and density for the prediction area for 1998-2019. CV and intervals estimated as described for the previous figure.

Month	Abundance	CV	95% Interval	Area (km^2)	Density (individuals / 100 km^2)
1	108,960	0.148	81,650 - 145,404	1,272,925	8.6
2	87,170	0.204	58,731 - 129,382	1,272,925	6.8
3	81,466	0.263	49,043 - 135,325	1,272,925	6.4
4	94,162	0.269	56,089 - 158,079	1,272,925	7.4
5	125,590	0.226	81,137 - 194,398	1,272,925	9.9
6	155,985	0.183	109,264 - 222,685	1,272,925	12.3
7	141,585	0.162	103,345 - 193,976	1,272,925	11.1
8	121,405	0.161	88,706 - 166,157	1,272,925	9.5
9	142,109	0.166	102,911 - 196,236	1,272,925	11.2
10	177,543	0.150	132,557 - 237,795	1,272,925	13.9
11	170,882	0.152	126,999 - 229,929	1,272,925	13.4
12	136,307	0.128	106,258 - 174,854	1,272,925	10.7

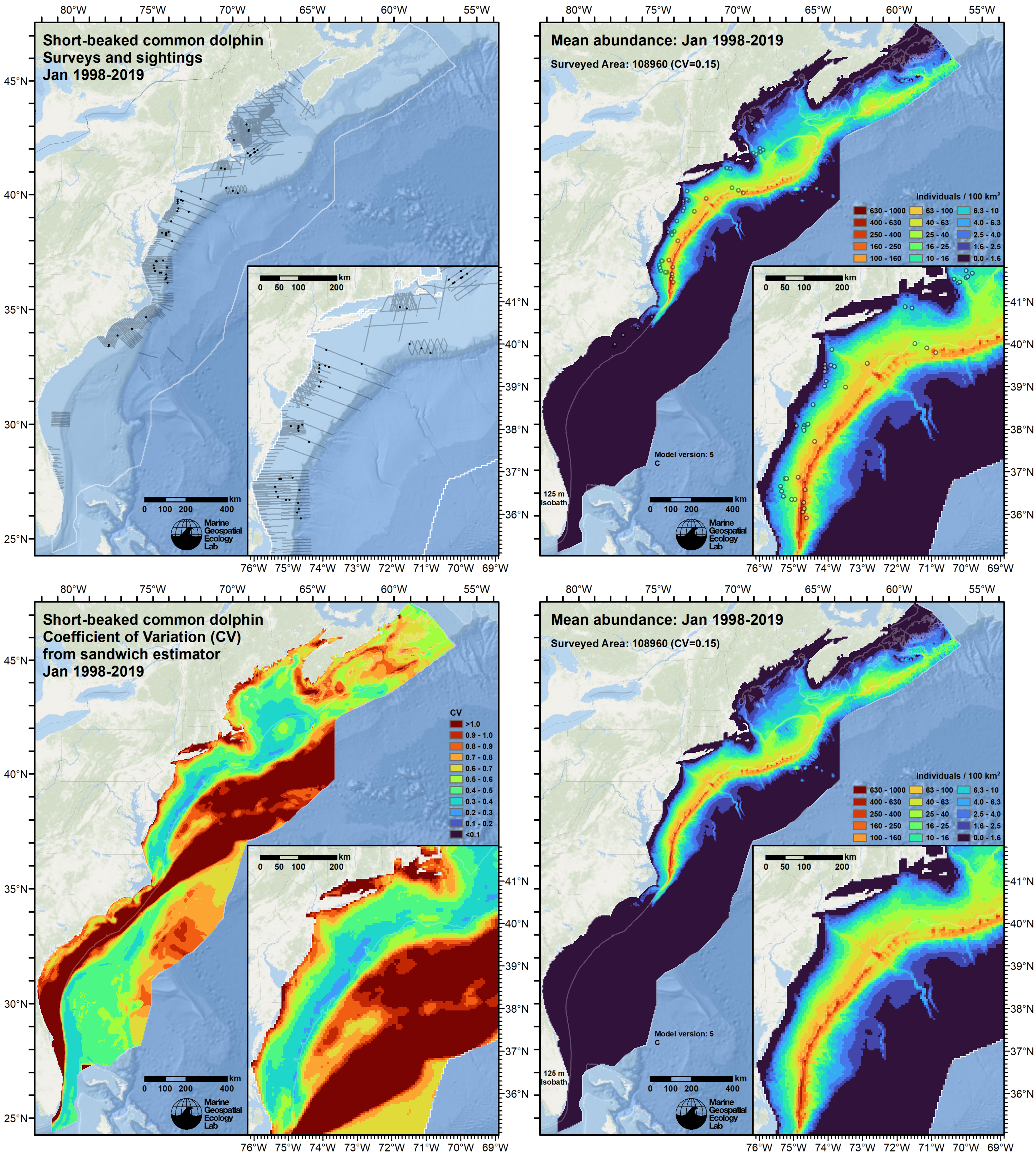

Figure 77: Survey effort and observations (top left), predicted density with observations (top right), predicted density without observations (bottom right), and coefficient of variation of predicted density (bottom left), for the month of January for the given era. Variance was estimated with the analytic approach given by Miller et al. (2022), Appendix S1, and accounts both for uncertainty in model parameter estimates and for temporal variability in dynamic covariates.

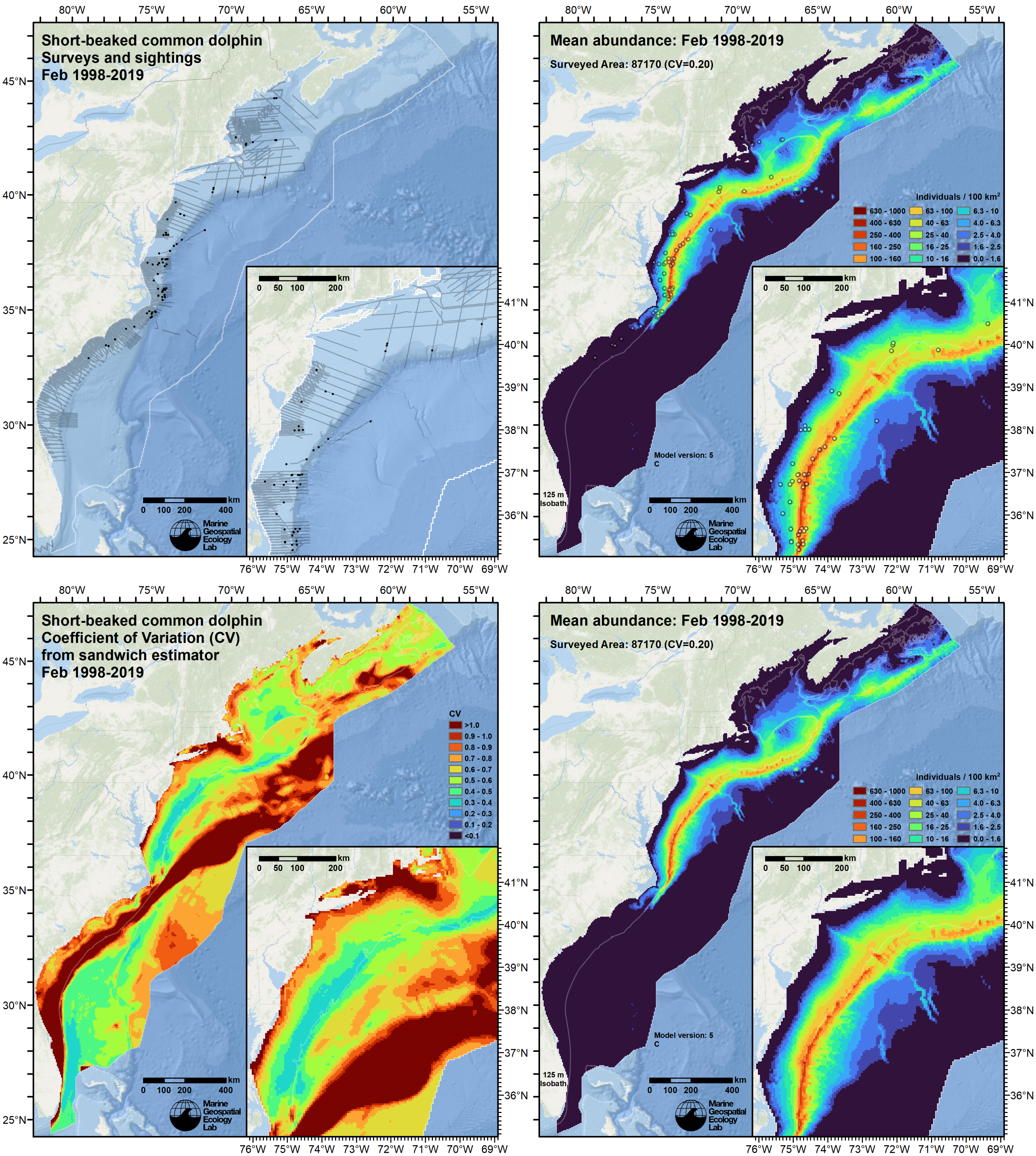

Figure 78: Survey effort and observations (top left), predicted density with observations (top right), predicted density without observations (bottom right), and coefficient of variation of predicted density (bottom left), for the month of February for the given era. Variance was estimated with the analytic approach given by Miller et al. (2022), Appendix S1, and accounts both for uncertainty in model parameter estimates and for temporal variability in dynamic covariates.

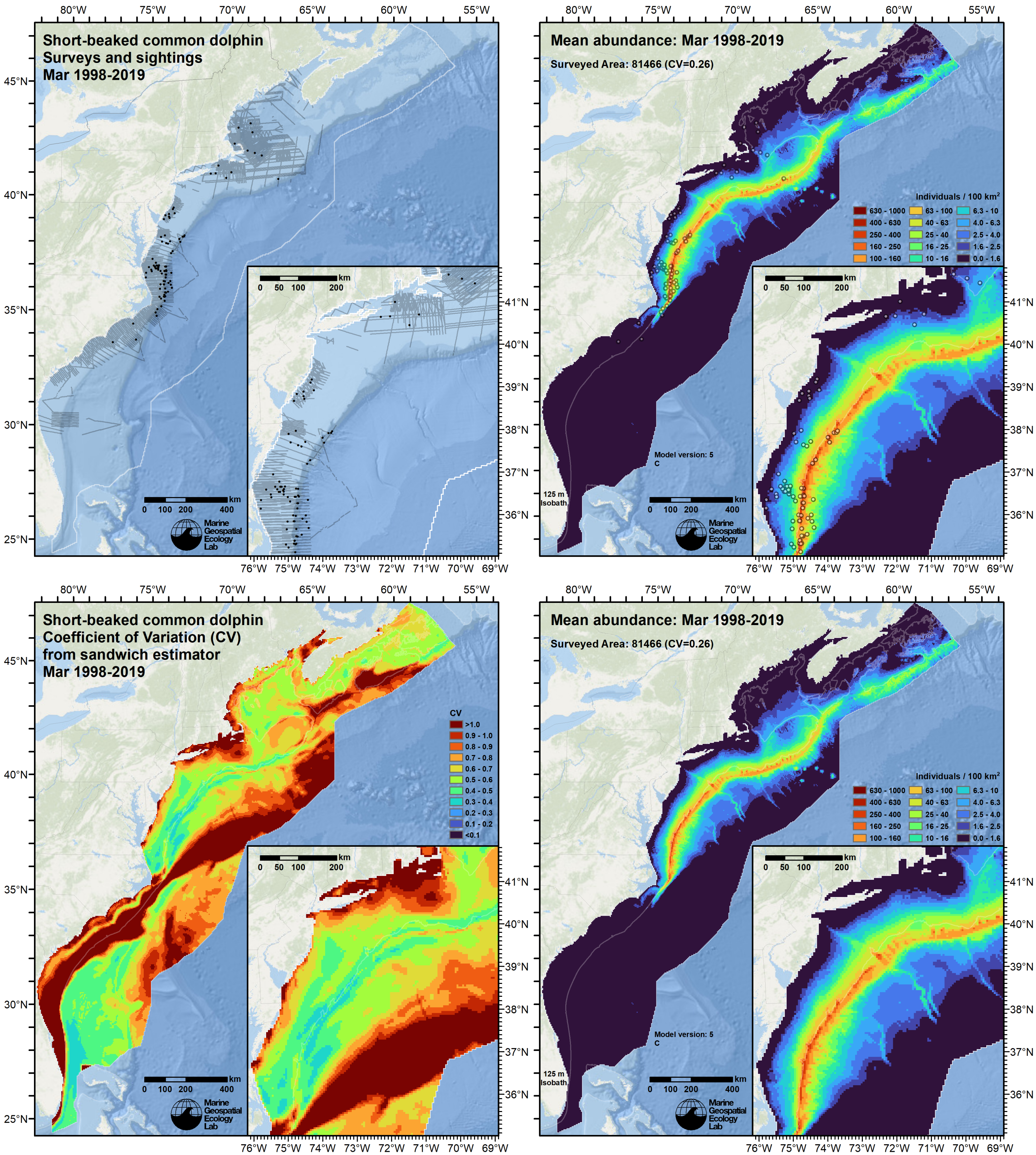

Figure 79: Survey effort and observations (top left), predicted density with observations (top right), predicted density without observations (bottom right), and coefficient of variation of predicted density (bottom left), for the month of March for the given era. Variance was estimated with the analytic approach given by Miller et al. (2022), Appendix S1, and accounts both for uncertainty in model parameter estimates and for temporal variability in dynamic covariates.

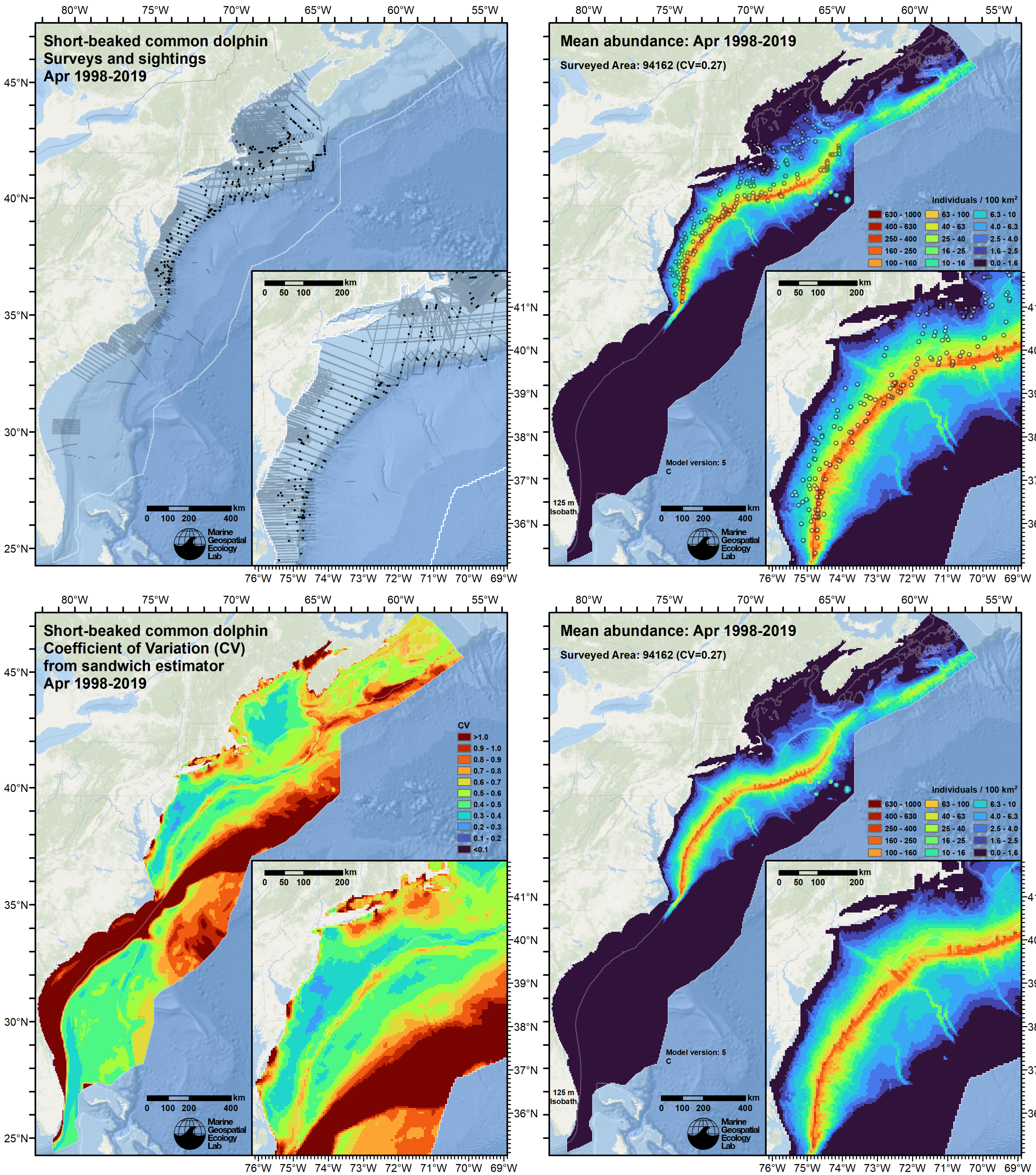

Figure 80: Survey effort and observations (top left), predicted density with observations (top right), predicted density without observations (bottom right), and coefficient of variation of predicted density (bottom left), for the month of April for the given era. Variance was estimated with the analytic approach given by Miller et al. (2022), Appendix S1, and accounts both for uncertainty in model parameter estimates and for temporal variability in dynamic covariates.

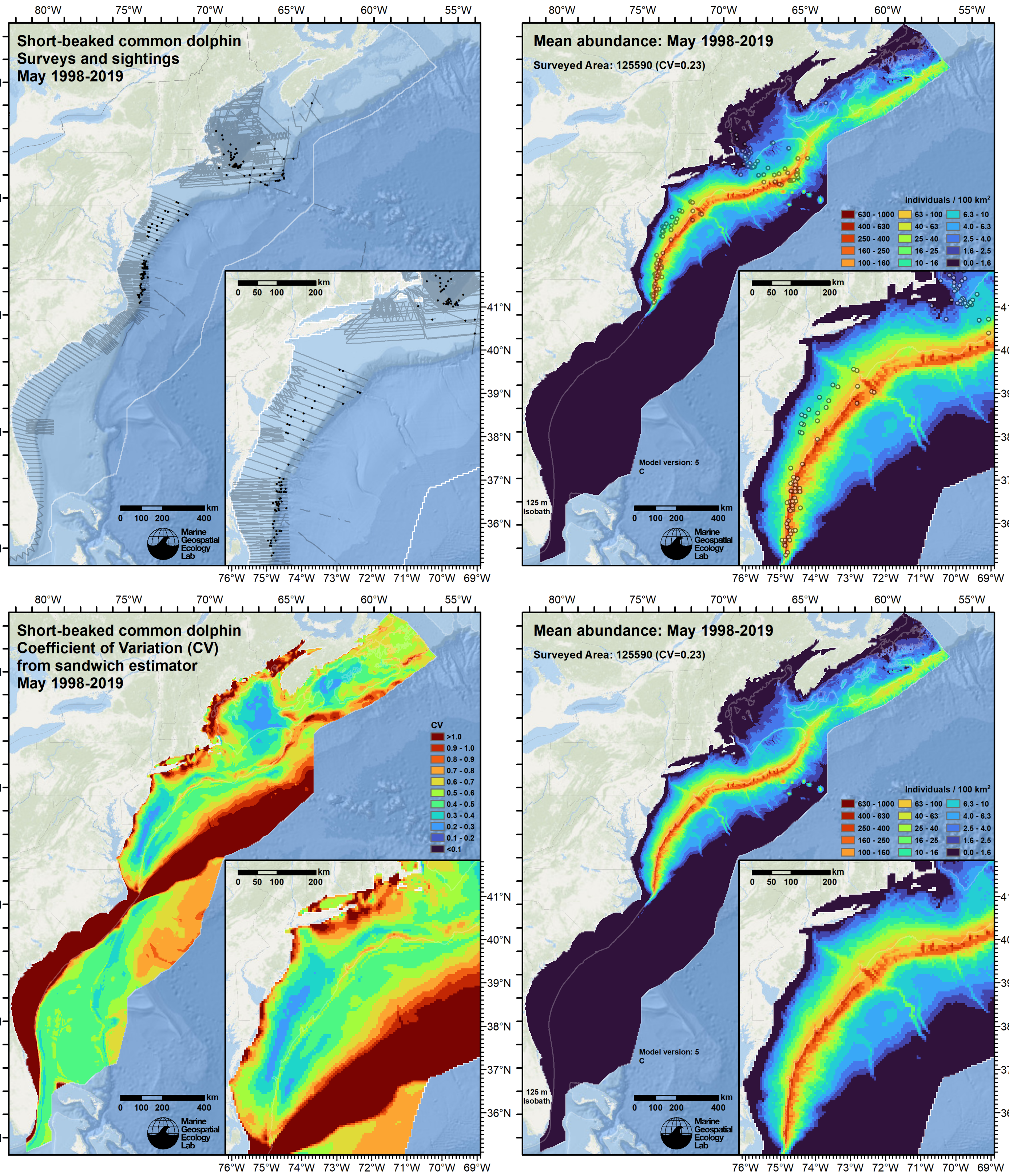

Figure 81: Survey effort and observations (top left), predicted density with observations (top right), predicted density without observations (bottom right), and coefficient of variation of predicted density (bottom left), for the month of May for the given era. Variance was estimated with the analytic approach given by Miller et al. (2022), Appendix S1, and accounts both for uncertainty in model parameter estimates and for temporal variability in dynamic covariates.

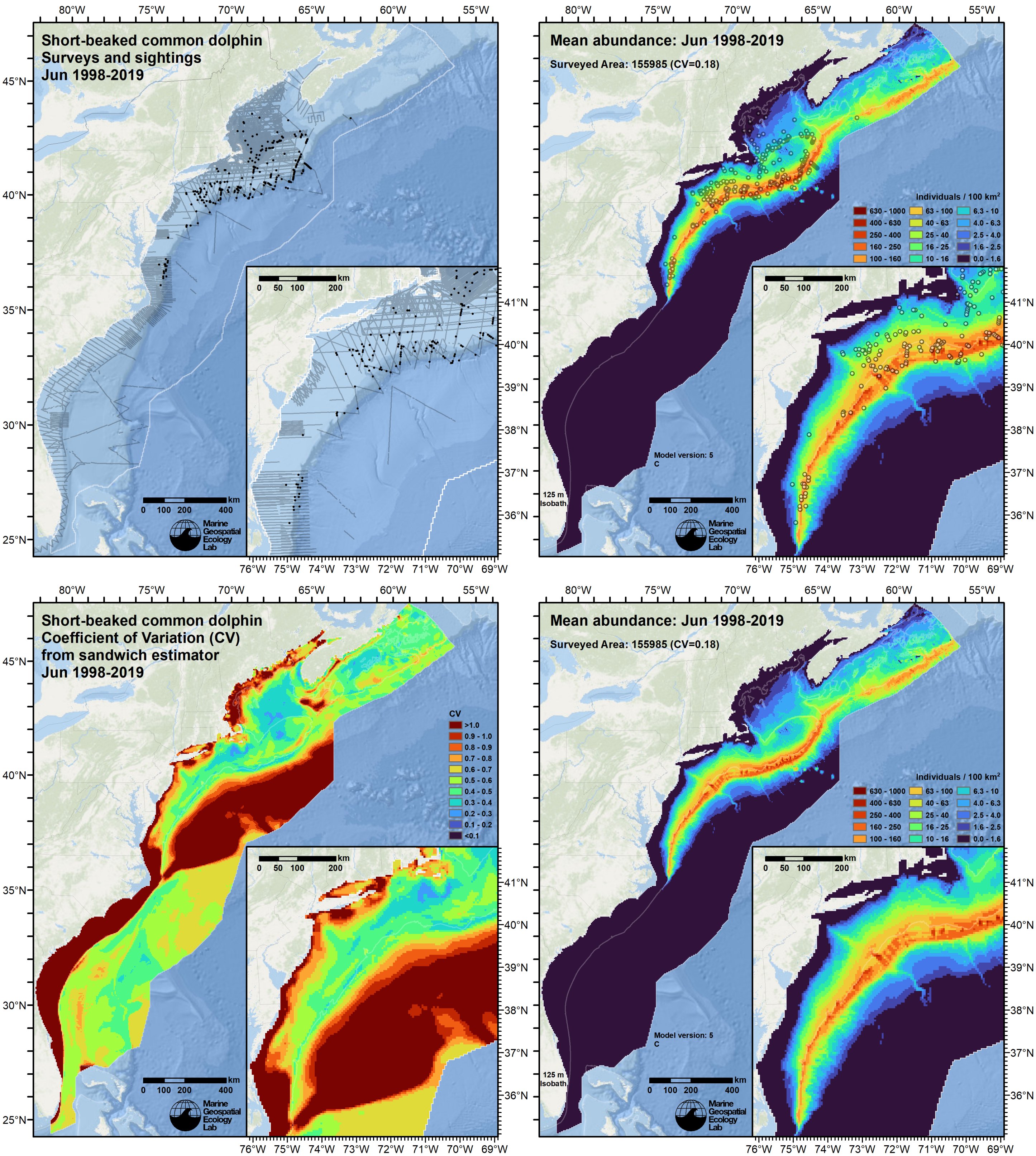

Figure 82: Survey effort and observations (top left), predicted density with observations (top right), predicted density without observations (bottom right), and coefficient of variation of predicted density (bottom left), for the month of June for the given era. Variance was estimated with the analytic approach given by Miller et al. (2022), Appendix S1, and accounts both for uncertainty in model parameter estimates and for temporal variability in dynamic covariates.

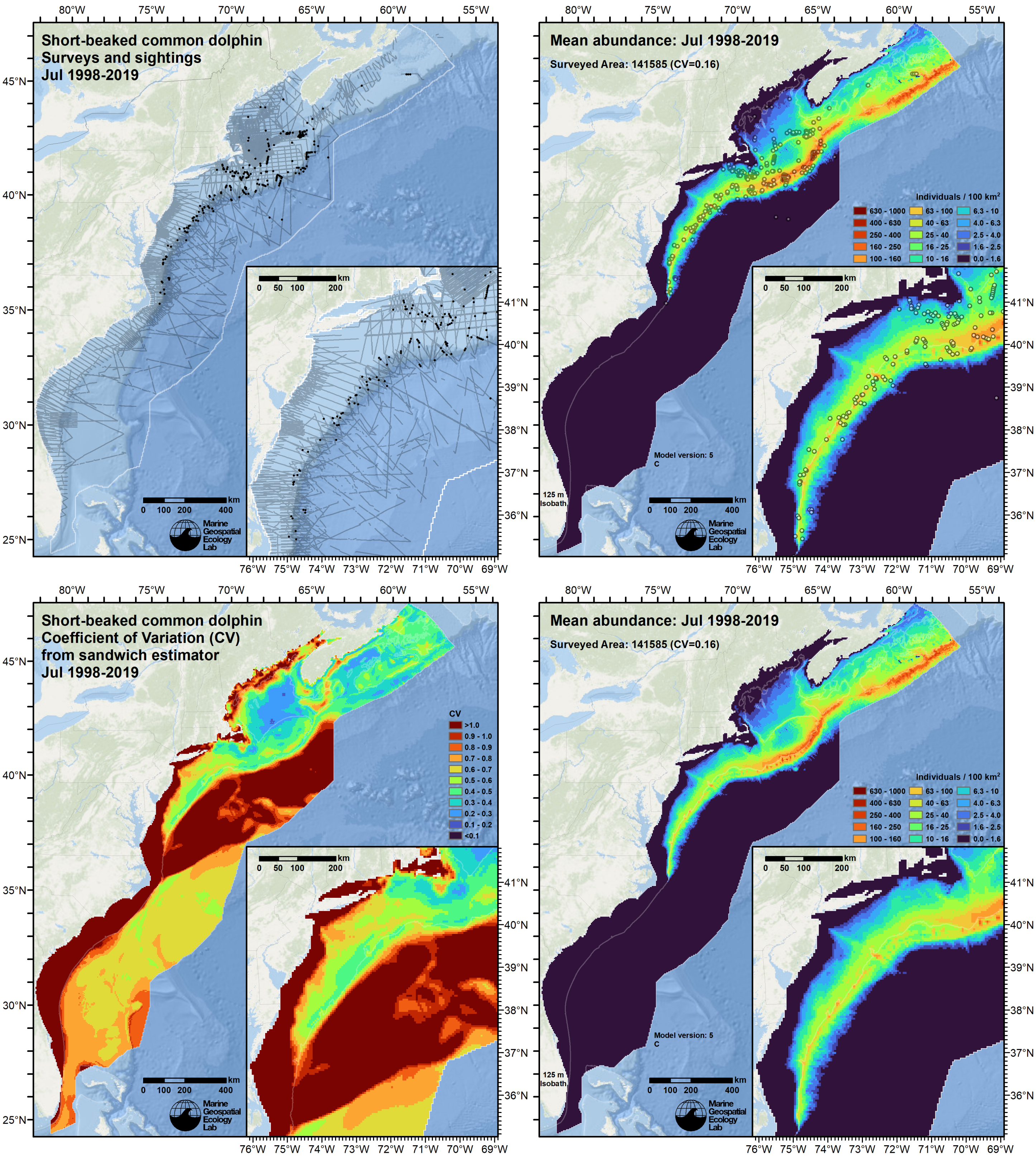

Figure 83: Survey effort and observations (top left), predicted density with observations (top right), predicted density without observations (bottom right), and coefficient of variation of predicted density (bottom left), for the month of July for the given era. Variance was estimated with the analytic approach given by Miller et al. (2022), Appendix S1, and accounts both for uncertainty in model parameter estimates and for temporal variability in dynamic covariates.

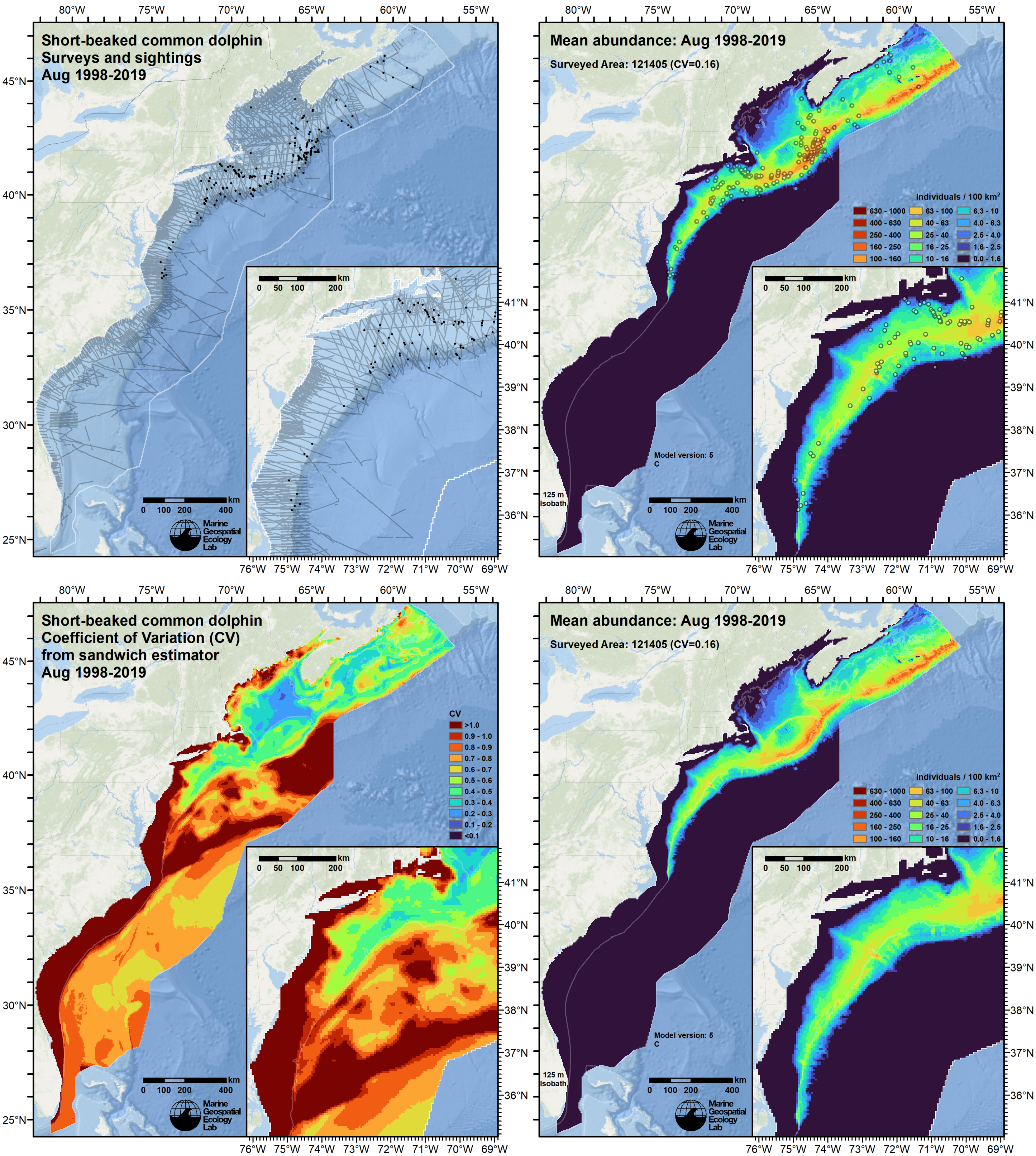

Figure 84: Survey effort and observations (top left), predicted density with observations (top right), predicted density without observations (bottom right), and coefficient of variation of predicted density (bottom left), for the month of August for the given era. Variance was estimated with the analytic approach given by Miller et al. (2022), Appendix S1, and accounts both for uncertainty in model parameter estimates and for temporal variability in dynamic covariates.

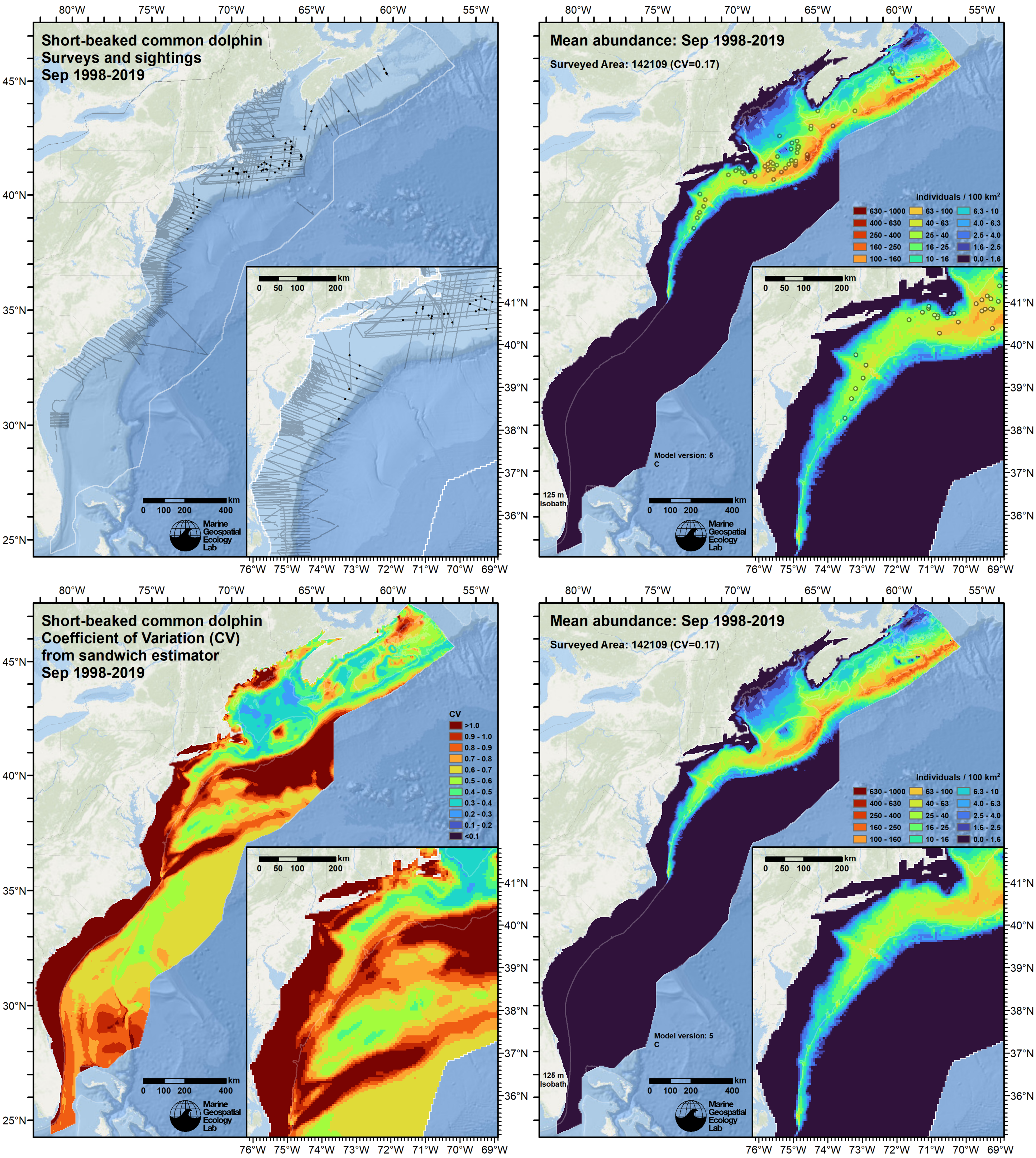

Figure 85: Survey effort and observations (top left), predicted density with observations (top right), predicted density without observations (bottom right), and coefficient of variation of predicted density (bottom left), for the month of September for the given era. Variance was estimated with the analytic approach given by Miller et al. (2022), Appendix S1, and accounts both for uncertainty in model parameter estimates and for temporal variability in dynamic covariates.

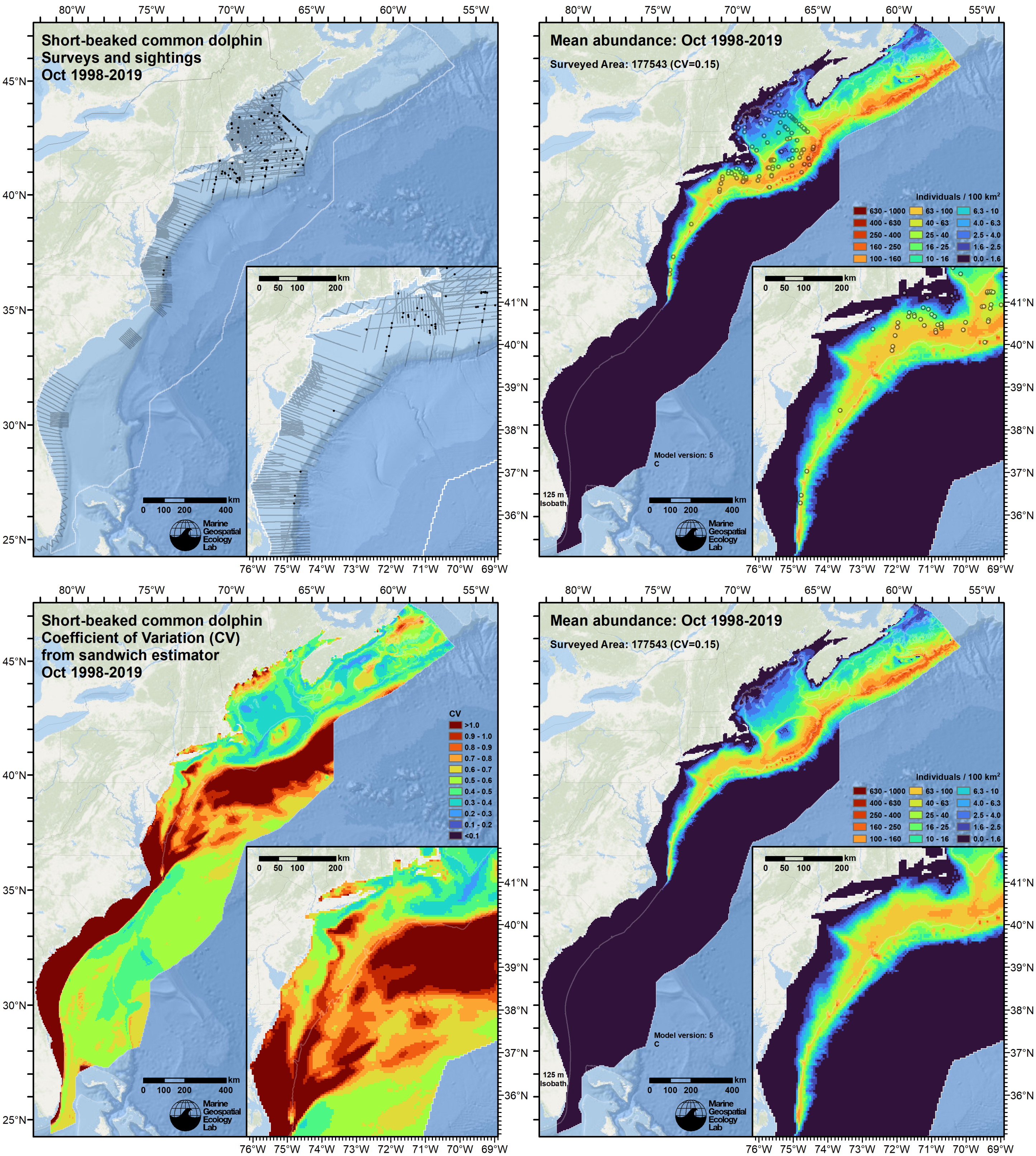

Figure 86: Survey effort and observations (top left), predicted density with observations (top right), predicted density without observations (bottom right), and coefficient of variation of predicted density (bottom left), for the month of October for the given era. Variance was estimated with the analytic approach given by Miller et al. (2022), Appendix S1, and accounts both for uncertainty in model parameter estimates and for temporal variability in dynamic covariates.

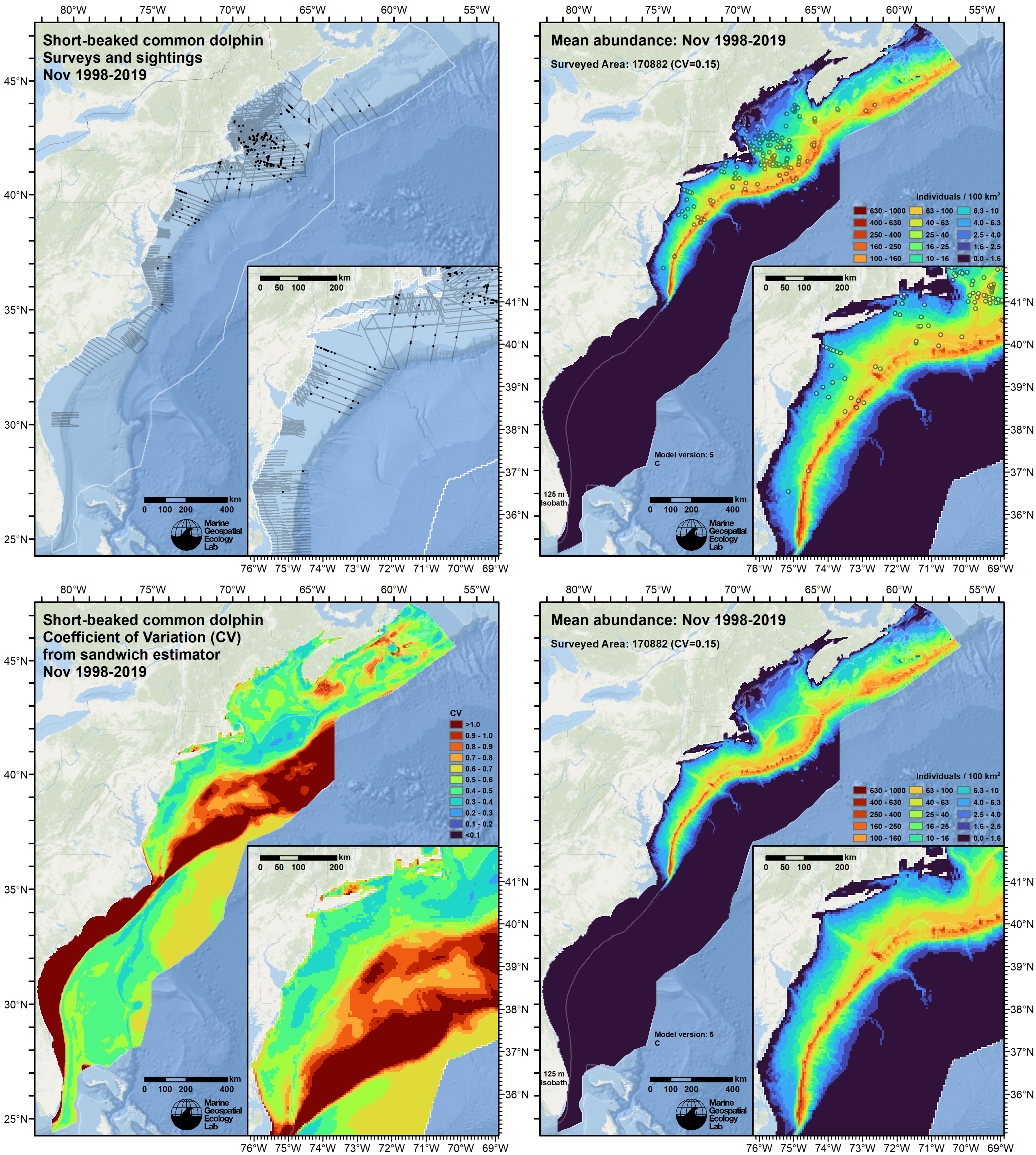

Figure 87: Survey effort and observations (top left), predicted density with observations (top right), predicted density without observations (bottom right), and coefficient of variation of predicted density (bottom left), for the month of November for the given era. Variance was estimated with the analytic approach given by Miller et al. (2022), Appendix S1, and accounts both for uncertainty in model parameter estimates and for temporal variability in dynamic covariates.

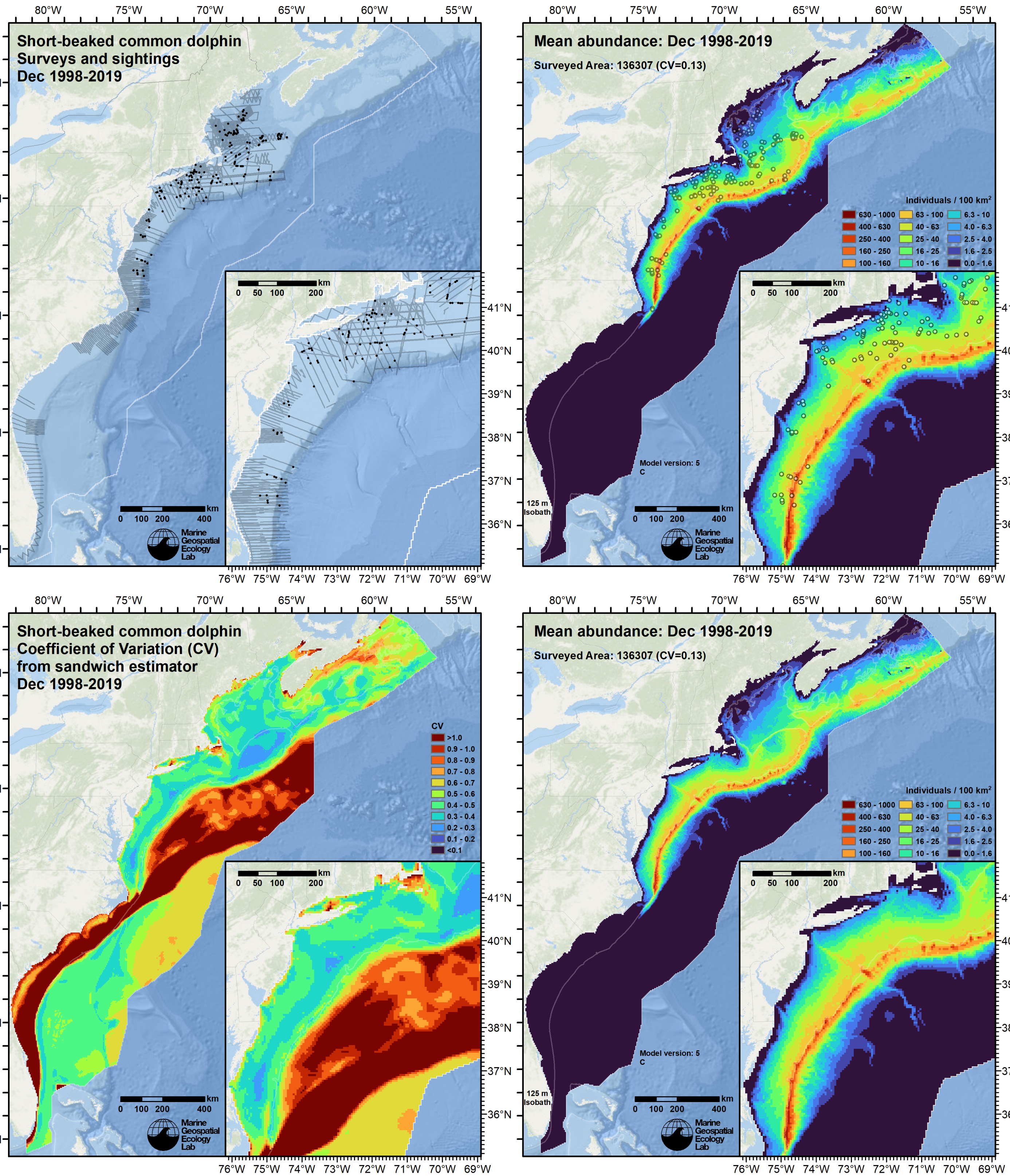

Figure 88: Survey effort and observations (top left), predicted density with observations (top right), predicted density without observations (bottom right), and coefficient of variation of predicted density (bottom left), for the month of December for the given era. Variance was estimated with the analytic approach given by Miller et al. (2022), Appendix S1, and accounts both for uncertainty in model parameter estimates and for temporal variability in dynamic covariates.

6.2 Abundance Comparisons

6.2.1 NOAA Stock Assessment Report

Table 29: Comparison of regional abundance estimates from the 2021 NOAA Stock Assessment Report (SAR) (Hayes et al. (2022)) to estimates from this density model extracted from roughly comparable zones (Figure 89 below). The SAR estimates were based on a single year of surveying, while the model estimates were taken from the multi-year mean density surfaces we provide to model users (Section 6.1).

2021 Stock Assessment Report			Density Model		
Month/Year	Area	N_{est}	Period	Zone	Abundance
Jun-Sep 2016	Central Virginia to lower Bay of Fundy[a]	80,227	Jun-Sep 1998-2019	NEFSC	60,464
Jun-Aug 2016	Florida to central Virginia[b]	900	Jun-Aug 1998-2019	SEFSC	7,294
Jun-Sep 2016	Bay of Fundy/Scotian Shelf/Gulf of St. Lawrence[c]	43,124	Jun-Sep 1998-2019	Canada[d]	73,859
Jun-Sep 2016	Total	124,251	Jun-Sep 1998-2019	Total	141,617

[a] Estimate originally from Palka (2020).
[b] Estimate originally from Garrison (2020).
[c] Estimate originally from Lawson and Gosselin (2018). Very few sightings were reported in the Gulf of St. Lawrence (see Figure 1 of the 2021 SAR) so we presume most of N_{est} occurred in the Bay of Fundy/Scotian Shelf area.
[d] Our Canada zone is roughly comparable to the SAR's "Bay of Fundy/Scotian Shelf" area but does not include the Gulf of St. Lawrence.

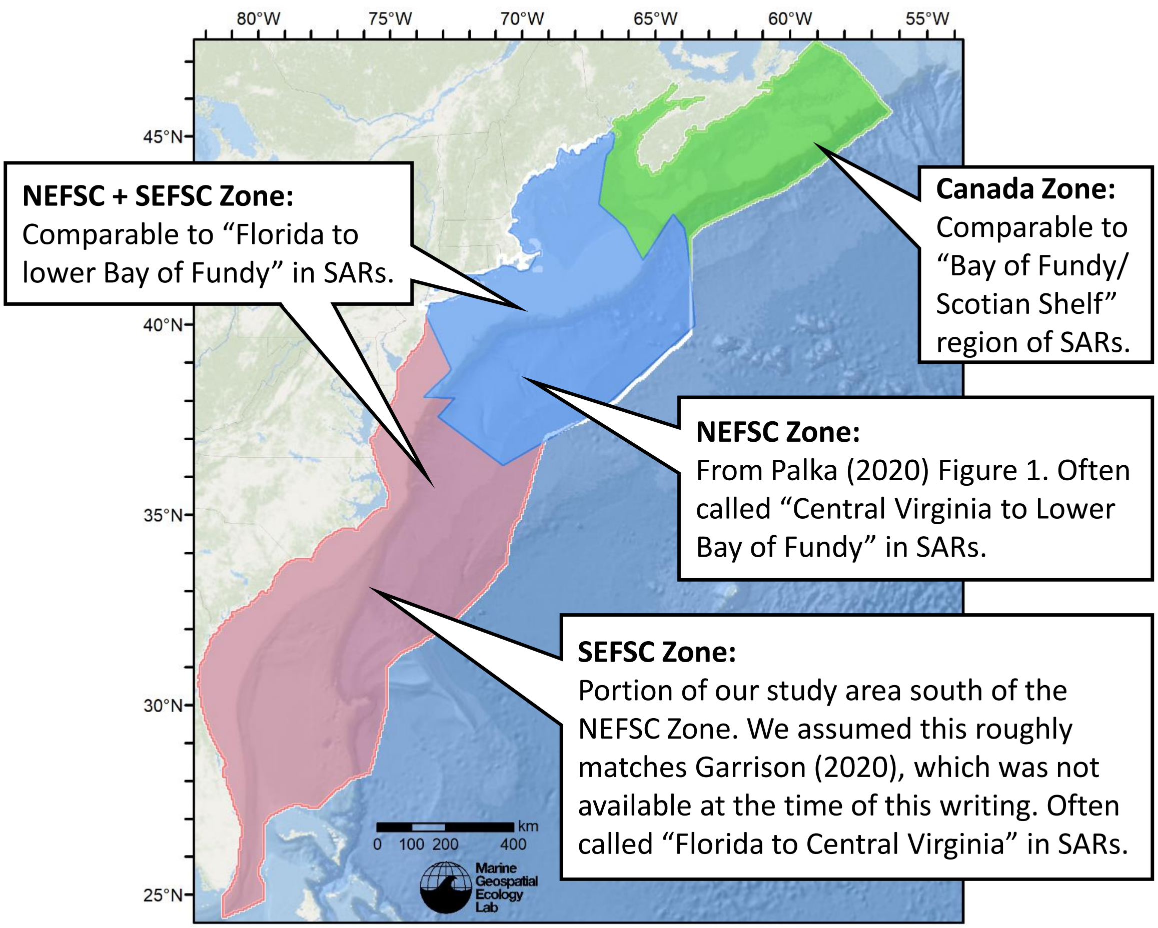

Figure 89: Zones for which we extracted abundance estimates from the density model for comparison to estimates from the NOAA Stock Assessment Report.

6.2.2 Previous Density Model

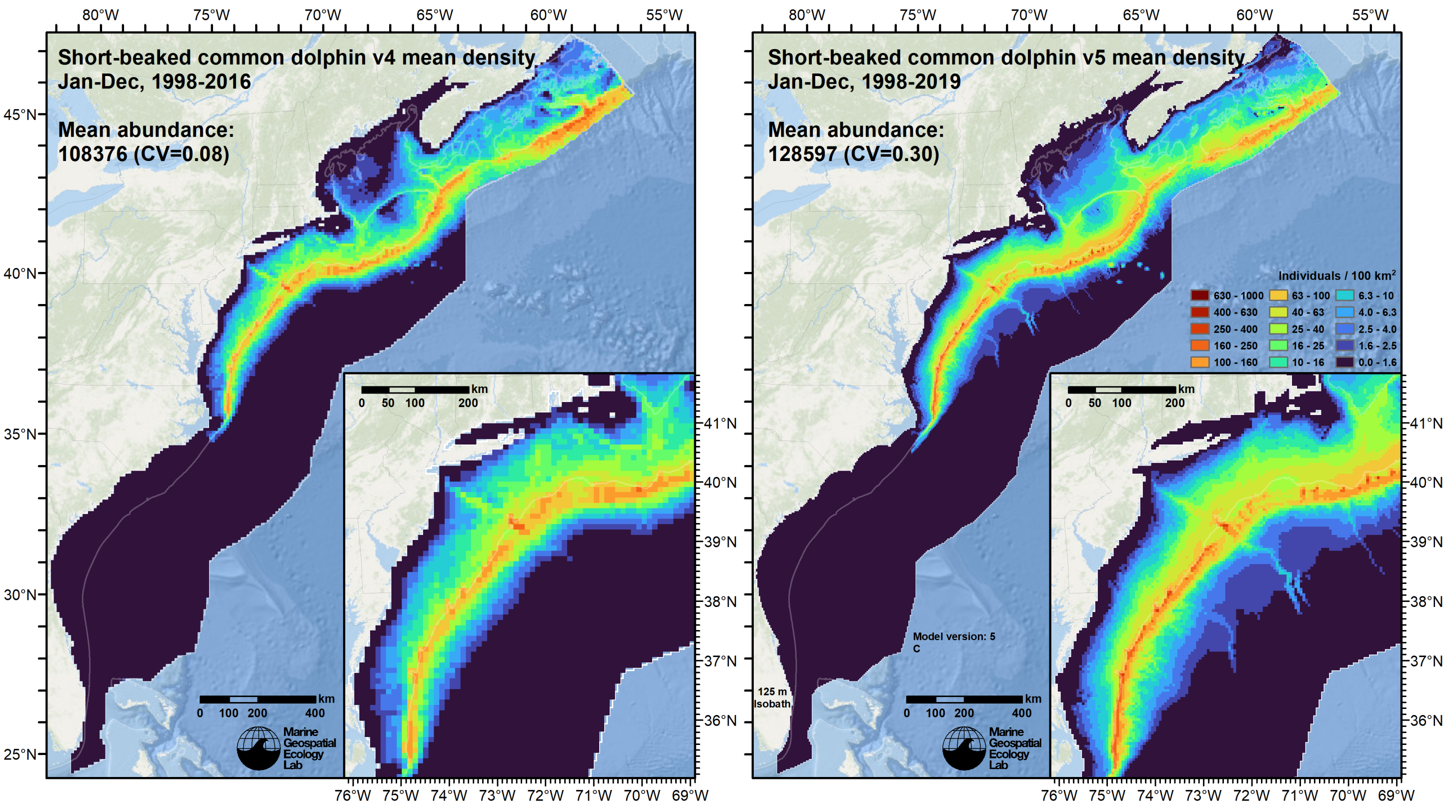

Figure 90: Comparison of the mean density predictions from the previous model (left) released by Roberts et al. (2018) to those from this model (right).

7 Discussion

When summarized across the modeled period (1998-2019), mean monthly density maps (Figures 77-88) broadly agreed with the overall distribution and seasonal pattern described by Jefferson et al. (2009), with a strong movement north along the shelf break in late spring and retreat south at the end of autumn. Jefferson et al. (2009) reported that in January to May, short-beaked common dolphins regularly range north only as far as Georges Bank. Although our model predicted high densities north of Georges Bank starting in June, concentrated along the Scotian Shelf break, it also predicted low but non-zero density in January to May.

This non-zero prediction is supported by sightings archived in the OBIS-SEAMAP system (Halpin et al. 2009; Fujioka et al. 2014), which suggest the species' range now likely extends into Canada year-round. For example, DFO (2017) reported opportunistic sightings along the slope of the Scotian Shelf and over the Grand Banks as early as April. Similarly, the NOAA AMAPPS program (Palka et al. 2021) reported sightings in April 2019 in the eastern Gulf of Maine off Yarmouth, over Browns Bank, and over LaHave Basin on the Scotian Shelf. (NOAA's AMAPPS surveys were utilized in our model but DFO's opportunistic sightings were not.)

The non-zero winter and spring density in Canada is also supported by recent evidence of a distribution shift driven by climate change. The shelf north of Cape Hatteras, and the Gulf of Maine in particular, is one of the most rapidly warming marine ecosystems in the world (Pershing et al. 2015). Thorne et al. (2022) tested stranding records of odontocetes reported along the eastern U.S. from 1996 to 2020 for evidence of distribution shifts. They reported that common dolphin showed strong evidence of a poleward (i.e. northward) shift in distribution, and suggested it could be traced to warming sea surface temperatures and associated changes in the dynamics of the Gulf Stream. However, they cautioned that in their analysis, which examined nine species using power analysis simulations, while the poleward shift for common dolphin was statistically significant at $\alpha = 0.05$, it was not significant when α was adjusted to account for their analysis being a multiple comparison test.

Mean monthly abundance predicted by our model for the prediction region ranged from a low of 81,466 in March to a high of 177,543 in October (Figure 76; Table 28). The mean summer (June-September) abundance of 141,617 was 14% higher than the most recent NOAA Stock Assessment Report (Hayes et al. 2022). Regionally, our model predicted lower abundance for the "Central Virginia to lower Bay of Fundy" area, and higher abundance predicted both to the south and to the north, in Canada (Table 29). Because the SAR was based on a single year of surveying, and our analysis on multiple years of surveys conducted over two decades, we do not find these differences surprising, given the interannual variability in this ecosystem.

Given the general match between the model's predictions and what has been reported in the literature, the differences discussed above notwithstanding, we elected to offer density predictions for this species at monthly temporal resolution.

References

Atlas R, Hoffman RN, Ardizzone J, Leidner SM, Jusem JC, Smith DK, Gombos D (2011) A Cross-calibrated, Multiplatform Ocean Surface Wind Velocity Product for Meteorological and Oceanographic Applications. Bulletin of the American Meteorological Society 92:157–174. doi: 10.1175/2010BAMS2946.1

Barco SG, Burt L, DePerte A, Digiovanni R Jr. (2015) Marine Mammal and Sea Turtle Sightings in the Vicinity of the Maryland Wind Energy Area July 2013-June 2015, VAQF Scientific Report #2015-06. Virginia Aquarium & Marine Science Center Foundation, Virginia Beach, VA

Barlow J, Forney KA (2007) Abundance and population density of cetaceans in the California Current ecosystem. Fishery Bulletin 105:509–526.

Becker JJ, Sandwell DT, Smith WHF, Braud J, Binder B, Depner J, Fabre D, Factor J, Ingalls S, Kim S-H, Ladner R, Marks K, Nelson S, Pharaoh A, Trimmer R, Von Rosenberg J, Wallace G, Weatherall P (2009) Global Bathymetry and Elevation Data at 30 Arc Seconds Resolution: SRTM30_PLUS. Marine Geodesy 32:355–371. doi: 10.1080/01490410903297766

Brasnett B (2008) The impact of satellite retrievals in a global sea-surface-temperature analysis. Quarterly Journal of the Royal Meteorological Society 134:1745–1760. doi: 10.1002/qj.319

Breiman L (2001) Random Forests. Machine Learning 45:5–32. doi: 10.1023/A:1010933404324

Buckland ST, Anderson DR, Burnham KP, Laake JL, Borchers DL, Thomas L (2001) Introduction to Distance Sampling: Estimating Abundance of Biological Populations. Oxford University Press, Oxford, UK

Burt ML, Borchers DL, Jenkins KJ, Marques TA (2014) Using mark-recapture distance sampling methods on line transect surveys. Methods in Ecology and Evolution 5:1180–1191. doi: 10.1111/2041-210X.12294

Canada Meteorological Center (2012) GHRSST Level 4 CMC0.2deg Global Foundation Sea Surface Temperature Analysis Version 2.0. PODAAC, CA, USA. doi: 10.5067/GHCMC-4FM02

Canada Meteorological Center (2016) GHRSST Level 4 CMC0.1deg Global Foundation Sea Surface Temperature Analysis Version 3.0. PODAAC, CA, USA. doi: 10.5067/GHCMC-4FM03

Cañadas A, Desportes G, Borchers D (2004) The estimation of the detection function and g (0) for short-beaked common dolphins (Delphinus delphis), using double-platform data collected during the NASS-95 Faroese survey. J Cetacean Res Manage 6:191–98.

Canny JF (1986) A computational approach to edge detection. IEEE Transactions on Pattern Analysis and Machine Intelligence 8:679–698. doi: 10.1016/B978-0-08-051581-6.50024-6

Carretta JV, Lowry MS, Stinchcomb CE, Lynn MS, E. CR (2000) Distribution and abundance of marine mammals at San Clemente Island and surrounding offshore waters: Results from aerial and ground surveys in 1998 and 1999. NOAA Administrative Report LJ-00-02. NOAA National Marine Fisheries Service, Southwest Fisheries Center, La Jolla, CA

Chassignet E, Hurlburt H, Metzger EJ, Smedstad O, Cummings J, Halliwell G, Bleck R, Baraille R, Wallcraft A, Lozano C, Tolman H, Srinivasan A, Hankin S, Cornillon P, Weisberg R, Barth A, He R, Werner F, Wilkin J (2009) US GODAE: Global Ocean Prediction with the HYbrid Coordinate Ocean Model (HYCOM). Oceanog 22:64–75. doi: 10.5670/oceanog.2009.39

Cole T, Gerrior P, Merrick RL (2007) Methodologies of the NOAA National Marine Fisheries Service Aerial Survey Program for Right Whales (Eubalaena glacialis) in the Northeast U.S., 1998-2006. U.S. Department of Commerce, Woods Hole, MA

Cotter MP (2019) Aerial Surveys for Protected Marine Species in the Norfolk Canyon Region: 2018–2019 Final Report. HDR, Inc., Virginia Beach, VA

DFO (2017) DFO Maritimes Region Cetacean Sightings. Version 7 In OBIS Canada Digital Collections. Bedford Institute of Oceanography, Dartmouth, NS, Canada

Foley HJ, Paxton CGM, McAlarney RJ, Pabst DA, Read AJ (2019) Occurrence, Distribution, and Density of Protected Species in the Jacksonville, Florida, Atlantic Fleet Training and Testing (AFTT) Study Area. Duke University Marine Lab, Beaufort, NC

Fujioka E, Kot CY, Wallace BP, Best BD, Moxley J, Cleary J, Donnelly B, Halpin PN (2014) Data integration for conservation: Leveraging multiple data types to advance ecological assessments and habitat modeling for marine megavertebrates using OBIS–SEAMAP. Ecological Informatics 20:13–26.

Garnesson P, Mangin A, Fanton d'Andon O, Demaria J, Bretagnon M (2019) The CMEMS GlobColour chlorophyll *a* product based on satellite observation: Multi-sensor merging and flagging strategies. Ocean Science 15:819–830. doi: 10.5194/os-15-819-2019

Garrison LP (2020) Abundance of cetaceans along the southeast U.S. East coast from a summer 2016 vessel survey. PRD Contribution # PRD-2020-04. NOAA National Marine Fisheries Service, Southeast Fisheries Science Center, Miami, FL

Garrison LP, Martinez A, Maze-Foley K (2010) Habitat and abundance of cetaceans in Atlantic Ocean continental slope waters off the eastern USA. Journal of Cetacean Research and Management 11:267–277.

Geo-Marine, Inc. (2010) New Jersey Department of Environmental Protection Baseline Studies Final Report Volume III: Marine Mammal and Sea Turtle Studies. Geo-Marine, Inc., Plano, TX

Gowans S, Whitehead H (1995) Distribution and habitat partitioning by small odontocetes in the Gully, a submarine canyon on the Scotian Shelf. Can J Zool 73:1599–1608. doi: 10.1139/z95-190

Halpin P, Read A, Fujioka E, Best B, Donnelly B, Hazen L, Kot C, Urian K, LaBrecque E, Dimatteo A, Cleary J, Good C, Crowder L, Hyrenbach KD (2009) OBIS-SEAMAP: The World Data Center for Marine Mammal, Sea Bird, and Sea Turtle Distributions. Oceanography 22:104–115. doi: 10.5670/oceanog.2009.42

Harris PT, Macmillan-Lawler M, Rupp J, Baker EK (2014) Geomorphology of the oceans. Marine Geology 352:4–24. doi: 10.1016/j.margeo.2014.01.011

Hayes SA, Josephson E, Maze-Foley K, Rosel PE, Wallace J, Brossard A, Chavez-Rosales S, Cole TVN, Garrison LP, Hatch J, Henry A, Horstman SC, Litz J, Lyssikatos MC, Mullin KD, Murray K, Orphanides C, Ortega-Ortiz J, Pace RM, Palka DL, Powell J, Rappucci G, Soldevilla M, Wenzel FW (2022) US Atlantic and Gulf of Mexico Marine Mammal Stock Assessments 2021. NOAA National Marine Fisheries Service, Northeast Fisheries Science Center, Woods Hole, MA

Hothorn T, Hornik K, Zeileis A (2006) Unbiased Recursive Partitioning: A Conditional Inference Framework. Journal of Computational and Graphical Statistics 15:651–674. doi: 10.1198/106186006X133933

Jefferson TA, Fertl D, Bolaños-Jiménez J, Zerbini AN (2009) Distribution of common dolphins (Delphinus spp.) In the western Atlantic Ocean: A critical re-examination. Mar Biol 156:1109–1124. doi: 10.1007/s00227-009-1152-y

Laake JL, Calambokidis J, Osmek SD, Rugh DJ (1997) Probability of Detecting Harbor Porpoise From Aerial Surveys: Estimating g(0). Journal of Wildlife Management 61:63–75. doi: 10.2307/3802415

Lawson JW, Gosselin J-F (2018) Estimates of cetacean abundance from the 2016 NAISS aerial surveys of eastern Canadian waters, with a comparison to estimates from the 2007 TNASS. NAMMCO SC/25/AE/09. In: Proceedings of the NAMMCO 25th Scientific Committee (SC). North Atlantic Marine Mammal Commission, Bergen-Tromsø, Norway,

Lehodey P, Senina I, Murtugudde R (2008) A spatial ecosystem and populations dynamics model (SEAPODYM)–Modeling of tuna and tuna-like populations. Progress in Oceanography 78:304–318. doi: 10.1016/j.pocean.2008.06.004

Lehodey P, Conchon A, Senina I, Domokos R, Calmettes B, Jouanno J, Hernandez O, Kloser R (2015) Optimization of a micronekton model with acoustic data. ICES Journal of Marine Science 72:1399–1412. doi: 10.1093/icesjms/fsu233

Mallette SD, Lockhart GG, McAlarney RJ, Cummings EW, McLellan WA, Pabst DA, Barco SG (2014) Documenting Whale Migration off Virginia's Coast for Use in Marine Spatial Planning: Aerial and Vessel Surveys in the Proximity of the Virginia Wind Energy Area (VA WEA), VAQF Scientific Report 2014-08. Virginia Aquarium & Marine Science Center Foundation, Virginia Beach, VA

Mallette SD, Lockhart GG, McAlarney RJ, Cummings EW, McLellan WA, Pabst DA, Barco SG (2015) Documenting Whale Migration off Virginia's Coast for Use in Marine Spatial Planning: Aerial Surveys in the Proximity of the Virginia Wind Energy Area (VA WEA) Survey/Reporting Period: May 2014 - December 2014, VAQF Scientific Report 2015-02. Virginia Aquarium & Marine Science Center Foundation, Virginia Beach, VA

Mallette SD, McAlarney RJ, Lockhart GG, Cummings EW, Pabst DA, McLellan WA, Barco SG (2017) Aerial Survey Baseline Monitoring in the Continental Shelf Region of the VACAPES OPAREA: 2016 Annual Progress Report. Virginia Aquarium & Marine Science Center Foundation, Virginia Beach, VA

Marsh H, Sinclair DF (1989) Correcting for Visibility Bias in Strip Transect Aerial Surveys of Aquatic Fauna. The Journal of Wildlife Management 53:1017. doi: 10.2307/3809604

McAlarney R, Cummings E, McLellan W, Pabst A (2018) Aerial Surveys for Protected Marine Species in the Norfolk Canyon Region: 2017 Annual Progress Report. University of North Carolina Wilmington, Wilmington, NC

McLellan WA, McAlarney RJ, Cummings EW, Read AJ, Paxton CGM, Bell JT, Pabst DA (2018) Distribution and abundance of beaked whales (Family Ziphiidae) Off Cape Hatteras, North Carolina, U.S.A. Marine Mammal Science. doi: 10.1111/mms.12500

Meissner T, Wentz FJ, Scott J, Vazquez-Cuervo J (2016) Sensitivity of Ocean Surface Salinity Measurements From Spaceborne L-Band Radiometers to Ancillary Sea Surface Temperature. IEEE Trans Geosci Remote Sensing 54:7105–7111. doi: 10.1109/TGRS.2016.2596100

Mesgaran MB, Cousens RD, Webber BL (2014) Here be dragons: A tool for quantifying novelty due to covariate range and correlation change when projecting species distribution models. Diversity Distrib 20:1147–1159. doi: 10.1111/ddi.12209

Miller DL, Becker EA, Forney KA, Roberts JJ, Cañadas A, Schick RS (2022) Estimating uncertainty in density surface models. PeerJ 10:e13950. doi: 10.7717/peerj.13950

Mullin KD, Fulling GL (2003) Abundance of cetaceans in the southern U.S. North Atlantic Ocean during summer 1998. Fishery Bulletin 101:603–613.

Palka D (2020) Cetacean Abundance in the US Northwestern Atlantic Ocean Summer 2016. Northeast Fish Sci Cent Ref Doc. 20-05. NOAA National Marine Fisheries Service, Northeast Fisheries Science Center, Woods Hole, MA

Palka D, Aichinger Dias L, Broughton E, Chavez-Rosales S, Cholewiak D, Davis G, DeAngelis A, Garrison L, Haas H, Hatch J, Hyde K, Jech M, Josephson E, Mueller-Brennan L, Orphanides C, Pegg N, Sasso C, Sigourney D, Soldevilla M, Walsh H (2021) Atlantic Marine Assessment Program for Protected Species: FY15 – FY19 (OCS Study BOEM 2021-051). U.S. Deptartment of the Interior, Bureau of Ocean Energy Management, Washington, DC

Palka DL (2006) Summer abundance estimates of cetaceans in US North Atlantic navy operating areas (NEFSC Reference Document 06-03). U.S. Department of Commerce, Northeast Fisheries Science Center, Woods Hole, MA

Palka DL, Chavez-Rosales S, Josephson E, Cholewiak D, Haas HL, Garrison L, Jones M, Sigourney D, Waring G, Jech M, Broughton E, Soldevilla M, Davis G, DeAngelis A, Sasso CR, Winton MV, Smolowitz RJ, Fay G, LaBrecque E, Leiness JB, Dettloff K, Warden M, Murray K, Orphanides C (2017) Atlantic Marine Assessment Program for Protected Species: 2010-2014 (OCS Study BOEM 2017-071). U.S. Deptartment of the Interior, Bureau of Ocean Energy Management, Washington, DC

Perkins NJ, Schisterman EF (2006) The Inconsistency of "Optimal" Cutpoints Obtained using Two Criteria based on the Receiver Operating Characteristic Curve. American Journal of Epidemiology 670–675.

Pershing AJ, Alexander MA, Hernandez CM, Kerr LA, Le Bris A, Mills KE, Nye JA, Record NR, Scannell HA, Scott JD, Sherwood GD, Thomas AC (2015) Slow adaptation in the face of rapid warming leads to collapse of the Gulf of Maine cod fishery. Science 350:809–812. doi: 10.1126/science.aac9819

Read AJ, Barco S, Bell J, Borchers DL, Burt ML, Cummings EW, Dunn J, Fougeres EM, Hazen L, Hodge LEW, Laura A-M, McAlarney RJ, Peter N, Pabst DA, Paxton CGM, Schneider SZ, Urian KW, Waples DM, McLellan WA (2014) Occurrence, distribution and abundance of cetaceans in Onslow Bay, North Carolina, USA. Journal of Cetacean Research and Management 14:23–35.

Roberts JJ, Best BD, Dunn DC, Treml EA, Halpin PN (2010) Marine Geospatial Ecology Tools: An integrated framework for ecological geoprocessing with ArcGIS, Python, R, MATLAB, and C++. Environmental Modelling & Software 25:1197–1207. doi: 10.1016/j.envsoft.2010.03.029

Roberts JJ, Best BD, Mannocci L, Fujioka E, Halpin PN, Palka DL, Garrison LP, Mullin KD, Cole TVN, Khan CB, McLellan WA, Pabst DA, Lockhart GG (2016) Habitat-based cetacean density models for the U.S. Atlantic and Gulf of Mexico. Scientific Reports 6:22615. doi: 10.1038/srep22615

Roberts JJ, Mannocci L, Schick RS, Halpin PN (2018) Final Project Report: Marine Species Density Data Gap Assessments and Update for the AFTT Study Area, 2017-2018 (Opt. Year 2), Document Version 1.2. Duke University Marine Geospatial Ecology Lab, Durham, NC

Roberts JJ, Yack TM, Halpin PN (2023) Marine mammal density models for the U.S. Navy Atlantic Fleet Training and Testing (AFTT) study area for the Phase IV Navy Marine Species Density Database (NMSDD), Document Version 1.3. Duke University Marine Geospatial Ecology Lab, Durham, NC

Robertson FC, Koski WR, Brandon JR, Thomas TA, Trites AW (2015) Correction factors account for the availability of bowhead whales exposed to seismic operations in the Beaufort Sea. Journal of Cetacean Research and Management 15:35–44.

Ryan C, Boisseau O, Cucknell A, Romagosa M, Moscrop A, McLanaghan R (2013) Final report for trans-Atlantic research passages between the UK and USA via the Azores and Iceland, conducted from R/V Song of the Whale 26 March to 28 September 2012. Marine Conservation Research International, Essex, UK

Silsbe GM, Behrenfeld MJ, Halsey KH, Milligan AJ, Westberry TK (2016) The CAFE model: A net production model for global ocean phytoplankton. Global Biogeochemical Cycles 30:1756–1777. doi: 10.1002/2016GB005521

Thorne LH, Heywood EI, Hirtle NO (2022) Rapid restructuring of the odontocete community in an ocean warming hotspot. Global Change Biology gcb.16382. doi: 10.1111/gcb.16382

Torres LG, Mclellan WA, Meagher E, Pabst DA (2005) Seasonal distribution and relative abundance of bottlenose dolphins, Tursiops truncatus, along the US mid-Atlantic coast. Journal of Cetacean Research and Management 7:153.

Wentz FJ, Scott J, Hofflman R, Leidner M, Atlas R, Ardizzone J (2015) Remote Sensing Systems Cross-Calibrated Multi-Platform (CCMP) 6-hourly ocean vector wind analysis product on 0.25 deg grid, Version 2.0. Remote Sensing Systems, Santa Rosa, CA

Whitt AD, Powell JA, Richardson AG, Bosyk JR (2015) Abundance and distribution of marine mammals in nearshore waters off New Jersey, USA. Journal of Cetacean Research and Management 15:45–59.

Wood SN (2011) Fast stable restricted maximum likelihood and marginal likelihood estimation of semiparametric generalized linear models. Journal of the Royal Statistical Society: Series B (Statistical Methodology) 73:3–36. doi: 10.1111/j.1467-9868.2010.00749.x